Single lift blade alignment for large offshore wind turbines

Master Thesis

K. de Leeuw

Delft University of Technology

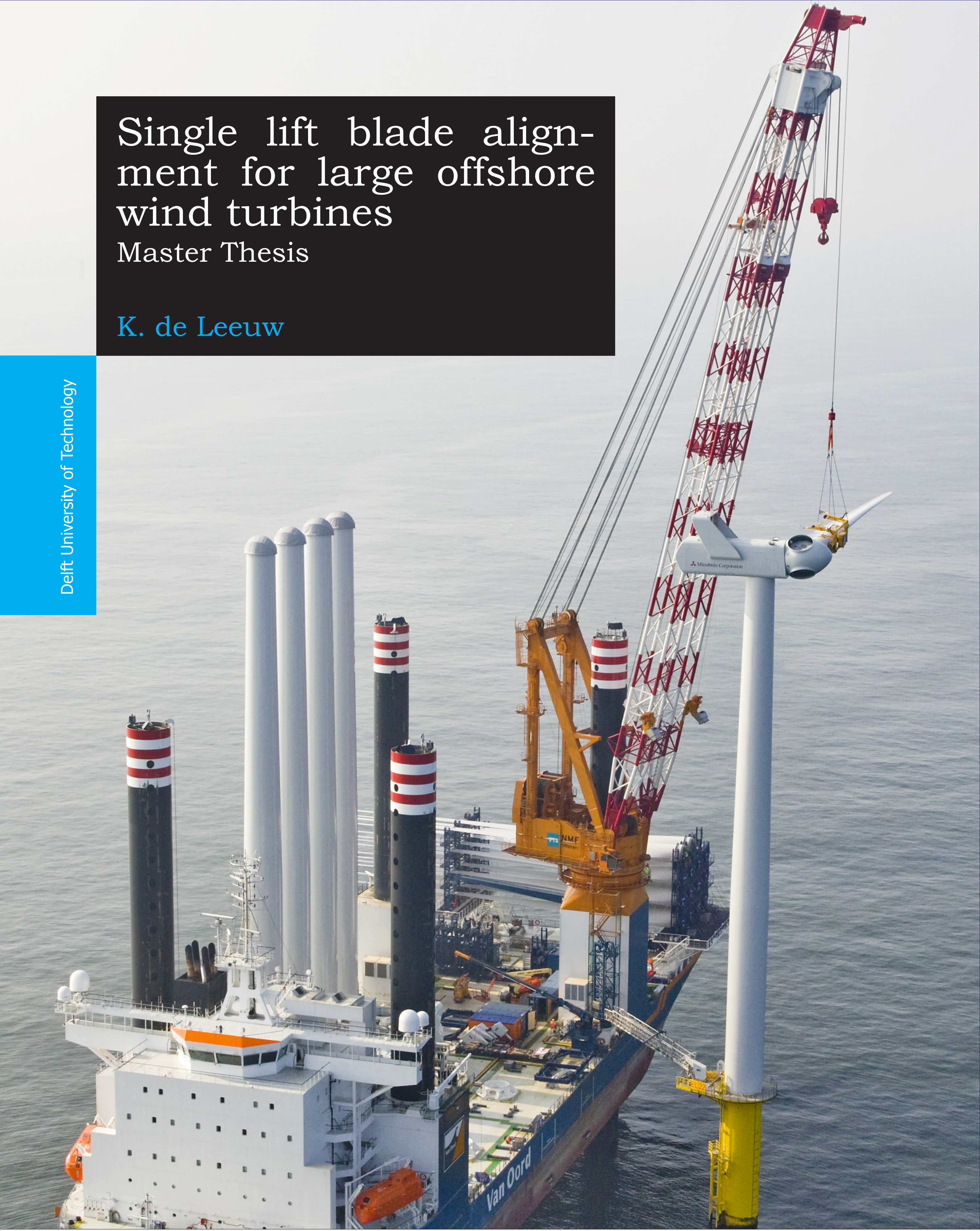

TU Delft
Delft
University of
Technology

Challenge the future

Single lift blade alignment for large offshore wind turbines

A critical assessment of the alignment process of next generation wind turbine blades

by

K. de Leeuw

in partial fulfillment of the requirements for the degree of

Master of Science
in Offshore and Dredging Engineering

at the Delft University of Technology.
to be defended publicly on Wednesday 11, 2019 at 13:00 AM.

Student number:	4337840	
Project duration:	September 1, 2018– December 11, 2019	
Chairman:	Ir. P.G.F. Sliggers	TU Delft
Thesis committee:	Dr.ir. A. Jarquin Laguna	TU Delft
	Ir. J. Voormolen	Van Oord

TU Delft

Van Oord
Marine ingenuity

Preface

The installation of larger offshore wind turbine blades is one of Van Oords concerns for the future. Motions of the blade in the alignment phase, where the blade is mated into the hub, are causing problems during single blade installations. An analysis of the parameters that influence the motion of a wind turbine blade is performed and the effects on the motions of installing larger blades are investigated. A numerical model is developed to determine the dynamic responses of the system subjected to wind loading. The results of a time domain analysis together with a frequency domain analysis show the main causes of the dynamic behaviour of the blade root. Suggestions to improve the current lift setup are made, which aim to decrease the motion of the blade root and thereby increase the workability for future offshore wind turbine blade installations.

During this graduation project I was surrounded by people who kept me going through the tough times. I would like to thank Antonio Jarquin Laguna for guiding me through this thesis project and providing me with all the knowledge I needed to finish this project. I would also like to thank Frank Sliggers for sharing his extensive experience. Futhermore I would like to thank Job Voormolen for his patience and guidance during this project. In addition I would like to thank the TU Delft and Van Oord for giving me the opportunity to combine this thesis with an international sport career. I would like to thank all the graduates in the graduate office and my colleagues at Van Oord for being able to work in a great atmosphere. Lastly, I would like to thank my family and friends for their continuous support. In particular my parents and my girlfriend Laura who where supporting me as much as they could. Without them I couldn't have managed to combine my graduation project and perform at the highest level in sport.

At the end of this thesis project I am convinced that this project shaped me in many ways. Not only I became a better engineer, but I also learned how to deal with stressful situations, how I can reach my goals, how to deal and learn from mistakes and how to never give up.

K. de Leeuw
Delft, December 2019

Abstract

In 2022 the first 12 MW offshore wind turbines are expected to be installed. Due to the continuous upscaling of wind turbine generators new problems are expected to arise during the installation of wind turbines. Especially the workability of the installation of larger wind turbine blades, which are already causing problems during the installation of 8.4 MW turbine blades, are questioned by Van Oord. This research focuses on the alignment process of the blade with the hub, which is considered to be the limiting factor in installing wind turbine blades. The ultimate goal is to reduce single blade installation times by facilitating the alignment process.

To investigate how different environmental conditions affect the dynamic behaviour of the blade in the alignment process, a numerical model is developed. The motions of the blade, forces in the taglines and aerodynamic forces on the blade are evaluated for different environmental conditions during 30-minute simulations in the time domain. Wind velocity, turbulence intensity and the angle of the incoming wind relative to the blade are environmental parameters that influence the motion of a blade. Results for a 8.4 MW reference turbine blade are compared to a 12 MW turbine blade and conclusions are made concerning the installation workability for larger turbine blades.

Results show that the displacement of the blade root is caused by the rotation of the blade and installation tool around its x- and z-axis. The response spectrum of the blade root motions contains a significant amount of energy at the lower frequency part of the spectrum. In this part the first and second natural frequency of the system occur, which correspond to the rotations that are the main causes for the displacement of the blade root. The effect of wind speed, turbulence and incoming wind angle on the response of the blade is significant. Furthermore simulations are conducted for different rotation angles of the blade in the blade installation tool, which can result in large reduction, around 50%, of blade root motions. The responses of larger turbine blades (length 107 metre) increase compared to a smaller turbine blade (length 80 metre). Workability is expected to decrease due to the increase in blade root motions.

Based on the results of the analysis, several improvements are proposed for decreasing the blade root motions using the existing tagline set up. Using a different angle of the blade in the installation tool and increasing the tagline tension both decrease blade root motions. A solution using an additional tagline is proposed and discussed to show how the current setup could be improved.

Contents

List of Tables ix

List of Figures xi

Nomenclature xiv

1 Introduction 1
- 1.1 Background 1
- 1.2 Problem Definition 2
- 1.3 Thesis Objective And Outline 3

2 Case Description 5
- 2.1 Blade Installation Procedure 5
- 2.2 Equipment 7
- 2.3 Reference Site 11
- 2.4 Limit Operation Criteria 12

3 Numerical Model 15
- 3.1 Assumptions 15
- 3.2 Kinematics 16
  - 3.2.1 Whip Hoist Hook System 16
  - 3.2.2 Blade Installation Tool & Blade 18
- 3.3 Loads 22
  - 3.3.1 Slings And Taglines 22
  - 3.3.2 Bearing Damping 22
  - 3.3.3 Aerodynamic Loading 23
- 3.4 Bodies Equations of Motions 27
  - 3.4.1 Generalized Coordinates 27
  - 3.4.2 Kinetic Energy 28
  - 3.4.3 Potential Energy 28
  - 3.4.4 Derivation EOM 29
  - 3.4.5 Simulation 29
- 3.5 Software Tools 31
- 3.6 Model Verification 32
- 3.7 Input 36

4 Model Results 39
- 4.1 Load Cases And Environmental Conditions 39
- 4.2 Results Reference Case 41
  - 4.2.1 Relative Motion Blade And Hub 43
- 4.3 Results 12MW Turbine Blade 44
  - 4.3.1 Eigenvalue Analysis 44
  - 4.3.2 Simulation Results 47
  - 4.3.3 Sensitivity Analysis 51
- 4.4 Improvements 54

5 Conclusion and Recommendations 59
- 5.1 Conclusions 59
- 5.2 Recommendations 59

A Case Description 61
- A.1 Restricted or Unrestricted operation 61
- A.2 Traverse system 62

B Model Verification 63
B.1 Simple Pendulum Motion Lift Wires . . . 63
B.2 Double Pendulum Motion Lift Wires . . . 63
B.3 Symmetry M-Matrix . . . 64

C Tower Fore-Aft Motion 69

D Blade 71
D.1 Blade Notes . . . 71
D.2 Segments . . . 72

E Input Lift Plan 73
E.1 Lift wires . . . 73
E.2 Whip Hoist . . . 74
E.3 BIT and blade . . . 75

F Research questions 77

Bibliography 79

List of Tables

1.1 Modelled parts . . . 4

2.1 Wire and rope properties . . . 9
2.2 Rigging equipment . . . 10
2.3 BIT information . . . 11
2.4 Reference location . . . 11
2.5 Limit operation criteria . . . 13

3.1 Damping and stiffness parameters . . . 23
3.2 TI for different wind speeds and I_{15} . . . 26
3.3 Degrees of freedom . . . 27
3.4 Model structure . . . 31
3.5 Turbine description . . . 36

4.1 Definition of load cases . . . 39
4.2 Definition of sensitivity cases . . . 40
4.3 Eigen modes and natural periods for BIT,blade and hook rigid body motions . . . 44
4.4 Simulation results for different angles of the blade in the BIT . . . 51
4.5 Simulation results for different damping values . . . 52

B.1 Random verification input . . . 65
B.2 Realistic verification input . . . 65
B.3 Verification: M-matrix symmetry for random input values . . . 66
B.4 Verification: M-matrix symmetry for realistic input values . . . 67

E.1 Lift wires properties . . . 73
E.2 Whip hoist properties . . . 74
E.3 BIT and blade properties . . . 75

List of Figures

1.1 Blade installation by the Aeolus 1
1.2 Blade transport and installation 2
1.3 Research methodology 4

2.1 Blade installation phases 6
2.2 Operation time 7
2.3 Side- and topview Aeolus 8
2.4 Overview lifting arrangement 8
2.5 Whip hoist overview 9
2.6 Rigging blade installation tool 10
2.7 Connection BIT-tagline 10
2.8 Blade Installation Tool 11
2.9 Dogger Bank location 12
2.10 Wind Rose 12
2.11 Wind Speed (August) 12
2.12 Misalignment of axes (hub and blade root) 13

3.1 Coordinate system: lift wires and whip hoist sheave 17
3.2 Coordinate system: whip hoist system 19
3.3 Coordinate system: blade installation tool and blade (back view) 20
3.4 Coordinate system: blade installation tool and blade (side view) 21
3.5 Blade root end 21
3.6 Tagline coordinates 21
3.7 Blade segments 23
3.8 Body-fixed and aerodynamic coordinate system 24
3.9 Wind speed time series (u,v and w) for $TI = 0.16$ and $\bar{U} = 15$ m/s 26
3.10 Wind speed time series for $TI = 0.16$ and $TI = 0.12$ at $\bar{U} = 6$ m/s 27
3.11 Pendulum motion lift wires: simulation- (left) and verification setup (right) 32
3.12 Verification result: pendulum motion hoist wires around x-axis 32
3.13 Verification result: pendulum motion hoist wires around y-axis 33
3.14 Double pendulum angles: test vs model 33
3.15 Energy in system (without energy dissipation) 35
3.16 Energy in system (with energy dissipation) 35
3.17 Imposed tower displacement 36
3.18 Overview lift installation plan 37

4.1 Track of the blade root center for 30-min simulations 41
4.2 Mean and standard deviation for 3 different wind speeds and 4 different angles 42
4.3 Mean displacement 42
4.4 Number of outcrossing of the safe boundary 42
4.5 Track of the hub displacement in x-direction 43
4.6 Number of outcrossing considering the relative motion between the blade root and hub 43
4.7 The dominant motion of the blade and BIT visualised: eigenmode 1 (bottom) and eigen mode 2 (top) 45
4.8 Wind speed spectrum (top) and blade root displacement frequency spectrum (bottom) 46
4.9 Kaimal and Jonswap spectrum 46
4.10 Track of the blade root center for 30-min simulations (12MW) 47
4.11 Workability for a 8.4MW (a) and 12MW (b) turbine blade installatin at the Dogger Bank in August 47

4.12 Track of the blade root (top figure) and moment (bottom figure) 48
4.13 Mean and standard deviation of the relative motion between the blade root and hub . . 49
4.14 Maximum tagline tension for V = 6 m/s and V = 9 m/s 49
4.15 Motions of the blade root towards the hub for V = 6m/s (top) and V=9m/s (bottom) . 50
4.16 Blade aerodynamic moments around x and z axis for different blade angles in the BIT for a wind speed V = 10 m/s 51
4.17 Number of outcrossing considering the relative motion between the blade root and hub 52
4.18 Results turbulence intensity sensitivity values 53
4.19 Tagline setup 54
4.20 Track of the blade root center for 30-min simulations using a different tagline tension . 55
4.21 Additional tagline 2 55
4.22 Track of the blade root centre with an additional tagline 56
4.23 Wind spectrum (top) and blade root displacement spectrum for the old and new lift setup 56
4.24 Results of the old setup compared to the results of the proposed improvements 57

A.1 Flow chart 61
A.2 Snatch Blocks 62

C.1 Results fore-aft displacement hub for $h_s = 0.5m$ 69
C.2 Results fore-aft displacement hub for $h_s = 1m$ 69

Nomenclature

Abbreviations

AOA	Anlge Of Attack
BDF	Backward Differentation Formula
BIT	Blade Installation Tool
DOF	Degrees Of Freedom
EOM	Equations of Motions
GE	General Electric
NTM	Normal Turbulence Model
ODE	Ordinary Differential Equation
OWT	Offshore Wind Turbine
PFL	Pull Force Limit
RNA	Rotor Nacelle Assymbly
SWL	Safe Working Load
TGM	Tagline Master
TI	Turbulence Intensity
TP	Transition Piece
WIV	Wind turbine Installation Vessel
WLL	Working Load Limit

Symbols

α	Angle of rotation around x-axis lift wires	[°]
α_{wf}	Alpha Factor Weather Forecast	[-]
β	Angle of rotation around y-axis lift wires	[°]
δ	Angle of rotation around x-axis whip hoist bearing	[°]
ϵ	Angle of rotation around z-axis whip hoist hook	[°]
η	Angle of rotation around y-axis blade and blade installation tool	[°]
γ	Angle of rotation around y-axis whip hoist sheave	[°]
θ	Angle of rotation around z-axis blade and blade installation tool	[°]
ζ	Angle of rotation around x-axis blade and blade installation tool	[°]
D	Rayleigh dissipation function	[J]
d	Diameter	[m]

d_{hb}	Outcrossing Rate Safe Boundary	[Hz]
E	Elastic potential energy	[J]
F	Force vector	[N]
h	Water Depth	[m]
h_{ave}	Average Water Depth	[m]
I	Moment of inertia	[kg/m^2]
I_u	Turbulence intensity	[-]
k_{axial}	Axial stiffness of a sling	[m]
L	Langrangian	[J]
l	Length	[m]
L_{LAT}	Latitude	[$^\circ$]
L_{LON}	Longitude	[$^\circ$]
M	Moment vector	[Nm]
OP_{LIM}	Operational Limiting Criteria	[-]
OP_{WF}	Operational Criteria Weather Window	[s]
p_i	Point *i* described in inertial coordinates	[m]
p_i	Transformation Matrix *i*	[m]
q_i	Generalized coordinate *i*	[$^\circ$],[m]
T	Kinetic Energy	[J]
T_C	Estimated Maximum Contingency Time	[s]
T_R	Operation Reference Period	[s]
T_{POP}	Planned Operation Period	[s]
V	Potential Energy	[J]
x_{CoGBIT}	Translation in x-direction blade and blade installation tool	[m]
y_{CoGBIT}	Translation in y-direction blade and blade installation tool	[m]
z_{CoGBIT}	Translation in z-direction blade and blade installation tool	[m]

1

Introduction

1.1. Background

Van Oord is a leading international contractor offering innovative solutions for the dredging, marine and offshore industry. Van Oord's activities are subdivided in four fields of activity: Oil & Gas, Dredging, The Netherlands and Offshore Wind. Especially the offshore wind sector is growing rapidly due to the growing demand for green energy solutions. In 2007 the business unit Offshore Wind was established and responsible for all activities involving offshore wind farm construction. Since 2007 Van Oord has been responsible for the engineering, procurement, construction and installation (EPCI) of many wind farms.

One of Van Oord's responsibilities involves the installation of offshore wind turbines (OWT). An OWT consist of a substructure, transition piece, tower and rotor nacelle assymbly (RNA). The substructure and transition piece (TP) are installed separately. The installation of the tower and RNA could be done in different ways, but for large-scale OWT installation single lift operations are the preferred installation method. Single blade installations are easier to control than, for example, a bunny ear setup where two blades and the hub are installed simultaneously . Deck usage and crane capacity also play a role in selecting the installation method [1].

This thesis considers the blade lift operations to be done by the Aeolus. The Aeolus is a purpose-built jack-up vessel that installs OWTs. The OWT parts are subjected to wind loads during lifting operations. Especially the blades are sensitive to wind loads. The motion of the blades is often damped by a tagline system which is installed on the Aeolus crane. During the alignment phase, just before the blade is connected to the hub, these motions cause problems. Large motions during the alignment phase are a problem in single blade lift operations. Van Oord expects these motions to cause even bigger problems when larger blades have to be installed.

Figure 1.1: Blade installation by the Aeolus

OWT Blade Installation

Together with the tower and nacelle, the blades are loaded on the Aeolus (see figure 2.1a). A blade rack system is used to safely store the blades during shipping and operation (see figure 2.1b). At the desired location the jacking system elevates the vessel to provide a stable installation platform. The tower is installed on top of the transition piece and the nacelle on top of the tower. For the installation of the blades, the hub is rotated to the desired position. A blade installation tool (BIT) is lowered and fastened to the blade. Taglines are attached to the BIT and keep the blade away from undesired motion during lifting (see figure 1.2d). The blade is lifted to hub height and the alignment phase starts (see figure 2.1d). After the alignment phase, the blade is bolted to the hub and the BIT is retracted. This process is repeated for next blade.

(a) Loading blades (b) Blade rack system

(c) Aeolus at location

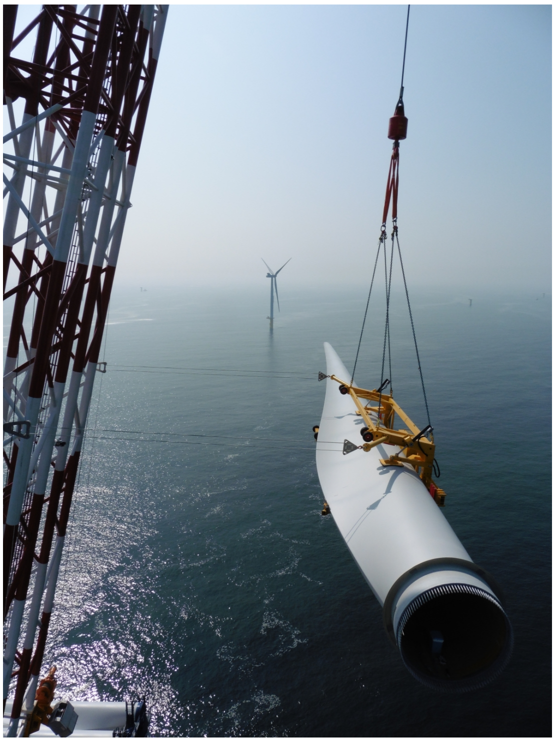

(d) Lifting blade to hub height

(e) Alignment phase

Figure 1.2: Blade transport and installation

1.2. Problem Definition

General Electric Company (GE) recently installed a prototype of the Haliade-X 12MW in Rotterdam and won two deals for installing 12MW turbines along the U.S. East Coast and at the Dogger Bank. The dimension of this 12MW turbine have increased relative to the 'smaller' turbines. Due to the continuous upscaling of wind turbines new problems arise in the offshore wind industry. Offshore wind installation contractors are expected to install bigger wind turbines in offshore conditions. Especially heavy lift operations are more difficult to control when wind turbines are getting bigger. Offshore installation vessels should be able to perform the same installation precision for larger and heavier blades. Furthermore, the installation height increases and approaches the maximum installation height. The alignment process of the blade root and the hub are influenced by the aforementioned developments and the effects of upscaling these operations are not clear.

1.3. Thesis Objective And Outline

Company Objective

Installing blades is a time-consuming process due to the sensitivity to high wind speeds. State-of-the-art lift equipment allows single blade installations at mean wind speeds around 8-12 m/s (wind force: 5/6) at hub height [2]. Installation costs form a big part of the total capital expenditures of an OWF and are potentially the largest cost reduction opportunity to 2025 [3]. New techniques are expected to be necessary to be able to install 12MW turbine blades and shorten installation times. Design solutions should be based on the underlying problems.

Safety is another topic to consider when installing blades. In the final installation phase guide pins in the blade flange are used to facilitate the mating process. This mating process is assisted by banksmen whose job is to make sure the guide pins do not damage. During this process safety of the banksmen is an issue when the blade is moving unexpected. Getting a feeling for this unexpected movements is essential to improve safety for banksmen and reducing potential risks. Wind turbine suppliers expect EPCI contractors, such as Van Oord, to continuously invest and adapt to new circumstances and create a safe working environment.

Graduation Aim

The main objective of this research is to determine the feasibility of future blade installation based on wind loading during blade lift operations and improve the alignment process. To investigate the main objective, the research focuses on defining a representative numerical model to calculate blade - wind interaction during the alignment phase. Based on this model the effects of some critical input parameters are investigated in a sensitivity analyses to gain knowledge about the blade motion in different operational conditions. The feasibility of future turbine blade installation is determined based on the results in the time domain, frequency domain and the results of the sensitivity analyses.

Research Question

The following research question is established:

> *What effect on workability does the upscaling to future 12MW wind turbines have on the alignment process of single blade installation of turbine blades using a jack-up vessel?*

To be able to answer the research question, the following sub-questions:

> What effect does wind have on the dynamics of a wind turbine blade in the alignment phase?
>
> Under which environmental conditions will the movement of the blade relative to the hub stay within workability limits?
>
> What are the main causes for excessive blade root displacement?
>
> Are future blade installations expected to create an unsafe operation environment for employees?

Scope of Work

This research focuses on blade installation of offshore wind turbines. Wind is found to be limiting the operations of blade lift operations. Most critical is the alignment phase, where the blade root is aligned with the hub and ready to be connected. Other phases in the installation process of blades are not incorporated in this research. The focus of this research is on aerodynamic loading and dynamics of the blade and providing suggestions to improve the alignment process. The crane and vessel motions are not taken into account in this research. For the motion of the hub an imposed fore-aft displacement is considered.

Part	Components
Environmental conditions	Wind speed | Wind direction | Wind Turbulence
Installation equipment	Taglines | Blade Installation Tool | Whip hoist hook | Slings | Lift wires
Blade parameters	Dimensions | Aerodynamic Coefficients | Angle of Attack
System responses	Displacement | Accelerations | Forces | Tagline Tension

Table 1.1: Modelled parts

Methodology

A numerical computational model is build to describe the effects of wind on single-blade installations. Assumptions are stated to describe the limitations of the model. The model is based on rigid body dynamics. In total the system consist of 4 rigid bodies and 11 degrees of freedom. The taglines are modelled as springs, which control the motion of the blade. The blade experiences wind induced loads from an artificial wind field. The simulations are performed for different wind field characteristics, such as mean wind velocity and turbulence intensity. The responses of the system during this aerodynamic loading of the blade are monitored. The motion of the blade root centre, the tagline tension, the wind induced loads on the blade are tracked for each simulation. After processing the data of the simulations, information about the workability for specific wind conditions is obtained. After validation of the model, a reference load case with a 8.4MW turbine blade is worked out to be able to compare these results with the results for a 12MW turbine blade. Time domain simulations are performed to simulate real offshore conditions and to produce results which can be evaluated against the limiting operation criteria. After the results are interpreted a sensitivity analysis is performed. A sensitivity analysis is done to check how different values of a set of certain independent variables affect a specific dependent variable under specific conditions. The results can be used to determine the workability of single blade installation under certain environmental conditions. A analysis in the frequency domain is performed to gain information about the basic dynamic behaviour of the complete lift system.

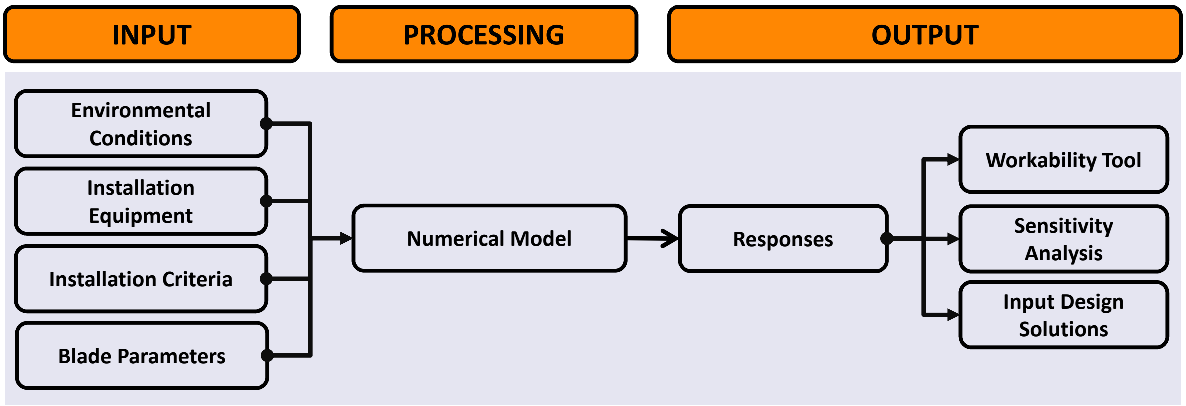

Figure 1.3: Research methodology

2

Case Description

This chapter starts with a discription of the logistics involved in the transportation process of a blade from quayside to the wind farm. Then the lifting procedures are explained. In the next section, typical equipment used for a single blade lift operation are described. This equipment also serves as input for the numerical model. In the third section the site conditions used for analysis are given. In the fourth and final section, the limit operation criteria are given.

2.1. Blade Installation Procedure

The logistic process for blade installation starts at the port where the Aeolus is docked. The Aeolus is one of Van Oord's wind turbine installation vessels (WIV). Different solutions to load the vessel exist and the selected method depends on the turbine supplier. For small turbines the blades can be loaded directly with their transport frame and seafastened on the wind turbine installation vessel. Usually a blade rack is already seafastened on the vessels deck and the blades are loaded without their transport frames. Turbine suppliers can also prescribe lifting operation methods for loading the blades from the marshalling harbour quayside. The placement and orientation on the WIV deck is also prescribed and differs from project to project.

After arranging the WIV with the superstructure parts it sails out to the wind farm location for installation of the wind turbine. At the given location the Aeolus is jacked. For some locations the spud cans are placed at the same location as where they were during the installation of the support substructure. For other locations a new area is chosen based on soil conditions. Therefore the orientation of the Aeolus is fixed beforehand and not based on ideal wind direction to install blades. After preloading of the legs of the Aeolus, which assures a stable lifting platform, the lifting operation of the blades initiates. Allowable environmental conditions for the tower, nacelle and blades are determined based on the equipment used. The installation of blades is often the limiting operation, because of the high sensitivity to wind. Blade yokes, used as lifting equipment to grab the blade, have a certain maximum wind speed. The WIV crane also has a wind speed limit. A marine warranty surveyor is present to provide independent third-party technical review and approval of the installation of the superstructure parts.

Each wind turbine supplier provides their own technical description for the installation methodology. Furthermore the wind turbine supplier is responsible for the installation process and installation equipment. Turbine suppliers Vestas and GE both use their own different installation methodology. For the Norther wind farm project Vestas prepared the Aeolus with their own tagline system to control the lifting of blades. The tagline system is remotely controlled by Vestas during lifting operations. Tension in the tagline system is controlled to keep the movement of the blade as low as possible.

In figure 2.1 the different phases of the blade installation are shown. The installation starts with the lift-off phase of the blade from the blade rack 2.1a. Then the crane follows the slew path to the hub. When the blade is at hub height, the alignment phase initiates 2.1b. If the lifting criteria requirements are met to mate the blade to the hub, the blade is bolted to the hub 2.1c. If the blade is succesfully bolted to the hub the BIT is removed and process is repeated for the next blade 2.1d.

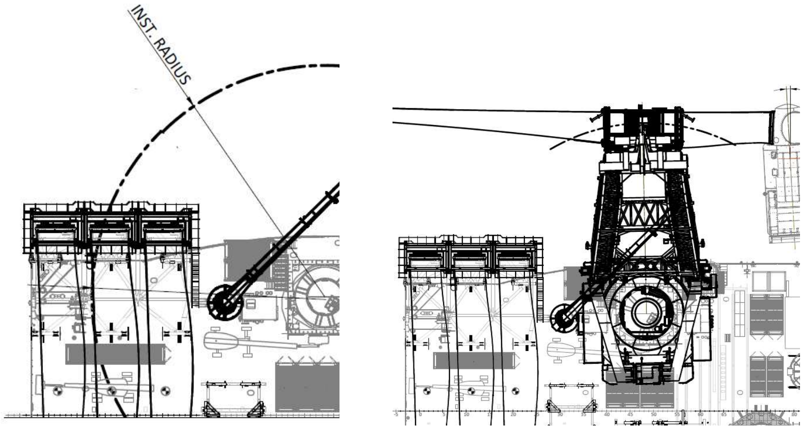

(a) Lift off to hub height (b) Alignment and mating phase

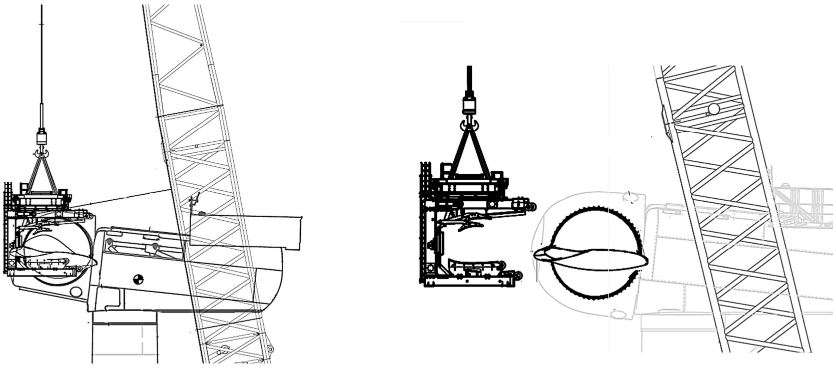

(c) Side view (d) BIT removal

Figure 2.1: Blade installation phases

Weather Window

Uncertainties related to weather forecasting must be taken into consideration in offshore lift operations. An offshore operation can be defined as weather restricted or unrestricted operation. The procedure to find the required weather window can be found in appendix A.1. Blade lift operations are defined as weather restricted operations. Therefore a required weather window needs to be established. The duration of one blade installation is defined by an operation reference period (T_R):

$$T_R = T_{POP} + T_C \tag{2.1}$$

where

T_R = Operation reference period
T_{POP} = Planned operation period
T_C = Estimated maximum contingency time

Blade lift operations are repetitive occurring offshore operations for which the planned operation time (T_{POP}) is scheduled in detail. Contingency time is added to cover uncertainty in the planned operation time. For repetitive operations a contingency time (T_C) of 50% of T_{POP} is normally accepted. If the planned operation period is 3 hours, after adding 1.5 hour as a contingency, the operation reference period T_R becomes 4.5 hour.

Next step is to define the operational limiting criteria (OP_{LIM}) for the lift installation. The limit criteria is often defined by the turbine supplier and depends on installation tools. For Norther the wind speed limit was $OP_{LIM} = 10 m/s$. By defining the forecasted operational criteria as $OP_{WF} = \alpha_{wf} \cdot OP_{LIM}$ the uncertainty in both forecasting and monitoring of the environmental conditions is accounted for. For an operational limiting wind speed of $10 m/s$ an alpha factor of 0.80 is found in DNV-OS-H101 [4]. Using this alpha factor the forecasted operational criteria becomes $OP_{WF} = 8 m/s$. At the start of the

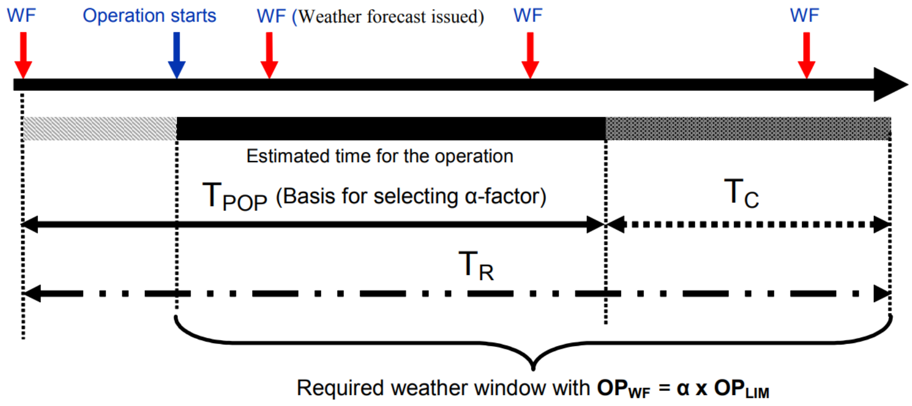

Figure 2.2: Operation time

operation the last 30 minutes should be below the operational limit and the forecast for the weather window should also be below the operational limit. The operation is interrupted when the wind speed exceeds $8m/s$ and the blade is returned to deck where it is seafastened again.

2.2. Equipment

Single blade installation for project Norther was performed by the jack-up vessel Aeolus. The equipment used during project Norther is used as input for the numerical simulation. Therefore only this equipment is described in this chapter.

Aeolus

The vessel used in this research project is the jack up vessel Aeolus (see figure 2.3). The Aeolus is a self elevating wind turbine installation unit and provides a stable platform for lifting operations. It was purpose-built to construct wind parks and put into service in 2014. It is equipped with an advanced single acting and continuous hydraulic pin-and-hole jacking system. Four giant legs allow the Aeolus to be jacked up and work in waters up to 45 metres deep. The jacking system provides a stable platform for lifting operations. The four legs (tubes) have a length of 81m and a diameter of 4.5 m.

Crane

The Aeolus is accommodated with a 1600t Huisman crane. This crane is a truss structure which consist of multiple beams that together form a rigid structure. Huisman is responsible for the main hoist (1600 ton) and auxiliary hoist system (100 ton) with a reach of 14m - 32m and 16m - 109m respectively. The whip hoist (auxiliary hoist system) is used to install blades.

Whip Hoist

The Aeolus is equipped with a whip hoist jib which is used to perform blade installations. Two sheaves are fixed to the whip hoist jib to guide the whip hoist wire through a sheave fixed to the whip hoist block and catcher (see figure 2.5a). The whip hook is connected to whip hoist block (see figure 2.5b). The safe working load (SWL) of the whip hoist hook is 100 mt and the total weight 6 ton. The dimensions are 6.2 m x 2.1 m. The hook is able to rotate around the hoist bearing block. The whip hoist wire is coupled to the whip hoist block. Slings attach the whip hoist hook with the blade installation tool. The whip hoist wire is a single reeving line starting from the whip hoist winch and on the other end fixed to the whip hoist jib. The steel whip hoist wire has a diameter of 0.05 m and total length of 515 m. The minimum breaking load is 233 ton.

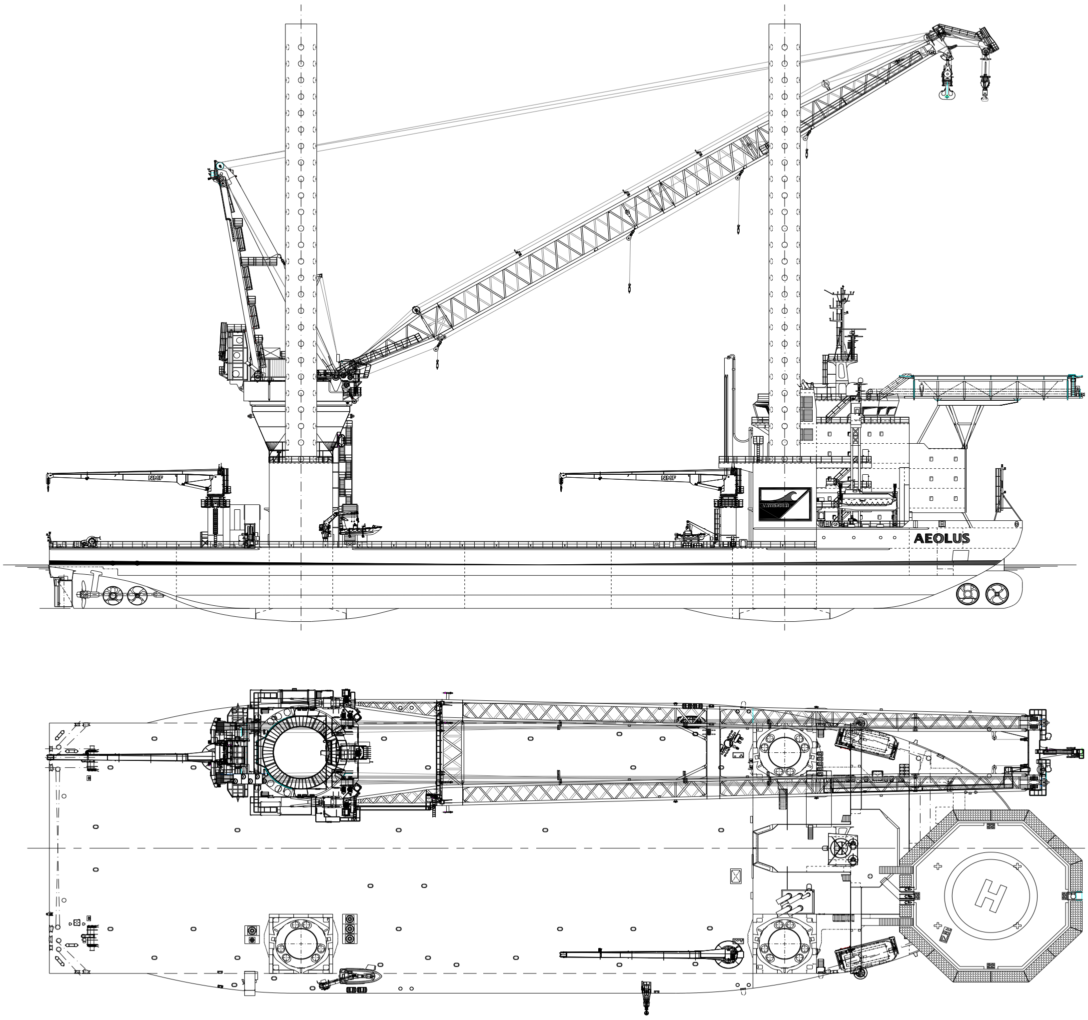

Figure 2.3: Side- and topview Aeolus

Traverse System

During the installation of wind turbine blades the horizontal direction of the BIT is controlled by a traverse system. The traverse system is composed of a guidewire winch, tagline master (TGM) and top traverse. The guidewire winch and tagline master are mounted on a frame which is attached to the crane pedestal. The guidewire winch is able to create a maximum pre-tension in the guide wire of 194kN. Vestas prefers a pre-tension of 24kN. The tagline master creates a constant tension in the tagline called the pull force limit (PFL). The PFL can be manually chosen before by the tagline operator. Vestas prefers a PFL of 15kN. If the pull force exceeds the PFL, the tagline will slide. The top traverse exist of the support clamps, the top traverse clamp and top traverse. Its primary function is to provide an anchor place for the guide wire and tagline.

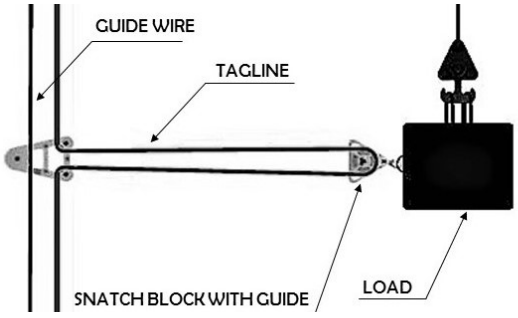

Figure 2.4: Overview lifting arrangement

A 60kN snatch block is connected to each guide wire. It serves as a guide between the guide wire and the tagline. The snatch block will follow the load when the BIT is lifted. Another snatch block with guide connects the tagline to the BIT. The tagline runs through two 60kN snatch blocks, out to the snatch block with guide, attached to the BIT, and up to the top traverse to be fastened (see appendix A.2). The snatch block between the wire stops is there to create a safe distance between the tagline and the guidewire. Wire stops prevent the snatch block from damaging the guidewire winch or top traverse. In figure 2.4 a simplified overview of the lifting arrangement is shown. The properties of the tagline and guide wire are shown in table 2.1.

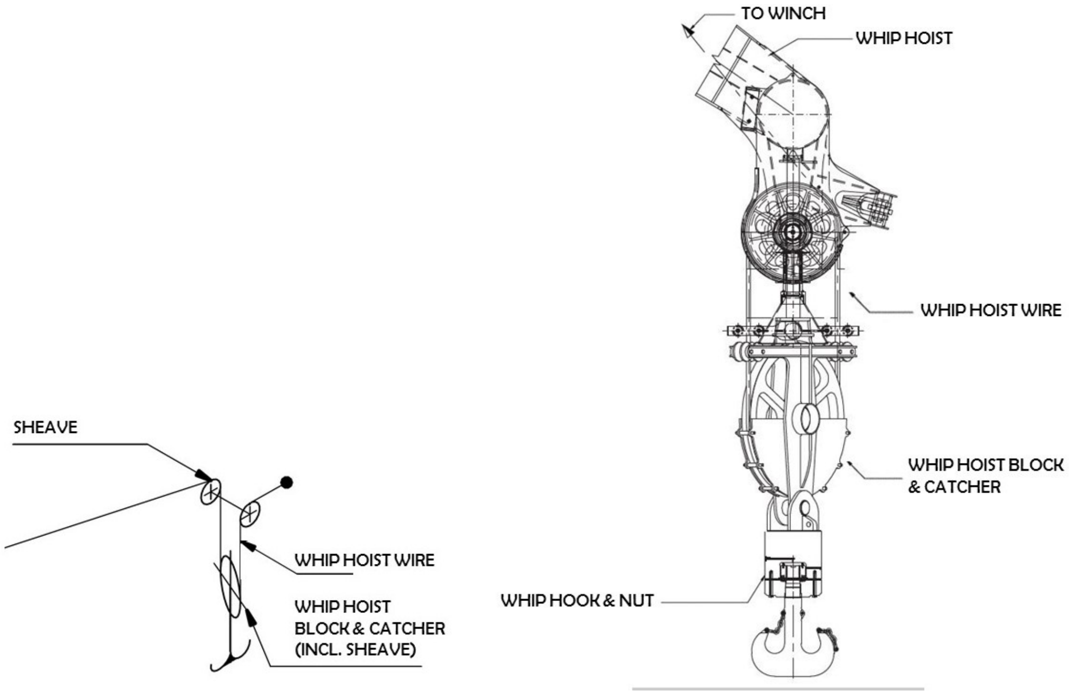

(a) Reeving whip hoist

(b) Whip hoist block and catcher

Figure 2.5: Whip hoist overview

Description	Diameter (m)	Material	MBL (mt)
Guide wire	0.30	Steel	91.8
Tagline	0.16	Dynema	24

Table 2.1: Wire and rope properties

Rigging

Rigging equipment is used to connect the BIT to the whip hoist hook. The rigging consist of four round slings which are connected with sling shackles to the BIT. In figure 2.6 the dimensions of the rigging are shown. Round slings also connect the BIT to the tagline system. To be able to control the movement of the blade the taglines are mounted on the BIT. On both ends of the BIT external tubes allow the taglines to be attached to the BIT. A steel link connects the round sling to the shackle fixed to the BIT (figure 2.7). The working load limit (WLL) of the round sling (tagline) is 3 ton. The round sling is connected to a safety hook. This safety hook is fixed to the pulley where the tagline is pulled through. The pulley is able to move vertically when the blades are lifted. The tagline returns to a zip trolley which rolls over the guide wire.

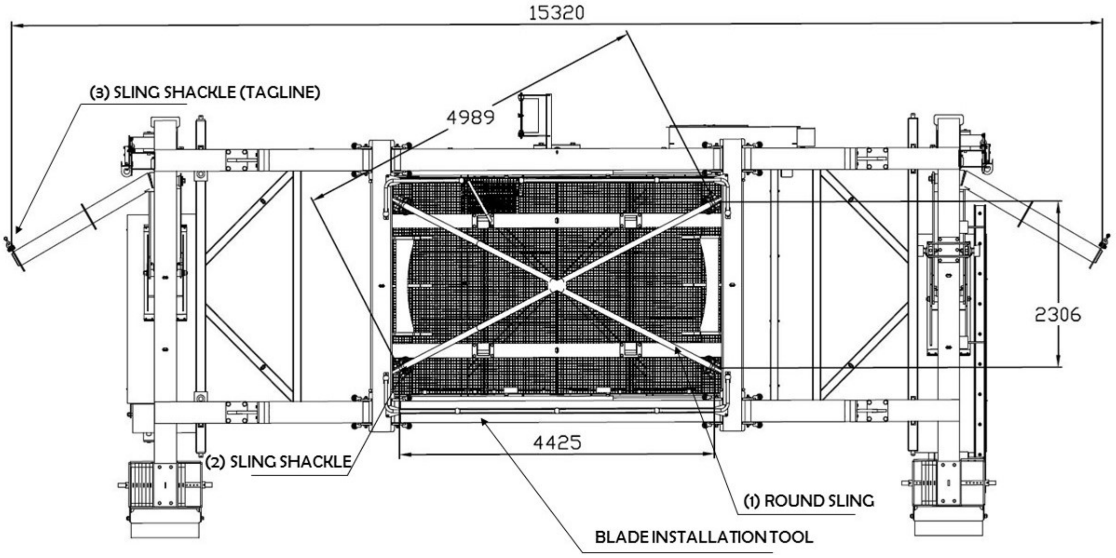

Figure 2.6: Rigging blade installation tool

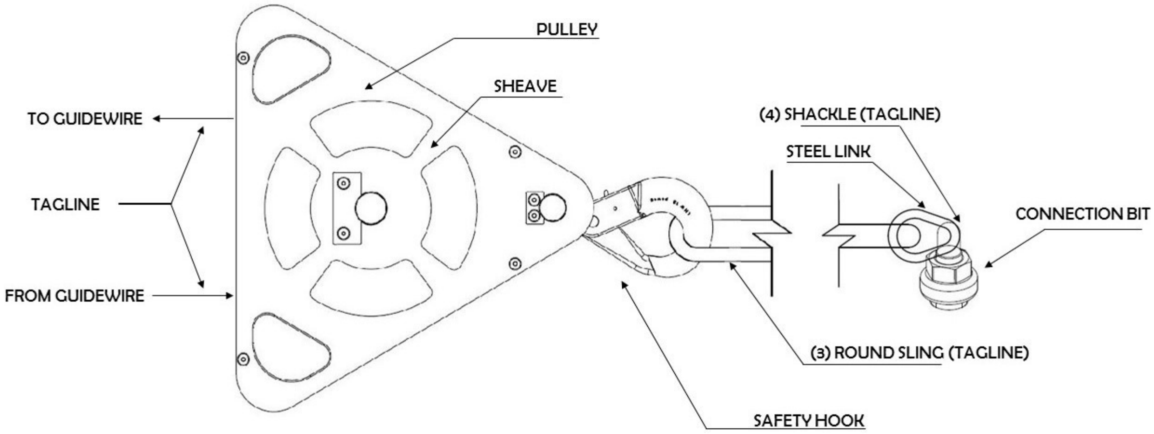

Figure 2.7: Connection BIT-tagline

Information about the rigging equipment is important input for the model. In table 2.2 properties of the rigging is shown.

No.	Description	Length (m)	Dimensions (mm)	Material	Total Weight (kg)	WLL (t)
1	Round sling	4	∅ 98	Dynema core	20	40
2	Sling shackle		253 x 97 x 350	Alloy steel	21	40
3	Round sling (Tagline)	3	∅ 98	Fiber	0.8	3
4	Shackle (Tagline)		114 x 64 x 43	Alloy steel	0.7	3.25

Table 2.2: Rigging equipment

Blade Installation Tool

The blade installation tool is used to lift and protect the blade from damaging. The BIT is blade specific and often purpose (re)build for one particular blade. The tool grabs the blade from the blade rack. High friction rubbers prevent the blade from damaging during installation. The weight of the tool is 32t and the SWL of the tool is 40t. On top of the blade installation tool a movable frame is attached to the slings. This frame can move in one (horizontal) direction. To get the CoG of the blade and BIT in vertical alignment with the hook, the frame is moved to the right position. The force in the slings is distributed equally when the CoG of the blade and BIT is right beneath the hook.

Description	Dimensions (m)	Material	Total Weight (t)	WLL (t)
Blade installation tool	15.5 x 5.0 x 8.7	Steel	32	40

Table 2.3: BIT information

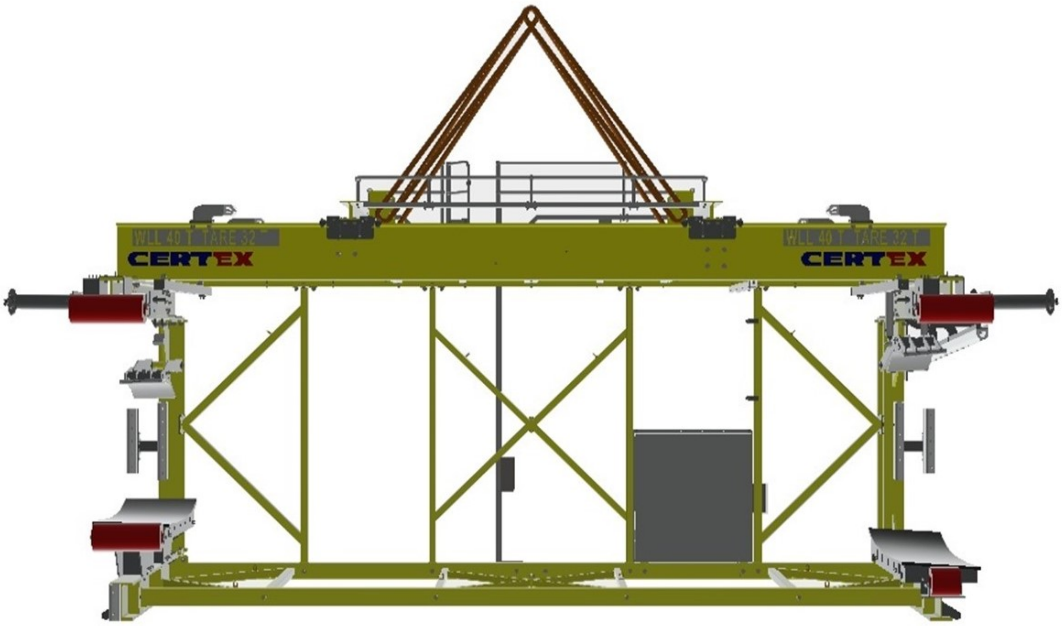

Figure 2.8: Blade Installation Tool

2.3. Reference Site

Situated in the southern central North Sea, the Dogger Bank is one of the locations where 12MW turbine will be installed in the near future. The Dogger Bank is therefore chosen as reference project site. With water depths ranging from 18 to 63 metres the seabed can be considered as shallow [5]. The average water depth of the Dogger Bank is 25 metre [6].

Parameter	Symbol	Value	Unit
Latitude	L_{LAT}	54°50′0”N	°
Longitude	L_{LON}	2°20′0”E	°
Water depth range	h	$18 - 63$	m
Assumed average water depth	h_{ave}	25	m

Table 2.4: Reference location

Environmental Conditions

Environmental conditions are input for the numerical model. Environmental input simulates realistic offshore conditions for the Dogger Bank. Wind is the environmental conditions that is assumed to have

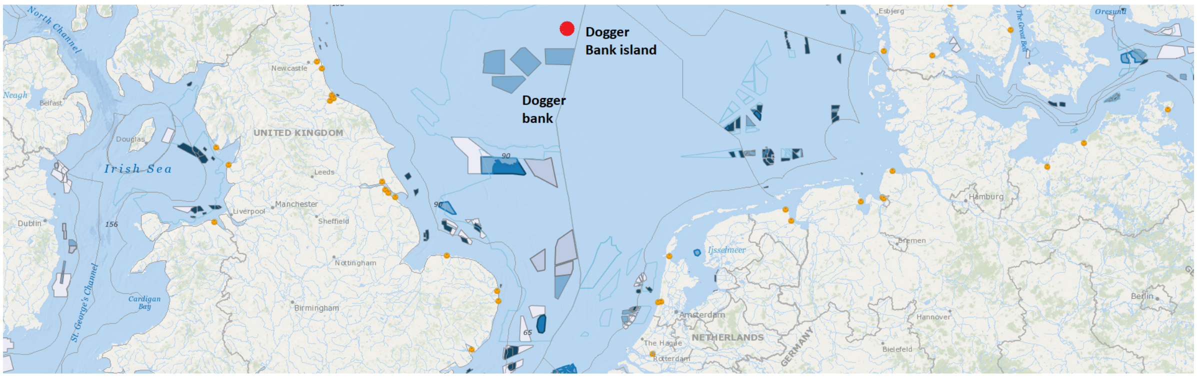

Figure 2.9: Dogger Bank location

the biggest impact on the installation of turbine blades. Current, tides, ice, earthquake, soil conditions and marine fouling are environmental conditions that may be important in certain cases, but are not taken into account in this research. Sufficient wind record data are available at Van Oord from the reference location (see figure 2.10 and 2.11)

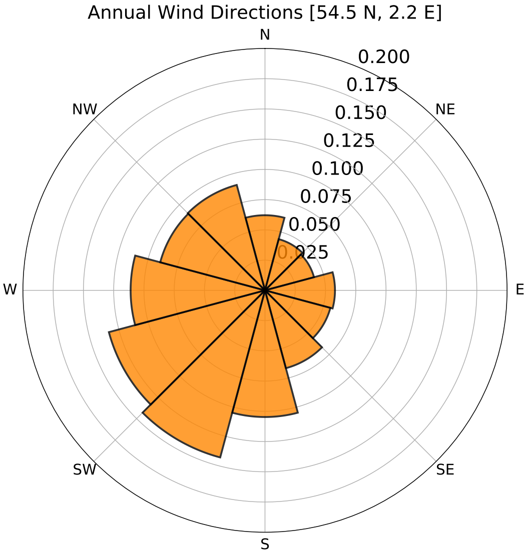

Figure 2.10: Wind Rose

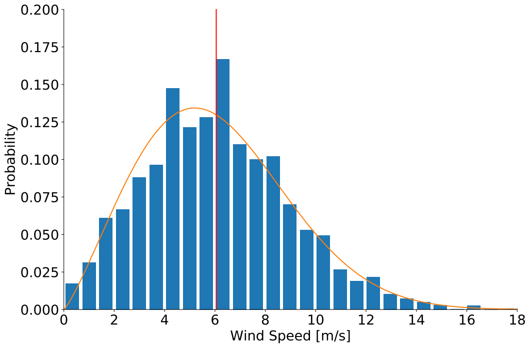

Figure 2.11: Wind Speed (August)

2.4. Limit Operation Criteria

Lift operations are subjected to certain criteria under which an operation is allowed to take place. The limiting operation criteria are given in 2.5. The displacement of the blade relative to the hub and the tagline tension is expected to be limiting the operation.

Parameter	Criteria
Critical outcrossing rate	$5.5 \cdot 10^{-3}$ Hz
Safe boundary	0.2 m
PFL tagline master	30 kN
Maximum side lead	5.1°
Maximum off lead	1.3°

Table 2.5: Limit operation criteria

Alignment criteria

The alignment phase starts when the blade is lifted to hub height. This final installation stage of a single-blade lift operation is assumed to last a maximum of 30 minutes. In the alignment phase the distance between the hub centre and blade root centre should not exceed the safe boundary. Together with a lifting supervisor the safe boundary is determined at 0.2 m. The outcrossing rate is the number of times d_{hb} exceeds the safe boundary. If the outcrossing rate is low enough the alignment process is successful. For a successful alignment process the number of outcrossings per minute should be one or less, which is equivalent to 30 or less outcrossings in 30 minutes [7].

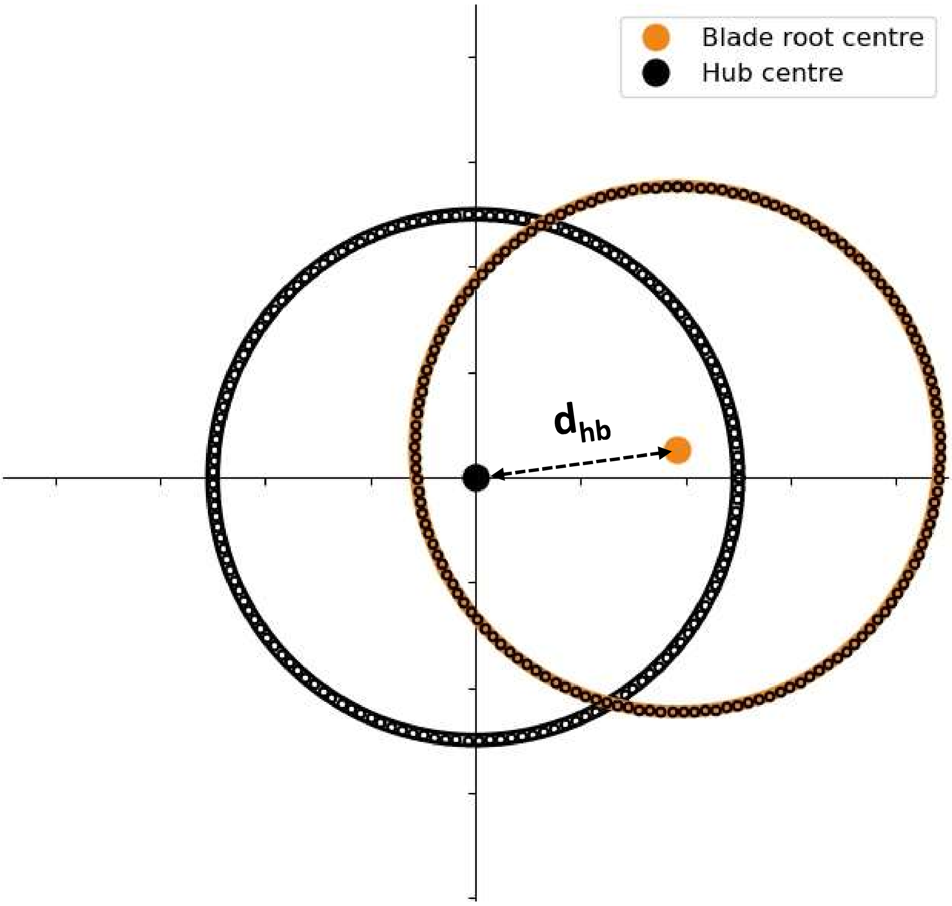

Figure 2.12: Misalignment of axes (hub and blade root)

3

Numerical Model

In this chapter the dynamical model of the blade and crane lifting gear is developed in steps to be able to analyse the dynamics of a blade lift operation. The model consist of two main bodies: the whip hoist and BIT (including the blade). The whip hoist block consist of several bodies which are described in more detail.

The most important assumptions are given before the model is explained. The next section describes the motion of points and bodies without considering any forces: kinematics. Then the loads present in the system are given, followed by the derivation of the equations of motions (EOM). In section 3.5 an overview of the programmed parts and the software used is given. In section 3.6 verification tests are executed to prove the numerical model is build properly. The lift setup, blade properties and tower displacement are explained in the final section.

In short, the following steps are taken to compute the EOM:

1. Determine the kinematics of the system. Identify the coordinate system, generalized coordinates and determine the positions of the CoGs of the bodies expressed in generalized coordinates using transformation matrices.
2. Determine the kinetic energy (T) and potential energy (V) expressed in generalized coordinates (q_i) and their derivatives ($\dot{q}_i$) .
3. Compute the Lagrangian for a system of particles:

$$L(q_i, \dot{q}_i, t) = T - V \tag{3.1}$$

4. Compute Euler-Lagrange's equation to find the EOM:

$$\frac{d}{dt}\left(\frac{\partial L}{\partial \dot{q}_i}\right) - \frac{\partial L}{\partial q_i} + \frac{\partial D}{\partial q_i} = F_{ext}(q_i) \tag{3.2}$$

3.1. Assumptions

The model explained in this chapter is a simplified representation of a realistic lift operation. The most important assumptions and limitations of the model are described in this section.

- The influence of the crane and the vessel are neglected. In the alignment phase of the blade with the hub the tip crane motions are neglected. The vessel's inertial and gravity loads are assumed to be substantially bigger compared to the loads acting on the blade.
- The lift wires are modelled as spherical pendulum based on the assumption that the rotation in the blade is small during the alignment phase. Allowing the lift wires to rotate around the x- and y-axis only. Rotation around the z-axis can occur in the hook bearing. Elasticity of the lift wires is not taken into account.
- Information about the different blades is estimated based on the DTU 10 MW reference wind turbine and internal turbine information available at Van Oord. The blade and BIT together form

one rigid body, where the location of their CoG is on the global z-axis. The cross-flow principle is applied for calculation of the aerodynamic loads on the blade sections. Only the inflow wind velocity perpendicular to the blade section is taken into account.

- An educated guess is made for the damping values based on available sources. Damping values for the taglines, slings and lift wires are based on references [1] and [8]. Conservative values for the bearing damping in the whip hoist bodies are used. Damping due to air friction of the rigid bodies is neglected.
- The taglines and slings are assumed to behave as linear tensile springs with damping. The axial stiffness of these wire ropes are determined using the formulas used in an Orcaflex simulation [9]. The weight of the tagline and slings are disregarded assumed that their influence on the system is negligible. Bending stiffness is also neglected as it is not expected to affect the dynamics of the system.
- Tower dynamics are not modelled, but the motions of the hub are substituted by imposed displacements (see section 3.7).

3.2. Kinematics

The kinematic equations are expressions for position, velocity and acceleration of the bodies in the model. Kinematics means the relations of the bodies of the model, without regarding forces. To describe the position of any point in the inertial frame of reference transformation matrices are used. The CoG of the rigid bodies expressed in inertial coordinates are calculated as followed:

$$\mathbf{p_i} = \mathbf{p_{Origin_i}} + \mathbf{T_i} \begin{bmatrix} p_{Local_{xi}} \\ p_{Local_{yi}} \\ p_{Local_{zi}} \end{bmatrix} \tag{3.3}$$

where $\mathbf{p_{Origin_i}}$ is the position vector of the origin of a local coordinate system i. The transformation matrix $\mathbf{T_i}$ is used to transform the coordinates of any point in the local coordinate system i to their corresponding coordinates in the inertial coordinate frame. The vectors described in this section are time dependent. The vectors with the subscript $t = 0$ are the initial position vectors in their local coordinate system and are not time dependent.

3.2.1. Whip Hoist Hook System

In this part the coordinate system and generalized coordinates of the position of the whip hoist hook bodies are given. The whip hoist hook system consist of three rigid bodies: the whip hoist sheave, the whip hoist hook bearing and the whip hoist hook. The whip hoist sheave is connected to the whip hoist lift wire. The lift wire is modelled as a spherical pendulum.

Lift Wire

The points $\mathbf{p_1}$ and $\mathbf{p_2}$ are fixed points in the inertial frame of reference. They represent the points where the lift wire is leaving the tip of the crane:

$$\mathbf{p_1} = \begin{bmatrix} p_{1x} \\ p_{1y} \\ p_{1z} \end{bmatrix} \tag{3.4}$$

$$\mathbf{p_2} = \begin{bmatrix} p_{2x} \\ p_{2y} \\ p_{2z} \end{bmatrix} \tag{3.5}$$

The CoG of the lift wires is given by $\mathbf{p_{CoGAW}}$ and $\mathbf{p_{CoGWW}}$, where AW (attached wire) is the part of the lift wire which is attached to the whip hoist boom and WW (winch wire) is the part of the lift wire which is connected to the winch. The lift wires are modelled as a double pendulum system which rotates around the x- and y-axis in the inertial frame. The rotation around the x- and y-axis for the lift wires introduces two generalized coordinates: $\alpha(t)$ and $\beta(t)$.

$$\mathbf{T_{Wx}} = \begin{bmatrix} 1 & 0 & 0 \\ 0 & c\alpha & s\alpha \\ 0 & -s\alpha & c\alpha \end{bmatrix} \quad (3.6) \qquad \mathbf{T_{Wy}} = \begin{bmatrix} c\beta & 0 & -s\beta \\ 0 & 1 & 0 \\ s\beta & 0 & c\beta \end{bmatrix} \quad (3.7) \qquad \mathbf{T_{Wz}} = \begin{bmatrix} 1 & 0 & 0 \\ 0 & 1 & 0 \\ 0 & 0 & 1 \end{bmatrix} \quad (3.8)$$

$$\mathbf{T_W} = \mathbf{T_{Wx}} \mathbf{T_{Wy}} \mathbf{T_{Wz}} = \begin{bmatrix} c\beta & 0 & -s\beta \\ s\alpha \cdot s\beta & c\alpha & s\alpha \cdot c\beta \\ c\alpha \cdot s\beta & -s\alpha & c\alpha \cdot c\beta \end{bmatrix} \quad (3.9)$$

Two sheaves at points $\mathbf{p_3}$ and $\mathbf{p_4}$ assure that the lift wire rope runs through the whip hoist sheave as smooth as possible. The coordinates in the inertial frame of reference of the points $\mathbf{p_3}$, $\mathbf{p_4}$, $\mathbf{p_{CoGAW}}$ and $\mathbf{p_{CoGWW}}$ are described in equation 3.10, 3.11, 3.12 and 3.13.

$$\mathbf{p_3} = \mathbf{p_1} + \mathbf{T_W} \mathbf{p_3}_{\mathbf{t=0}} \quad (3.10) \qquad \mathbf{p_4} = \mathbf{p_2} + \mathbf{T_W} \mathbf{p_4}_{\mathbf{t=0}} \quad (3.11)$$

$$\mathbf{p_{CoGWW}} = \mathbf{p_1} + \mathbf{T_W} \mathbf{p_{CoGWW}}_{\mathbf{t=0}} \quad (3.12) \qquad \mathbf{p_{CoGAW}} = \mathbf{p_2} + \mathbf{T_W} \mathbf{p_{CoGAW}}_{\mathbf{t=0}} \quad (3.13)$$

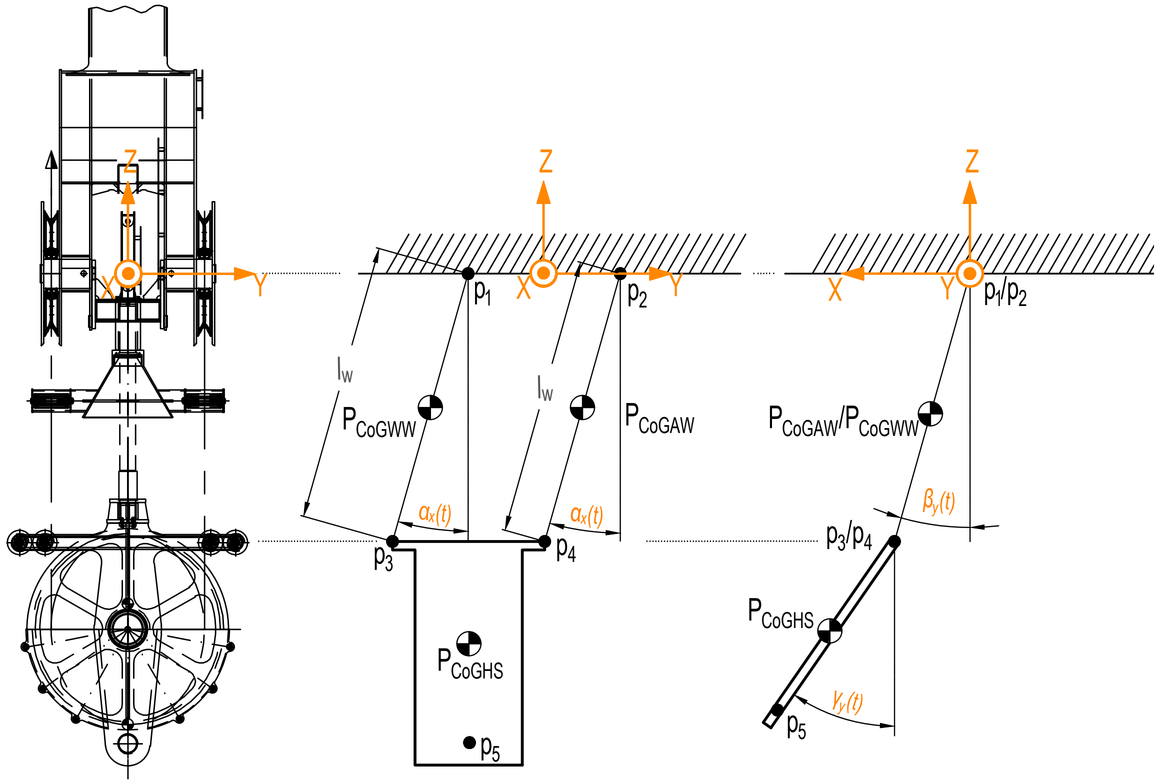

Figure 3.1: Coordinate system: lift wires and whip hoist sheave

Whip Hoist Sheave

The whip hoist sheave connects the hook to the lift wire. Rotation of the whip hoist sheave takes place in the x-z plane, which introduces a third generalized coordinate: $\gamma(t)$. The position of the CoG of the whip hoist is determined using the rotation matrix $\mathbf{T_{HS}}$:

$$\mathbf{T_{HSx}} = \begin{bmatrix} 1 & 0 & 0 \\ 0 & 1 & 0 \\ 0 & 0 & 1 \end{bmatrix} \quad (3.14) \qquad \mathbf{T_{HSy}} = \begin{bmatrix} c\gamma & 0 & -s\gamma \\ 0 & 1 & 0 \\ s\gamma & 0 & c\gamma \end{bmatrix} \quad (3.15) \qquad \mathbf{T_{HSz}} = \begin{bmatrix} 1 & 0 & 0 \\ 0 & 1 & 0 \\ 0 & 0 & 1 \end{bmatrix} \quad (3.16)$$

$$\mathbf{T_{HS}} = \mathbf{T_{HSx}}\mathbf{T_{HSy}}\mathbf{T_{HSz}} = \begin{bmatrix} c\gamma & 0 & -s\gamma \\ 0 & 1 & 0 \\ s\gamma & 0 & c\gamma \end{bmatrix} \tag{3.17}$$

With this transformation matrix the position of the whip hoist sheave CoG is determined:

$$\mathbf{p_{CoGHS}} = \frac{1}{2}\left(\mathbf{p_3} + \mathbf{p_4}\right) + \mathbf{T_{HS}}\left(\mathbf{p_{CoGHS_{t=0}}} - \frac{1}{2}\left(\mathbf{p_{3_{t=0}}} + \mathbf{p_{4_{t=0}}}\right)\right). \tag{3.18}$$

The whip hoist sheave is connected to the whip hoist bearing at $\mathbf{p_5}$:

$$\mathbf{p_5} = \frac{1}{2}\left(\mathbf{p_3} + \mathbf{p_4}\right) + \mathbf{T_{HS}}\left(\mathbf{p_{5_{t=0}}} - \frac{1}{2}\left(\mathbf{p_{3_{t=0}}} + \mathbf{p_{4_{t=0}}}\right)\right) \tag{3.19}$$

Whip Hoist Hook Bearing

The hook is able to rotate in the whip hoist hook bearing. The bearing is connected with the whip hook sheave through another bearing at $\mathbf{p_5}$. The rotation of the hook bearing around the whip hoist sheave is in the y-z plane:

$$\mathbf{T_{HBx}} = \begin{bmatrix} 1 & 0 & 0 \\ 0 & c\delta & s\delta \\ 0 & -s\delta & c\delta \end{bmatrix} \quad (3.20) \qquad \mathbf{T_{HBy}} = \begin{bmatrix} 1 & 0 & 0 \\ 0 & 1 & 0 \\ 0 & 0 & 1 \end{bmatrix} \quad (3.21) \qquad \mathbf{T_{HBz}} = \begin{bmatrix} 1 & 0 & 0 \\ 0 & 1 & 0 \\ 0 & 0 & 1 \end{bmatrix} \quad (3.22)$$

$$\mathbf{T_{HB}} = \mathbf{T_{HBx}}\mathbf{T_{HBy}}\mathbf{T_{HBz}} = \begin{bmatrix} 1 & 0 & 0 \\ 0 & c\delta & s\delta \\ 0 & -s\delta & c\delta \end{bmatrix} \tag{3.23}$$

which gives the following equation for the position of the hook bearing and $\mathbf{p_6}$

$$\mathbf{p_{CoGHB}} = \mathbf{p_5} + \mathbf{T_{HB}}\mathbf{T_{HS}}\left(\mathbf{p_{5_{t=0}}} - \mathbf{p_{CoGHB_{t=0}}}\right) \quad (3.24) \qquad \mathbf{p_6} = \mathbf{p_5} + \mathbf{T_{HB}}\mathbf{T_{HS}}\left(\mathbf{p_{5_{t=0}}} - \mathbf{p_{6_{t=0}}}\right) \quad (3.25)$$

Whip Hoist Hook

The whip hoist hook rotates around the local z-axis and the transformation matrix is given in 3.29.

$$\mathbf{T_{Hx}} = \begin{bmatrix} 1 & 0 & 0 \\ 0 & 1 & 0 \\ 0 & 0 & 1 \end{bmatrix} \quad (3.26) \qquad \mathbf{T_{Hy}} = \begin{bmatrix} 1 & 0 & 0 \\ 0 & 1 & 0 \\ 0 & 0 & 1 \end{bmatrix} \quad (3.27) \qquad \mathbf{T_{Hz}} = \begin{bmatrix} c\epsilon & s\epsilon & 0 \\ -s\epsilon & c\epsilon & 0 \\ 0 & 0 & 1 \end{bmatrix} \quad (3.28)$$

$$\mathbf{T_{H}} = \mathbf{T_{Hx}}\mathbf{T_{Hy}}\mathbf{T_{Hz}} = \begin{bmatrix} c\epsilon & s\epsilon & 0 \\ -s\epsilon & c\epsilon & 0 \\ 0 & 0 & 1 \end{bmatrix} \tag{3.29}$$

The position vector for the CoG of the hook becomes

$$\mathbf{p_{CoGH}} = \mathbf{p_6} + \mathbf{T_H}\mathbf{T_{HB}}\mathbf{T_{HS}}\left(\mathbf{p_{6_{t=0}}} - \mathbf{p_{CoGH_{t=0}}}\right). \tag{3.30}$$

3.2.2. Blade Installation Tool & Blade

The blade installation tool is connected to the whip hoist hook with four slings. The slings attachment points at the whip hoist hook are $\mathbf{p_{SH1}}$ and $\mathbf{p_{SH2}}$:

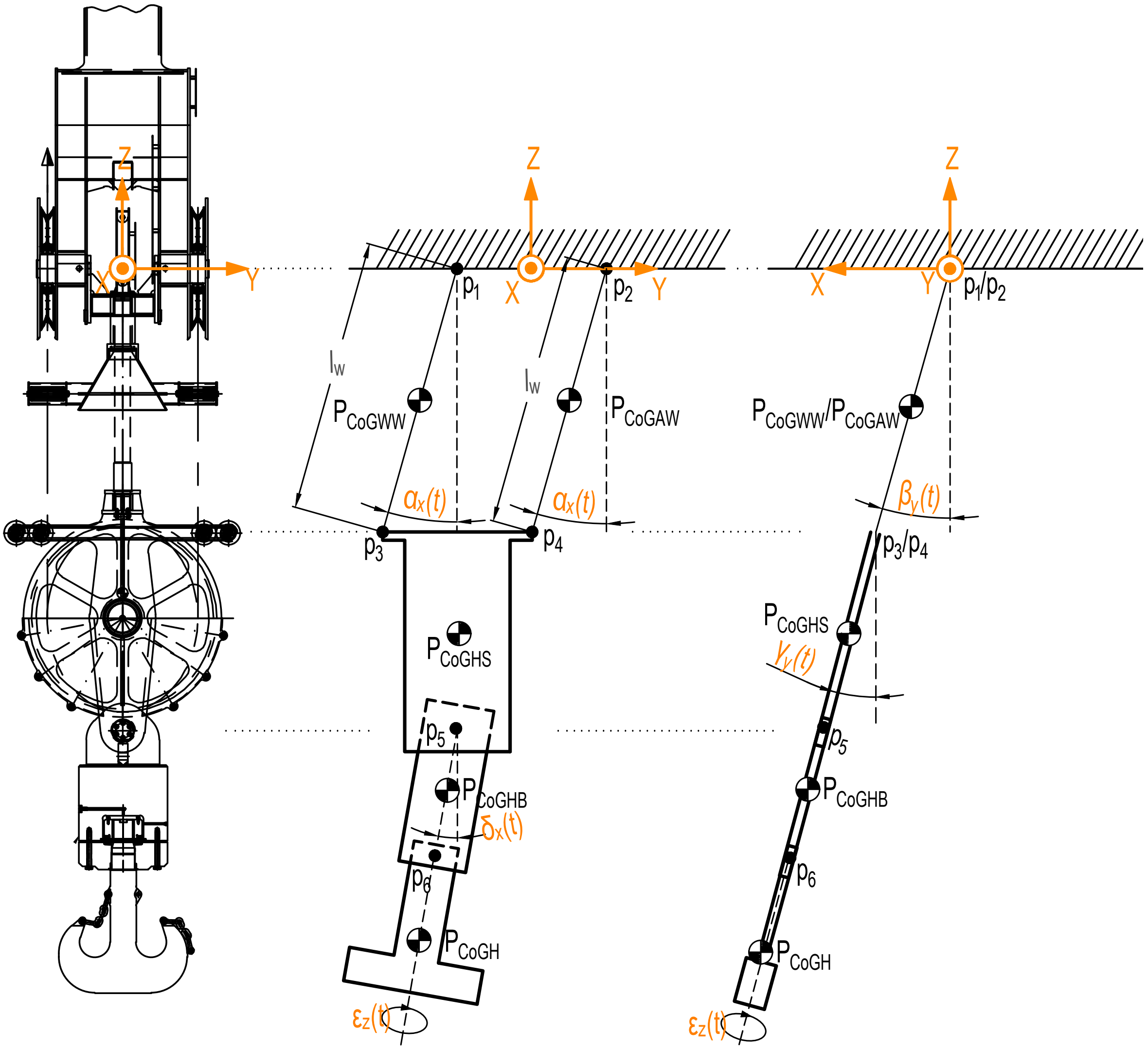

Figure 3.2: Coordinate system: whip hoist system

$$\mathbf{p_{SH1}} = \mathbf{p_6} + \mathbf{T_H T_{HB} T_{HS}} \cdot \mathbf{p_{SH1}} \quad (3.31) \qquad \mathbf{p_{SH2}} = \mathbf{p_6} + \mathbf{T_H T_{HB} T_{HS}} \cdot \mathbf{p_{SH2}} \quad (3.32)$$

The slings attachment points to the blade installation tool are $\mathbf{p_{SB1}}$, $\mathbf{p_{SB2}}$, $\mathbf{p_{SB3}}$ and $\mathbf{p_{SB4}}$:

$$\mathbf{p_{SBi}} = \mathbf{p_{CoGBIT}} + \mathbf{T_{BIT}} \cdot \mathbf{p_{SBi}} \tag{3.33}$$

The position and orientation of the blade installation tool in the inertial frame is described by three translational coordinates (x_{CoGBIT}, y_{CoGBIT} and z_{CoGBIT}) and three rotational coordinates (ζ, η and θ):

$$\mathbf{p_{CoGBIT}} = \begin{bmatrix} x_{CoGBIT}(t) \\ y_{CoGBIT}(t) \\ z_{CoGBIT}(t) \end{bmatrix} \tag{3.34}$$

and the orientation is determined by the rotation matrix for the BIT:

$$\mathbf{T_{BITx}} = \begin{bmatrix} 1 & 0 & 0 \\ 0 & c\delta & s\delta \\ 0 & -s\delta & c\delta \end{bmatrix} \quad (3.35) \qquad \mathbf{T_{BITy}} = \begin{bmatrix} c\epsilon & 0 & -s\epsilon \\ 0 & 1 & 0 \\ s\epsilon & 0 & c\epsilon \end{bmatrix} \quad (3.36) \qquad \mathbf{T_{BITz}} = \begin{bmatrix} c\zeta & s\zeta & 0 \\ -s\zeta & c\zeta & 0 \\ 0 & 0 & 1 \end{bmatrix} \quad (3.37)$$

$$\mathbf{T_{BIT}} = \mathbf{T_{BITx}}\mathbf{T_{BITy}}\mathbf{T_{BITz}} = \begin{bmatrix} c\epsilon \cdot c\zeta & c\epsilon \cdot s\zeta & -s\epsilon \\ c\zeta \cdot s\delta \cdot s\epsilon - c\delta \cdot s\zeta & c\delta \cdot c\zeta + s\delta \cdot s\epsilon \cdot s\zeta & c\epsilon \cdot s\delta \\ s\delta \cdot s\zeta + c\delta \cdot c\zeta \cdot s\epsilon & c\delta \cdot s\epsilon \cdot s\zeta - c\zeta \cdot s\delta & c\delta \cdot c\epsilon \end{bmatrix} \tag{3.38}$$

$$\mathbf{p_{CoGBIT}} = \mathbf{p_{CoGH}} + \mathbf{T_{BIT}} \cdot \begin{bmatrix} x_{CoGBIT}(t) \\ y_{CoGBIT}(t) \\ z_{CoGBIT}(t) \end{bmatrix} \tag{3.39}$$

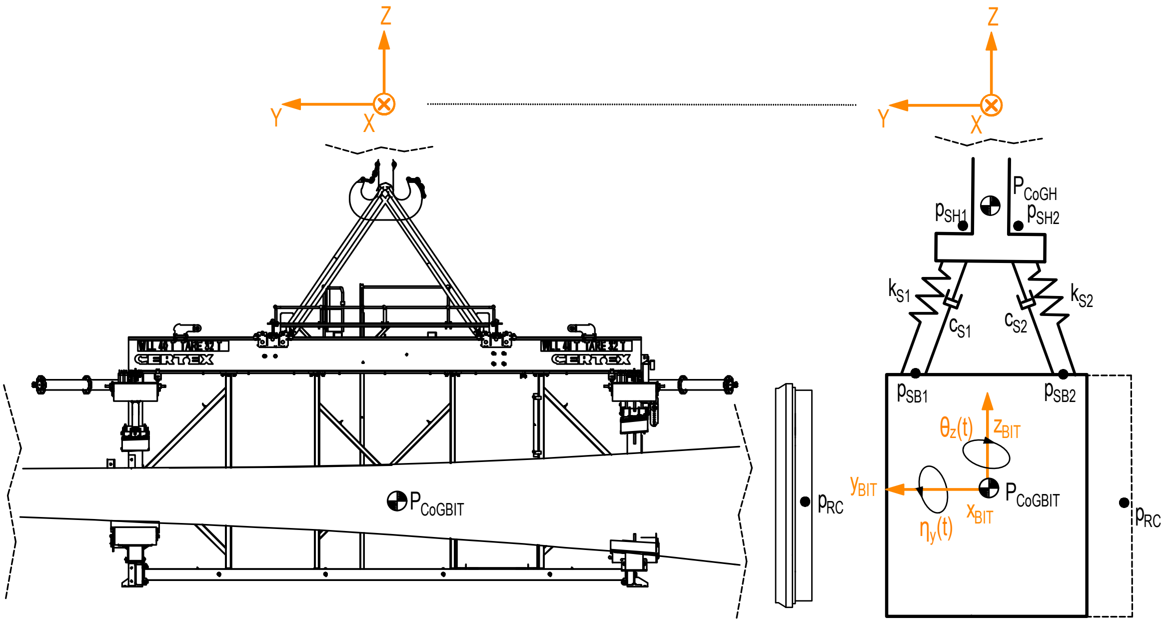

Figure 3.3: Coordinate system: blade installation tool and blade (back view)

The position of any location on the BIT or blade is determined in the same way the slings attachment location are determined. The centre of the root of the blade:

$$\mathbf{p_{RC}} = \mathbf{p_{CoGBIT}} + \mathbf{T_{BIT}} \cdot \mathbf{p_{root_{t=0}}} \tag{3.40}$$

The location $\mathbf{p_{RC}}$ is an important output variable of the simulation. Four other locations at the root of the blade ($\mathbf{p_{RC1}}, \mathbf{p_{RC2}}, \mathbf{p_{RC3}}, \mathbf{p_{RC4}}$) are also monitored to determine if the blade root end is rotating (see figure 3.5). For location j at the blade flange the position is determined with

$$\mathbf{p_{RC_j}} = \mathbf{p_{CoGBIT}} + \mathbf{T_{BIT}} \cdot \mathbf{p_{RC_{j,t=0}}} \tag{3.41}$$

The tagline connection locations at the BIT are:

$$\mathbf{p_{TB1}} = \mathbf{p_{CoGBIT}} + \mathbf{T_{CoGBIT}} \cdot \mathbf{p_{TB1_{t=0}}} \quad (3.42) \qquad \mathbf{p_{TB2}} = \mathbf{p_{CoGBIT}} + \mathbf{T_{CoGBIT}} \cdot \mathbf{p_{TB2_{t=0}}} \quad (3.43)$$

In the numerical model the tagline is fixed to the crane. These locations are important for load calculations. The locations at the crane are given as

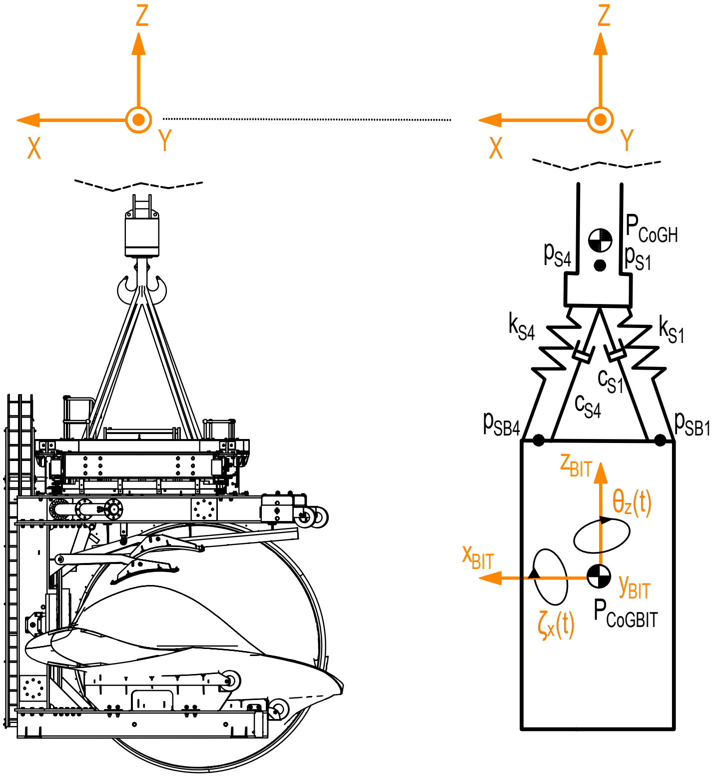

Figure 3.4: Coordinate system: blade installation tool and blade (side view)

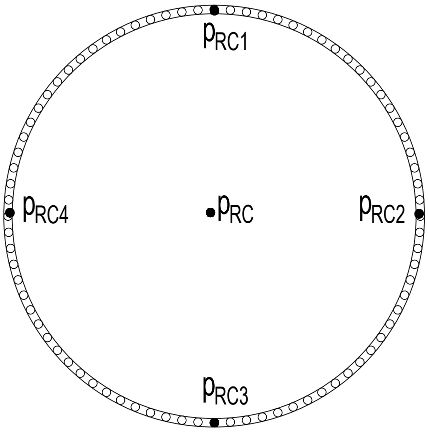

Figure 3.5: Blade root end

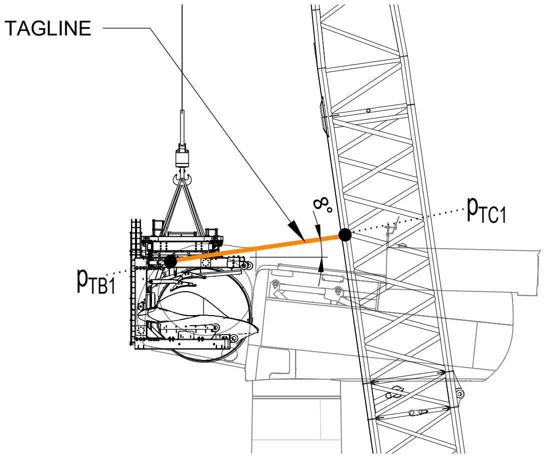

Figure 3.6: Tagline coordinates

$$\mathbf{p_{TC1}} = \begin{bmatrix} p_{TC1x} \\ p_{TC1y} \\ p_{TC1z} \end{bmatrix} \tag{3.44}$$

$$\mathbf{p_{TC2}} = \begin{bmatrix} p_{TC2x} \\ p_{TC2y} \\ p_{TC2z} \end{bmatrix} \tag{3.45}$$

.

3.3. Loads

In this section the different loads in system are described. First, the tagline and sling loads calculations are given. The loads due to bearing damping in the whip hoist hook are described in the next section. The wind-induced blade loads are described in the last section.

3.3.1. Slings And Taglines

The slings are modelled as tensile springs with damping. Elastic potential energy is stored in a spring when it is in compression or stretched. Slings only store energy when they are in tension. A sling does not store energy when it is in compression. As an example the tension in one sling is calculated. The same working principle holds for the other slings. The elastic potential energy stored in a spring is:

$$E_{s1} = \frac{1}{2} \cdot k_{axial_1} \cdot (\Delta l_{s1})^2 \cdot \tau(\Delta l_{s1}) \tag{3.46}$$

where Δl_{s1} is the elongation in sling 1:

$$\Delta l_{s1} = l_{0s1} - l_{s1} \tag{3.47}$$

$l_{0_{s1}}$ is the initial unstretched length of sling 1 and l_{s1} the length of the sling at a certain moment in time:

$$l_{s1} = \left|\left|\mathbf{p_{SH1}} - \mathbf{p_{SB1}}\right|\right| = \sqrt{(x_{p_{SH1}} - x_{p_{SB1}})^2 + (y_{p_{SH1}} - y_{p_{SB1}})^2 + (z_{p_{SH1}} - z_{p_{SB1}})^2} \tag{3.48}$$

To determine the axial stiffness ($k_{axial_{s1}}$) of a sling, Orcaflex [9] provides the following expression for the axial stiffness of fibre ropes:

$$k_{axial_{s1}} = 1.06 \cdot 10^6 \cdot d^2 \tag{3.49}$$

where d represents the diameter of sling 1. Slings are not capable to store energy when they are in compression. Therefore $\tau(\Delta l_{s1})$ is added to the elastic potential energy formula:

$$\tau(\Delta l_{s1}) = \begin{cases} 1, & \text{if} \Delta l_{s1} \geq 0 \\ 0, & \text{otherwise} \end{cases} \tag{3.50}$$

The Rayleigh Dissipation function for damping in sling 1 is calculated as

$$D_{s1} = \frac{1}{2} \cdot c_{s1} \cdot (\Delta \dot{l}_{s1})^2 \cdot \tau(\Delta l_{s1}) \tag{3.51}$$

where c_{s1} represents the damping coefficients for the taglines and slings. The elongation velocity of the sling is $\Delta \dot{l}_{s1}$. The load for each sling and tagline is derived in the same way as for sling 1. Damping and stiffness values are given in table 3.1.

3.3.2. Bearing Damping

The mechanical coupling between the hook bodies is possible due to roller bearings. The most common sources for damping in roller bearings are [10]:

- Material damping due to Hertzian deformation of the rolling elements and raceways.
- Damping due to squeezing lubricant within the so-called entry region where the oil is entrained into the Hertzian zone.
- Bearing interface damping between the bearing rings and housings or shaft respectively.
- Damping of the elasto-hydrodynamic lubrication film within the Hertzian zone between the rolling elements and raceways.

The tangential velocity in a roller bearing is used to calculate the damping loads. The bearing damping for the connection between the hook sheave and hook bearing is

$$D_{HB} = \frac{1}{2} \cdot c_{HB} \cdot (d_{b_{HB}} \dot{\delta})^2 \tag{3.52}$$

where $d_{b_{HB}}$ is the distance from the CoG of the hook bearing body to the bearing. The damping for the connection between the hook bearing and hook is calculated in the same way:

$$D_H = \frac{1}{2} \cdot c_H \cdot (d_{b_H} \dot{\epsilon})^2. \tag{3.53}$$

	Slings	Taglines	Hook Bearing	Hook
Stiffness [N/m]	$3 \cdot 10^7$	$1 \cdot 10^5$	[-]	[-]
Damping [Nm/s]	$1 \cdot 10^8$	$1 \cdot 10^4$	500	500

Table 3.1: Damping and stiffness parameters

3.3.3. Aerodynamic Loading

This section describes the aerodynamic modelling of the turbine blade. Wind acts as an environmental load on the blade and is expected to be the main cause for the dynamic behaviour of the blade. The section explains how blade forces and moments are calculated.

Aerodynamic model

The blade presented in this model is the DTU 10MW reference wind turbine which serves as a publicly available reference turbine for scientific purposes. The turbine blade is divided in a number of sections (see figure 3.7). Each section represents a small aerofoil with a specific chord length, geometric centre, twist angle and thickness/chord ratio (T/C). In appendix D the parameters for each section are given. The body fixed coordinate system for the blade is used to be able to calculate blade forces.

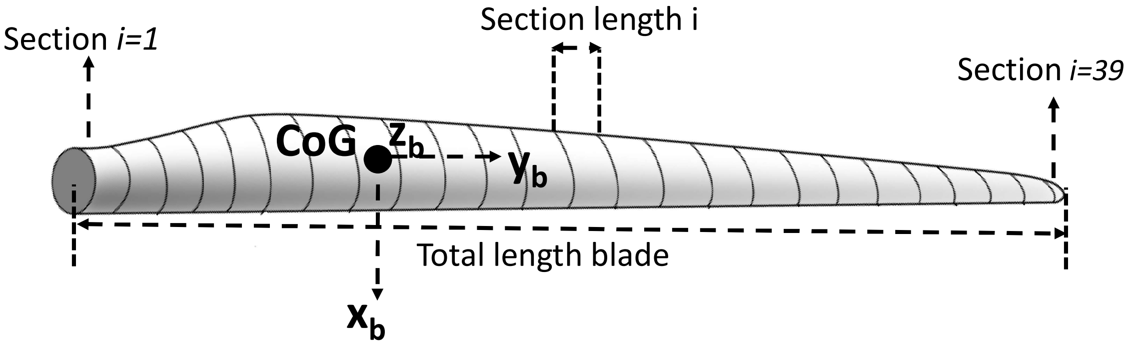

Figure 3.7: Blade segments

In figure 3.8 the orientation of the lift (L) and drag (D) forces are given. Drag forces act parallel to the wind direction. The forces perpendicular to the wind direction are lift forces. The wind vector is also given in the z-x plane. The wind vector has a x-direction component u and a z-direction component w. The y-direction component of the wind is v and is important when the wind direction is not perpendicular to the blade. If the wind direction is perpendicular to the blade the inflow velocity of wind in spanwise direction (y_b axis) of the blade is neglected according to the cross-flow principle. Besides the lift and drag forces, aerodynamic loading also creates a yaw moment (M) in each section of the blade.

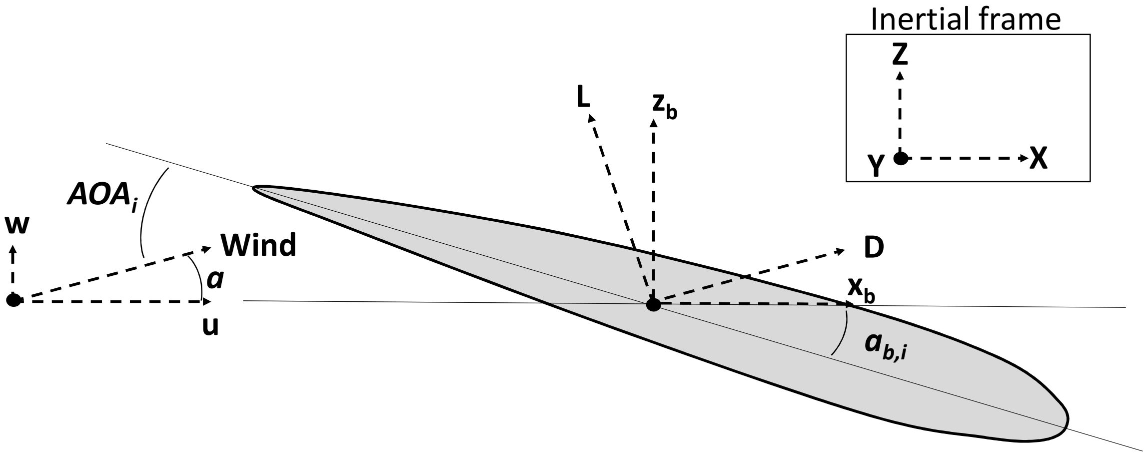

Figure 3.8: Body-fixed and aerodynamic coordinate system

Lift, drag and moment coefficients for each element are a function of the angle of attack (AOA) and thickness/chord ratio (t/c) in dynamic analysis. The DTU 10 MW reference wind turbine provides aerodynamic coefficients based on t/c and AOA. For each blade section i the drag force (D_i) , lift force (L_i) and pitching moment (M_i) are calculated based upon the cross-flow principle. Forces and moment for each element are given by:

$$L_i = 1/2\rho_a C_{L,i}(AOA_i, t_i/c_i)A_i V_i^2 \tag{3.54}$$

$$D_i = 1/2\rho_a C_{D,i}(AOA_i, t_i/c_i)A_i V_i^2 \tag{3.55}$$

$$M_i = 1/2\rho_a C_{M,i}(AOA_i, t_i/c_i)A_i V_i^2 \tag{3.56}$$

where

i = subscript representing blade section i
ρ_a = air density
$C_{L,i}$ = lift coefficient as a function of AOA and t_i/c_i
$C_{D,i}$ = drag coefficient as a function of AOA and t_i/c_i
$C_{D,i}$ = moment coefficient as a function of AOA and t_i/c_i
AOA = angle of attack
A_i = wing area blade
V_i = wind speed

For each blade section the t/c ratio is unique. The aerodynamic coefficients are available for six different values of t/c. Linear interpolation is used to find the aerodynamic coefficients for each section. The parameter A_i describes the wing area of section i [11]. The wing area of section i is approximated by

$$A_i = \frac{c_{i,begin}d_{i,begin}+c_{i,end}d_{i,end}}{2} \tag{3.57}$$

where $c_{i,begin}$ is the chord length at begin of section i and $d_{i,begin}$ the relative thickness at the begin of blade section i.

The angle of attack for an blade section i depends on the twist angle of blade section i ($\alpha_{b,i}$), the rotation of the blade around the y_b axis (η) and the incoming wind speed angle for section i (α). Adding these three angles, results in the AOA for a certain moment in time and for a specific aerofoil section:

$$AOA_i = \eta + a_{b,i} + a \tag{3.58}$$

$$a = \arctan(w_i, v_i sin(\theta_{wind}) + u_i cos(\theta_{wind})) \tag{3.59}$$

According the cross-flow flow principle span wise wind speed can be neglected. The wind velocity vector for each blade section is defined as

$$\mathbf{V_i} = \begin{bmatrix} u_i & v_i & w_i \end{bmatrix}^T \tag{3.60}$$

The wind speed V_i is quadratic related to the aerodynamic coefficients. The wind velocity vector is calculated for each blade section. Only perpendicular wind speed are taken into account. A transformation matrix is used to describe the perpendicular wind velocity in each section

$$\mathbf{T_{V_i}} = \begin{bmatrix} 1 & 0 & 0 \\ 0 & c\alpha & s\alpha \\ 0 & -s\alpha & c\alpha \end{bmatrix} \tag{3.61}$$

where the wind speed is calculated with

$$V_i = \sqrt{w_i^2 + (v_i sin(\theta_{wind}) + u_i cos(\theta_{wind}))^2} \tag{3.62}$$

For each element the wind loads are calculated and determine the total force on the blade centre of gravity. For every blade element i the contribution to the total drag force, lift force and pitch moment becomes

$$F_{tot} = \begin{bmatrix} F_{xb} \\ F_{yb} \\ F_{zb} \end{bmatrix} = \sum_{i=o}^{n} \begin{bmatrix} -D_{i,x} + L_{i,x} \\ 0 \\ D_{i,z} + L_{i,z} \end{bmatrix} \tag{3.63}$$

$$M_{tot} = \begin{bmatrix} M_{xb} \\ M_{yb} \\ M_{zb} \end{bmatrix} = \sum_{i=o}^{n} \begin{bmatrix} 0 \\ M_i \\ 0 \end{bmatrix} + \sum_{i=o}^{n} \begin{bmatrix} F_{zb,i} y_{center,i} \\ 0 \\ F_{xb,i} y_{center,i} \end{bmatrix} \tag{3.64}$$

Wind Speed Profile

Wind speed variation should be taken into account when simulating realistic offshore conditions [12]. These fluctuations over time, around a short-term mean wind speed, are called turbulence. The range of these fluctuations determine the turbulence intensity (TI). The degree of TI influences the dynamic behaviour of the blade during installation. The turbulence intensity is defined as:

$$I_u = \frac{\sigma_u}{\bar{U}} \tag{3.65}$$

where $\bar{U}$ is the mean wind speed and σ_u the standard deviation of the wind. The mean wind speed and standard deviation are assumed to remain constant within a 30-minute period. The normal turbulence model (NTM) is used to describe the turbulence intensity. The standard IEC 61400-1 [13] provides three turbulence categories based on I_{15}, which is the expected TI at a mean wind speed $\bar{U}$ of 15 m/s. The categories A (high TI), B (medium TI) and C (low TI) represent values for I_{15} of 0.16,0.14 and 0.12 respectively. The design values for TI should be conservative and the values are chosen with a 10% probability of exceedance (IEC 61400-1):

$$I_u = \frac{\sigma_u}{\bar{U}} = I_{15}(0.75 + \frac{5.6}{\bar{U}}) \tag{3.66}$$

where $\bar{U}$ is the mean wind speed at hub height and I_{15} defined as above. A higher mean wind speed at hub height corresponds to a lower turbulence intensity. In table 3.2 the TI values are given for the different TI categories and average wind speeds.

I_{15}	6 m/s	9 m/s	12 m/s	15 m/s
0.12	0.20	0.17	0.15	0.14
0.14	0.24	0.19	0.17	0.16
0.16	0.27	0.22	0.20	0.18

Table 3.2: TI for different wind speeds and I_{15}

The required wind speed time series for the numerical simulations are created with the simulation tool PyTurbSim [14]. Simulations of turbulent wind velocity time-series are produced by PyTurbSim and used as input for the numerical simulation. PyTurbSim is a statistical tool that matches the characteristics of a real flow. The most important characteristics are the mean velocity and standard deviation. The tool outputs a 2-D wind field with a predefined number of turbulence boxes. Each turbulence box contains a 3-D vector for which the velocity in u,v and w direction are stored. In figure 3.9 the results of a PyTurbSim simulation are shown for TI = 0.16, a mean wind speed $\bar{U}$ = 15 m/s and a duration of 1000 s for both the blade root and blade tip turbulence box. The wind fields differ for the blade root and tip, which is realistic for offshore wind conditions.

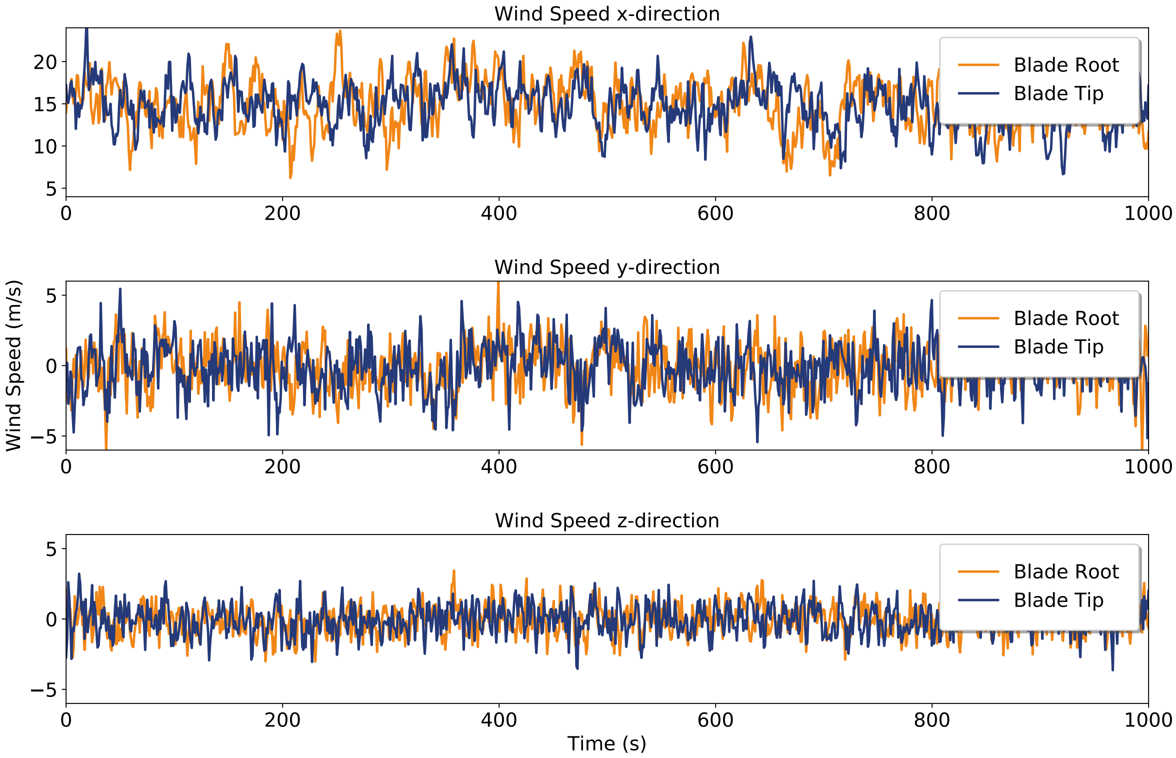

Figure 3.9: Wind speed time series (u,v and w) for TI = 0.16 and $\bar{U}$ = 15 m/s

Not only does the wind field differ for each blade section. For an offshore location the TI can differ as well. In figure 3.10 the wind speed values are given for a low TI and high TI. The wind serie with a higher TI results in larger variations from the mean wind speed. Sudden changes in wind speed result in a change in the loading of a turbine blade. Which changes the dynamic behaviour of the system.

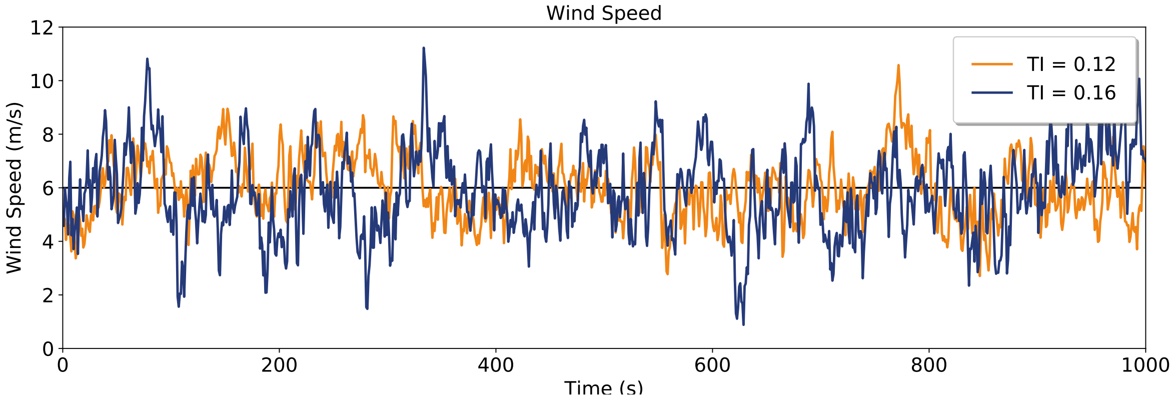

Figure 3.10: Wind speed time series for $TI = 0.16$ and $TI = 0.12$ at $\bar{U} = 6$ m/s

3.4. Bodies Equations of Motions

From the kinematic equations and loads the EOM are derived. This system of equations consists of a set of generalized coordinates, which are described in the kinematic section 3.2.

3.4.1. Generalized Coordinates

An overview of the generalized coordinates for the equipment is given in 3.3. The state of the system is described by the position of all bodies. These positions are described by a set of independent generalized coordinates:

$$\mathbf{q}(\mathbf{t}) = \left[\alpha, \beta, \gamma, \delta, \epsilon, x, y, z, \zeta, \eta, \theta\right]^T \tag{3.67}$$

The number of degrees of freedom should be the same as the number of generalized coordinates used to describe the EOM. Only then the generalized coordinates are independent of each other.

Equipment	Modelled as	DOF	Generalized Coordinates
Vessel	Rigid body (fixed)	0	[-]
Crane	Rigid body (fixed)	0	[-]
Crane hoist wires	Rigid body	2	$\alpha(t)$, $\beta(t)$
Whip Hoist Block	Rigid body	1	$\gamma(t)$
Whip Hoist Bearing	Rigid body	1	$\delta(t)$
Whip Hoist Hook	Rigid body	1	$\epsilon(t)$
Slings	Spring-Damper	0	[-]
Taglines	Spring-Damper	0	[-]
BIT and blade	Rigid Body	6	$x(t)$, $y(t)$, $z(t)$, $\zeta(t)$, $\eta(t)$, $\theta(t)$

Table 3.3: Degrees of freedom

3.4.2. Kinetic Energy

The kinetic energy for each rigid body in the system is calculated in the following equations:

$$T_{AW} = \frac{m_{AW}}{2}\left(\frac{d}{dt}\mathbf{p}_{\mathbf{CoGAW}}\right)^2 + \frac{1}{2}\mathbf{I}_{\mathbf{AW}}\left(\frac{d}{dt}\begin{bmatrix}\alpha\\ \beta\\ 0\end{bmatrix}\right)^2 \tag{3.68}$$

$$T_{WW} = \frac{m_{WW}}{2}\left(\frac{d}{dt}\mathbf{p}_{\mathbf{CoGWW}}\right)^2 + \frac{1}{2}\mathbf{I}_{\mathbf{WW}}\left(\frac{d}{dt}\begin{bmatrix}\alpha\\ \beta\\ 0\end{bmatrix}\right)^2 \tag{3.69}$$

$$T_{HS} = \frac{m_{HS}}{2}\left(\frac{d}{dt}\mathbf{p}_{\mathbf{CoGHS}}\right)^2 + \frac{1}{2}\mathbf{I}_{\mathbf{HS}}\left(\frac{d}{dt}\begin{bmatrix}0\\ \gamma\\ 0\end{bmatrix}\right)^2 \tag{3.70}$$

$$T_{HB} = \frac{m_{HB}}{2}\left(\frac{d}{dt}\mathbf{p}_{\mathbf{CoGHB}}\right)^2 + \frac{1}{2}\mathbf{I}_{\mathbf{HB}}\left(\frac{d}{dt}\begin{bmatrix}\delta\\ 0\\ 0\end{bmatrix}\right)^2 \tag{3.71}$$

$$T_{H} = \frac{m_{H}}{2}\left(\frac{d}{dt}\mathbf{p}_{\mathbf{CoGH}}\right)^2 + \frac{1}{2}\mathbf{I}_{\mathbf{H}}\left(\frac{d}{dt}\begin{bmatrix}0\\ 0\\ \epsilon\end{bmatrix}\right)^2 \tag{3.72}$$

$$T_{BIT} = \frac{m_{BIT}}{2}\left(\frac{d}{dt}\mathbf{p}_{\mathbf{CoGBIT}}\right)^2 + \frac{1}{2}\mathbf{I}_{\mathbf{BIT}}\left(\frac{d}{dt}\begin{bmatrix}\zeta\\ \eta\\ \theta\end{bmatrix}\right)^2 \tag{3.73}$$

The total kinetic energy in the system is:

$$T = T_{AW} + T_{WW} + T_{HS} + T_{HB} + T_{H} + T_{BIT} \tag{3.74}$$

3.4.3. Potential Energy

The potential energy in the system is calculated in the following equations:

$$U_{AW} = m_{AW}\begin{bmatrix}0\\ 0\\ g\end{bmatrix}\mathbf{p}_{\mathbf{CoGAW}} \tag{3.75}$$

$$U_{WW} = m_{WW}\begin{bmatrix}0\\ 0\\ g\end{bmatrix}\mathbf{p}_{\mathbf{CoGWW}} \tag{3.76}$$

$$U_{HS} = m_{HS}\begin{bmatrix}0\\ 0\\ g\end{bmatrix}\mathbf{p}_{\mathbf{CoGHS}} \tag{3.77}$$

$$U_{HB} = m_{HB}\begin{bmatrix}0\\ 0\\ g\end{bmatrix}\mathbf{p}_{\mathbf{CoGHB}} \tag{3.78}$$

$$U_{H} = m_{H}\begin{bmatrix}0\\ 0\\ g\end{bmatrix}\mathbf{p}_{\mathbf{CoGH}} \tag{3.79}$$

$$U_{BIT} = m_{BIT}\begin{bmatrix}0\\ 0\\ g\end{bmatrix}\mathbf{p}_{\mathbf{BIT}} \tag{3.80}$$

$$\tag{3.81}$$

The total potential energy in the dynamic system is:

$$U = U_{AW} + U_{WW} + U_{HS} + U_{HB} + U_{H} + U_{BIT} \tag{3.82}$$

3.4.4. Derivation EOM

The total energy in the system is the total kinetic and rotational energy minus the total potential energy

$$L = T - U \tag{3.83}$$

The equations of motions are determined using the Euler-Langrage equation for each generalized coordinate:

$$\frac{d}{dt}\left(\frac{\partial L}{\partial \dot{q}_i}\right) - \frac{\partial L}{\partial q_i} + \frac{\partial D}{\partial q_i} = F_{ext}(q_i) \tag{3.84}$$

Where the third term represents the damping in the system and the right hand sight of the equation the external forces. In these equations, motions coupling terms are present. The dynamics of a certain body in the system can affect the dynamics of any other body in the system.

3.4.5. Simulation

The state vector is given by $\mathbf{q_i}$ and the elements in this vector are state variables:

$$\mathbf{q_i} = \begin{bmatrix} \alpha_i \\ \beta_i \\ \gamma_i \\ \delta_i \\ \epsilon_i \\ x_i \\ y_i \\ z_i \\ \zeta_i \\ \eta_i \\ \theta_i \\ \dot{\alpha}_i \\ \dot{\beta}_i \\ \dot{\gamma}_i \\ \dot{\delta}_i \\ \dot{\epsilon}_i \\ \dot{x}_i \\ \dot{y}_i \\ \dot{z}_i \\ \dot{\zeta}_i \\ \dot{\eta}_i \\ \dot{\theta}_i \end{bmatrix} = \begin{bmatrix} u_{1i} \\ u_{2i} \\ u_{3i} \\ u_{4i} \\ u_{5i} \\ u_{6i} \\ u_{7i} \\ u_{8i} \\ u_{9i} \\ u_{10i} \\ u_{11i} \\ u_{12i} \\ u_{13i} \\ u_{14i} \\ u_{15i} \\ u_{16i} \\ u_{17i} \\ u_{18i} \\ u_{19i} \\ u_{20i} \\ u_{21i} \\ u_{22i} \end{bmatrix} \tag{3.85}$$

$$\dot{\mathbf{q}}_{\mathbf{i}} = \begin{bmatrix} \dot{\alpha}_i \\ \dot{\beta}_i \\ \dot{\gamma}_i \\ \dot{\delta}_i \\ \dot{\epsilon}_i \\ \dot{x}_i \\ \dot{y}_i \\ \dot{z}_i \\ \dot{\zeta}_i \\ \dot{\eta}_i \\ \dot{\theta}_i \\ \ddot{\alpha}_i \\ \ddot{\beta}_i \\ \ddot{\gamma}_i \\ \ddot{\delta}_i \\ \ddot{\epsilon}_i \\ \ddot{x}_i \\ \ddot{y}_i \\ \ddot{z}_i \\ \ddot{\zeta}_i \\ \ddot{\eta}_i \\ \ddot{\theta}_i \end{bmatrix} = \begin{bmatrix} \dot{u}_{1i} \\ \dot{u}_{2i} \\ \dot{u}_{3i} \\ \dot{u}_{4i} \\ \dot{u}_{5i} \\ \dot{u}_{6i} \\ \dot{u}_{7i} \\ \dot{u}_{8i} \\ \dot{u}_{9i} \\ \dot{u}_{10i} \\ \dot{u}_{11i} \\ \dot{u}_{12i} \\ \dot{u}_{13i} \\ \dot{u}_{14i} \\ \dot{u}_{15i} \\ \dot{u}_{16i} \\ \dot{u}_{17i} \\ \dot{u}_{18i} \\ \dot{u}_{19i} \\ \dot{u}_{20i} \\ \dot{u}_{21i} \\ \dot{u}_{22i} \end{bmatrix} \tag{3.86}$$

Parts of the formula including acceleration terms form the left hand side of the equation. The rest of the equations form the right hand side. The set of equations of motions is ordered based on acceleration terms to get the following general equation:

$$\mathbf{M}(q_i)\dot{\mathbf{q}}_{\mathbf{i}} = \mathbf{f}(q_i) \tag{3.87}$$

$$\left[\begin{array}{c|c} \begin{matrix} 1 & 0 & \dots & 0 \\ 0 & 1 & \dots & 0 \\ \vdots & \vdots & \ddots & \vdots \\ 0 & 0 & \dots & 1 \end{matrix} & \mathbf{0} \\ \hline \mathbf{0} & \begin{matrix} M_{1|1} & M_{2|1} & \dots & M_{22|1} \\ M_{1|2} & M_{2|2} & \dots & M_{22|2} \\ \vdots & \vdots & \ddots & \vdots \\ M_{1|22} & M_{2|22} & \dots & M_{22|22} \end{matrix} \end{array}\right] \begin{bmatrix} \dot{u}_{1i} \\ \dot{u}_{2i} \\ \vdots \\ \dot{u}_{22i} \end{bmatrix} = \begin{bmatrix} u_{12i} \\ u_{13i} \\ \vdots \\ u_{22i} \\ f_1(q_i) \\ f_2(q_i) \\ \vdots \\ f_{11}(q_i) \end{bmatrix} \tag{3.88}$$

From this set of first order differential equations the state vector $\dot{q}_i$ is determined:

$$\dot{\mathbf{q}}_{\mathbf{i}} = \mathbf{M}^{-1}\,\mathbf{f}(q_i) \tag{3.89}$$

Given the acceleration terms the state of the system for the next time step is numerically solved using an ODE solver

$$\mathbf{q_{i+1}} = f_{ODE}(\mathbf{q_i}, \mathbf{\dot{q}_i}) \tag{3.90}$$

The ODE solver takes the current state ($\mathbf{q_i}$) and its derivative ($\mathbf{\dot{q}_i}$) as input to compute the state at the next time step. The acceleration terms in the derivative state vector of the system are determined with equation 3.89.

3.5. Software Tools

Spyder and Maple are the software tools used in this research. These tools are chosen because they are both particularly useful at a different stage in building the model. Maple is math software that is very useful to easily solve mathematical problems and used to formulate the equations of motion. Spyder is a scientific environment written in the Python language and used to perform the numerical simulation. The results are also visualised with Spyder. The model is described in three sections: input (pre-processing), numerical simulation (processing) and results (post-processing). An overview is given in table 3.4.

Input

Before running the simulation, all time independent parameters of the system are defined. The hook and BIT equation of motion are formulated in Maple following Lagrangian mechanics as shown in previous section. Information about the blade and wind field is imported in Spyder. Other parameters are defined in the main file in Spyder. In this file the system parameters, simulation parameters and other constant are defined before executing the ODE solver.

Numerical Simulation

In the numerical simulation the equations of motions are solved for each generalized coordinate. The solving method used is the backward differentiation formula (BDF). Selecting the solving method depends on the type of ordinary differential equations. BDF is an implicit multi-step variable-order method and very appropriate for solving stiff problems [15]. The first 200 seconds are used for start-up of the simulation and not used in result analysis. At the start of the simulation the tagline tension and wind loads are added incrementally. In this way the start-up transient effects of the simulation are reduced. During the simulation some parameters are printed in the console to track the progress of the simulation and check the behaviour of the solver. Furthermore, bugs in the program are easier to find and locate while printing. When the numerical simulation is successfully finished, all useful information is stored as output in a Python dictionary file called ”results”.

Results

The required plots for analysing the results are produced in Spyder. Before running a script, that plots or animates a desired result, the results dictionary file is loaded and the data is extracted from this file. All plots and animations can be exported in several file formats.

	Module	Main Parts	Software
Input	Hook & BIT	Kinematics, masses, moment of intertia	Maple
	Blade data	Aerodynamic coefficients, section properties	Excel
	Wind Time Series	Mean wind speed, TI, angle	Spyder
	System	Lift set up, damping, stiffness	Spyder
	Simulation	Duration, error tolerances, ODE type	Spyder
Numerical Simulation	ODE solver	Blade loads, damping, slings, tagline	Spyder
Results	Plots	Displacements, acceleration, tagline tension, blade loads	Spyder

Table 3.4: Model structure

3.6. Model Verification

In this section code verification tests are conducted to prove that the model meets its specified requirements at a particular stage of its development.

Pendulum Motion Lift Wires

The lift wires should behave like a spherical pendulum. The rotation about the x- and y-axis are verified first.

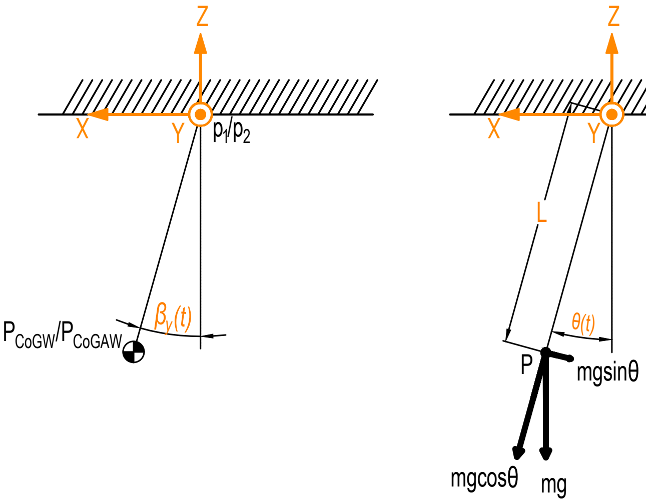

Figure 3.11: Pendulum motion lift wires: simulation- (left) and verification setup (right)

In the numerical model Langrangian mechanics are used to produce the equation of motion. Another method to find the equation of motion is by using Newtonian mechanics. Newton's second law is applied to derive the analytical harmonic solution of the pendulum motion around the y-axis and compared to the model solution (see B.1 for the derivation).

The test is performed for a length of $L = 18m$, $\theta_0 = 5^\circ$ and $\Theta_0 = 3^\circ$. For the given initial angles θ_0 and Θ_0 the Newtonian solution shows similar behaviour as the numerical model (see figure 3.12 and 3.13). Another simple check is the period of one pendulum motion $T = 2\pi\sqrt{L/g} \approx 8.5s$ correspond to the results, which is the case.

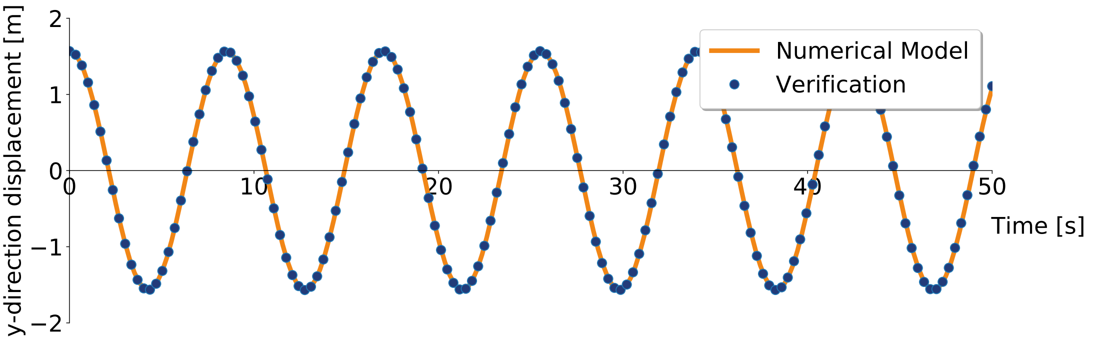

Figure 3.12: Verification result: pendulum motion hoist wires around x-axis

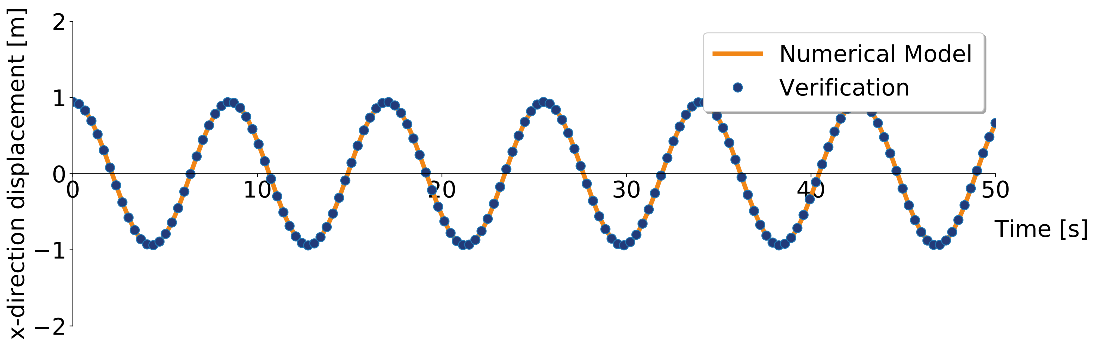

Figure 3.13: Verification result: pendulum motion hoist wires around y-axis

Double Pendulum Motion Lift Wires & Hook Sheave

Coupling between the masses of rigid bodies should be present. To verify these coupling motions the dynamics of the double pendulum motion between lift wires and hook sheave are investigated. Newton's equations are followed to find the EOM for the double pendulum. For the Newtonian derivation see B.2. The oscillation of the lift wires (p_{CoGWW} and p_{CoGAW}) and hook sheave block (p_{CoGHS}) are in the x-y plane. In the verificaiton method the m_1 respresent the mass of the lift wires together and m_2 the mass of the hook sheave block. Input values to run the simulation are: $m_1 = m_{CoGAW} = 5$, $m_2 = m_{CoGHS} = 30$, $L_1 = -p_{CoGAWz} = 18$, $L_2 = -p_{CoGHS} = 4$, $\theta_1(0) = 4$ and $\theta_2(0) = -2$. For the given masses, dimensions and initial angles the Newtonian double pendulum solution shows similar behaviour as the model (see figure 3.14).

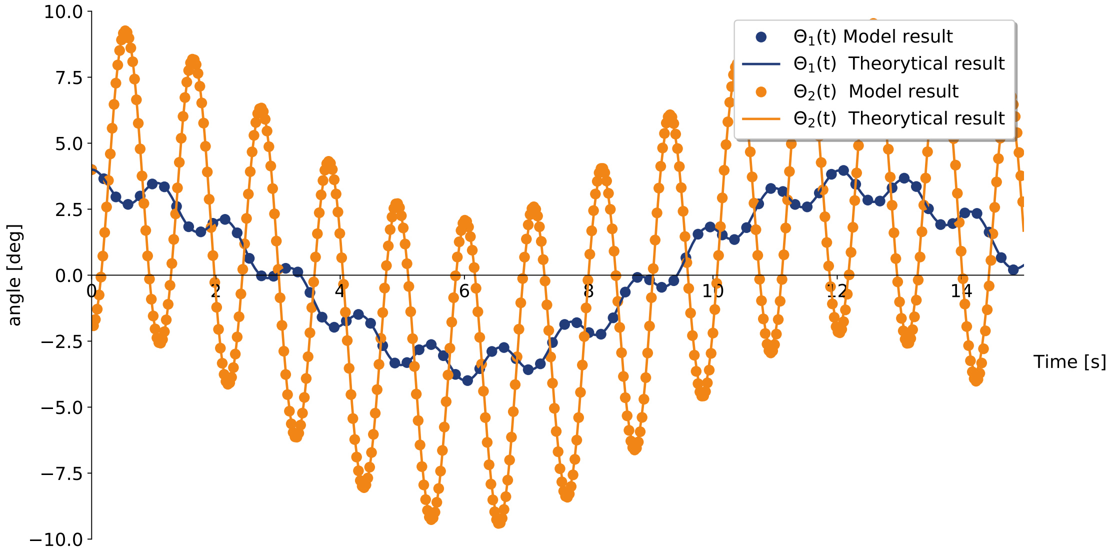

Figure 3.14: Double pendulum angles: test vs model

Symmetry M-Matrix

Based on the kinetic energy formula the mass matrix is validated. The mass matrix should be symmetric and the diagonal values should be positive. Non diagonal elements can be negative (see B.3). The symmetry of the M-matrix should hold for any state of the system. Therefore two test runs are done to check symmetry of the M-matrix. For the first run the set of generalized coordinates is randomly generated for values between 0 and 1 (3.91). For the second run a set of generalized coordinates is chosen which represent a realistic system state in an offshore lift operation (3.92). The M-matrix values for the random input are given in B.3 and for realistic input in B.4. Both matrices are symmetric and have no negative diagonal values.

$$\mathbf{q} = \begin{bmatrix} \alpha \\ \beta \\ \gamma \\ \delta \\ \epsilon \\ x \\ y \\ z \\ \zeta \\ \eta \\ \theta \end{bmatrix} = \begin{bmatrix} 0.61 \\ 0.57 \\ 0.52 \\ 0.25 \\ 0.46 \\ 0.49 \\ 0.48 \\ 0.95 \\ 0.97 \\ 0.72 \\ 0.57 \end{bmatrix} \quad (3.91) \qquad \mathbf{q} = \begin{bmatrix} \alpha \\ \beta \\ \gamma \\ \delta \\ \epsilon \\ x \\ y \\ z \\ \zeta \\ \eta \\ \theta \end{bmatrix} = \begin{bmatrix} 0.023 \\ 0.0080 \\ 0.024 \\ 0.031 \\ 0.0060 \\ 0.026 \\ 0.015 \\ -5.4 \\ 0.0091 \\ 0.0060 \\ 0.028 \end{bmatrix} \quad (3.92)$$

Energy Conservation

Looking at the conversation of mechanical energy is a useful method to understand and verificate the dynamic behaviour of the system. The mechanical energy in the system depends on the kinetic energy K, potential energy P and any form of energy dissipation. Kinetic energy is associated with linear and angular momentum. Potential energy is associated with contractions and expansions of springs and with gravitational potential. Roller bearing damping and damping in slings and taglines are examples of energy dissipation. External forces are also considered as a form of energy dissipation. These forms of energy dissipation are called non-conservative forces which do not have a potential energy term associated with them.

The total conserved energy in the system is

$$E = T + V \tag{3.93}$$

meaning the kinetic and potential can still vary within time, but the total energy is constant. To verify if the model complies to the law of conservation of energy the energy dissipation terms and external forces are removed from the EOM

$$\frac{d}{dt}\left(\frac{\partial L}{\partial \dot{q}_i}\right) - \frac{\partial L}{\partial q_i} + \frac{\partial D}{\partial q_i} = F_{ext}(q_i) \qquad \Rightarrow \qquad \frac{d}{dt}\left(\frac{\partial L}{\partial \dot{q}_i}\right) - \frac{\partial L}{\partial q_i} = 0. \tag{3.94}$$

The initial position vector $\mathbf{q}(t_0)$ equals to the initial position vector 3.92 and the initial velocity vector to $\dot{\mathbf{q}}(t_0) = \mathbf{0}$. The result is shown in figure 3.15. For reasons of visualisation the energy is normalised. Simulation results are shown for the first 3 seconds, because without damping the system becomes numerically unstable if the time step is too big. It is easy to see that the total energy remains constant, while an increase in potential energy shows a decrease in kinetic energy and vice versa.

If energy dissipation terms are added to the EOM, but external forces are excluded the Langrangian becomes

$$\frac{d}{dt}\left(\frac{\partial L}{\partial \dot{q}_i}\right) - \frac{\partial L}{\partial q_i} + \frac{\partial D}{\partial q_i} = F_{ext}(q_i) \qquad \Rightarrow \qquad \frac{d}{dt}\left(\frac{\partial L}{\partial \dot{q}_i}\right) - \frac{\partial L}{\partial q_i} + \frac{\partial D}{\partial q_i} = 0. \tag{3.95}$$

For the same initial conditions the results are shown in figure 3.16. As expected the total energy decreases over time. The system shows stable dynamical behaviour when damping terms are included. The coupled motion between the lift wires and BIT results in the sinusoidal kinetic and potential energy over time. If taglines are included, as external force in the model, the coupled motion between the lift wires and BIT is damped.

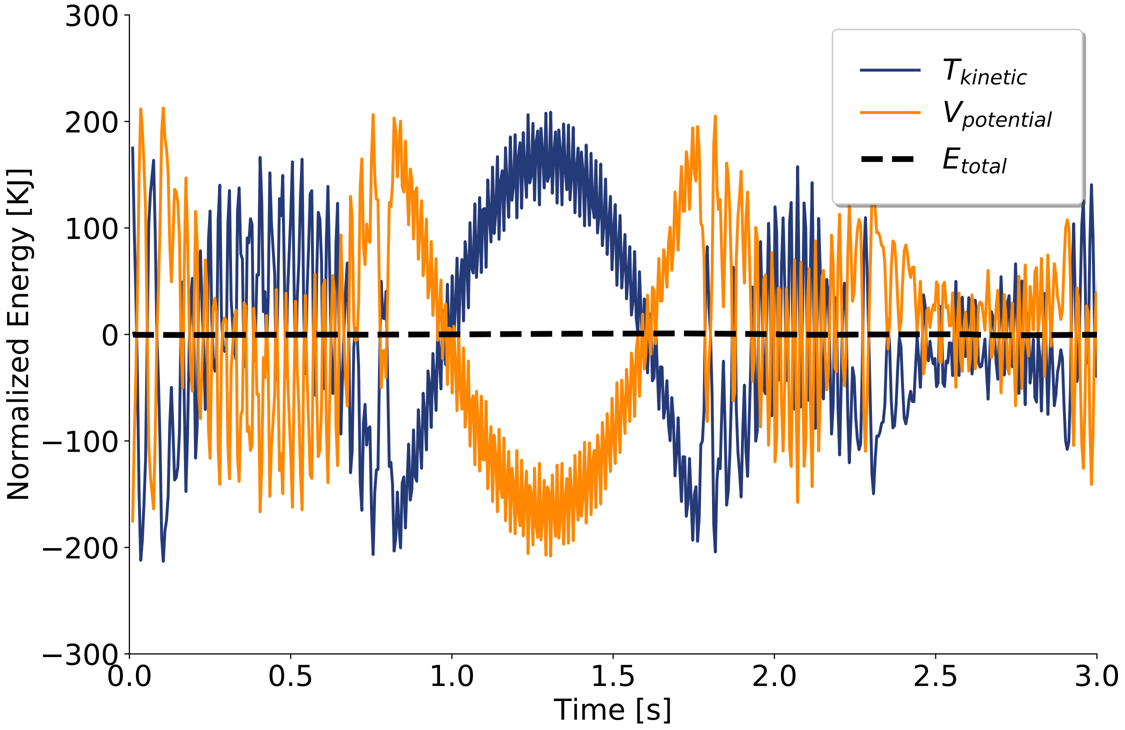

Figure 3.15: Energy in system (without energy dissipation)

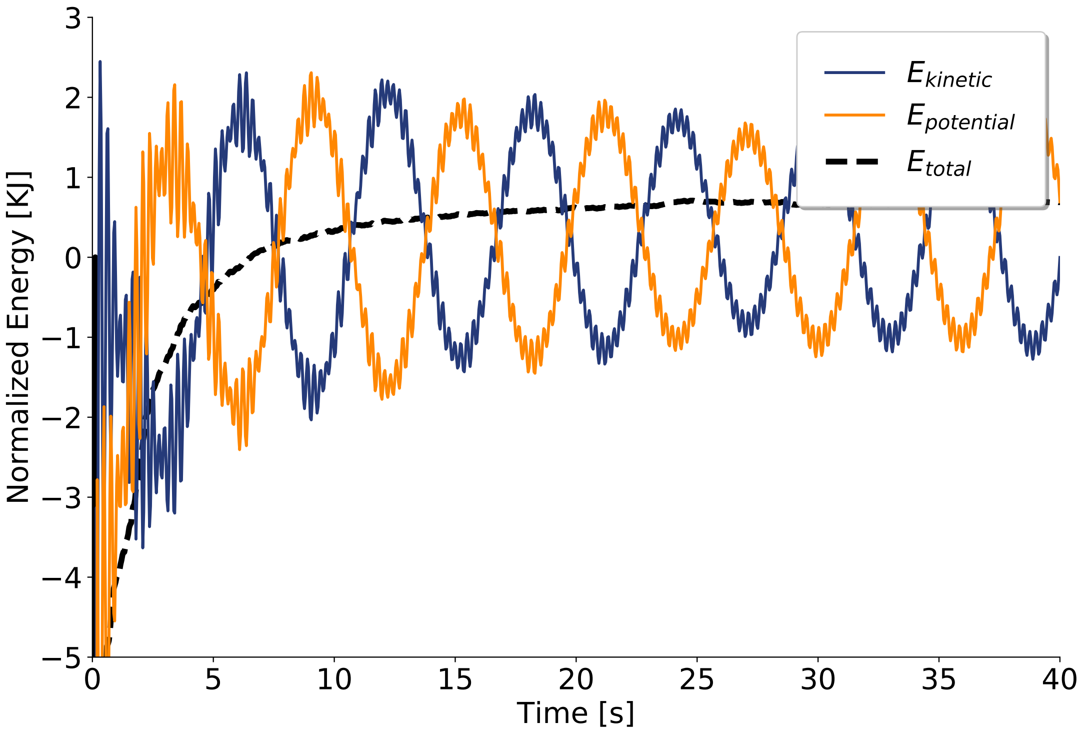

Figure 3.16: Energy in system (with energy dissipation)

3.7. Input

Tower displacement

The displacement of the hub relative to the blade complicates the alignment process. Hydrodynamic loading of monopile and aerodynamic loading of the tower and nacelle induce motions of the hub. A simplified model based on a discretized monopile and tower is build to analyse these hub motions. Wave loads are calculated using the Morrison equation and drag loads on the nacelle are also incorporated in the model. The results for a significant wave height of $h_s = 0.5m$ and $h_s = 1m$ are given in C. Because the model build to determine the hub motion is strongly simplified, an imposed tower displacement is used instead. The imposed motion is assumed to be sinusoidal with a frequency close to the natural frequency of the fore-aft motion of a wind turbine tower ($f = 0.25Hz$) and amplitude of 0.02m for tower input 1 and 0.06 for tower input 2. The imposed tower displacement shown in figure C.2 are added to the blade root displacement results in x-direction.

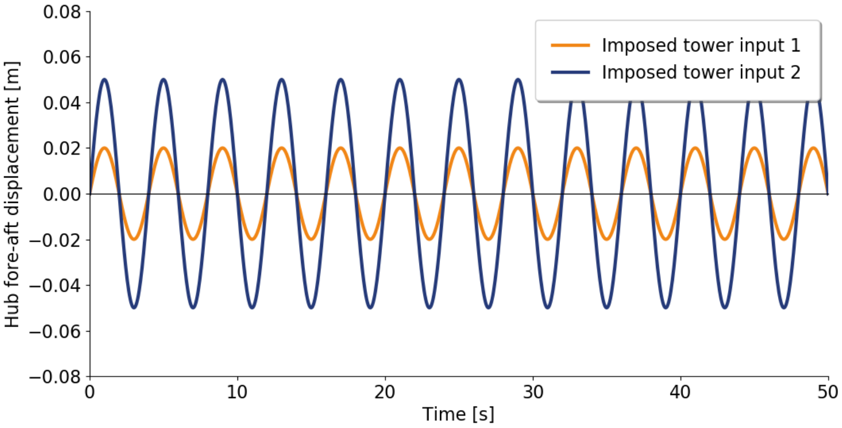

Figure 3.17: Imposed tower displacement

Blade properties

The main blade properties for a 8.4MW turbine and 12MW turbine are described in table 3.5. A 12 MW differs in length, mass, moment of inertia and blade section characteristics from a 8.4 MW blade.

Turbine	Vestas V164-8.4	DTU	Haliade-X
Rating	8.4 MW	10 MW	12 MW
Hub height	105 m	119 m	138 m
Blade mass	35.0 ton	41.7 ton	60 ton
Blade length	80 m	86.4	107 m
Root diameter	5.2 m	5.6 m	5.5 m
Moment of inertia	$I_x = I_z = 12.5 \cdot 10^6 kg/m^2$ $I_y = 23.7 \cdot 10^4 kg/m^2$	$I_x = I_z = 17.4 \cdot 10^6 kg/m^2$ $I_y = 32.7 \cdot 10^4 kg/m^2$	$I_x = I_z = 38.3 \cdot 10^6 kg/m^2$ $I_y = 45.4 \cdot 10^4 kg/m^2$

Table 3.5: Turbine description

Lift setup

At a hub height of 119m, the installation plan for the 10MW DTU turbine blades is close to the limits of the Aeolus and the crane boom. The minimum clearance of the BIT and crane should be 1.5 metre. This distance is most critical during the removal phase of the BIT. During the removal phase, the crane rotates towards the blade and the distance between the blade and the crane boom is close to 1.5 metre. This is the most critical phase in the lifting operation and the limiting factor in making the lift plan.

The following lift plan for blade installation with the Aeolus is considered based on the lift plan for Norther offshore wind farm. The crane boom is under an angle of 82°. The lift wires have a length of 36 metre, measured from the tip of the whip hoist to the hook. Shortening the length of the lift wires is not possible because of the minimum crane-blade clearance of 1.5 metre during the removal phase. All input values for the lift plan in the reference case (8.4MW) are given in appendix E.

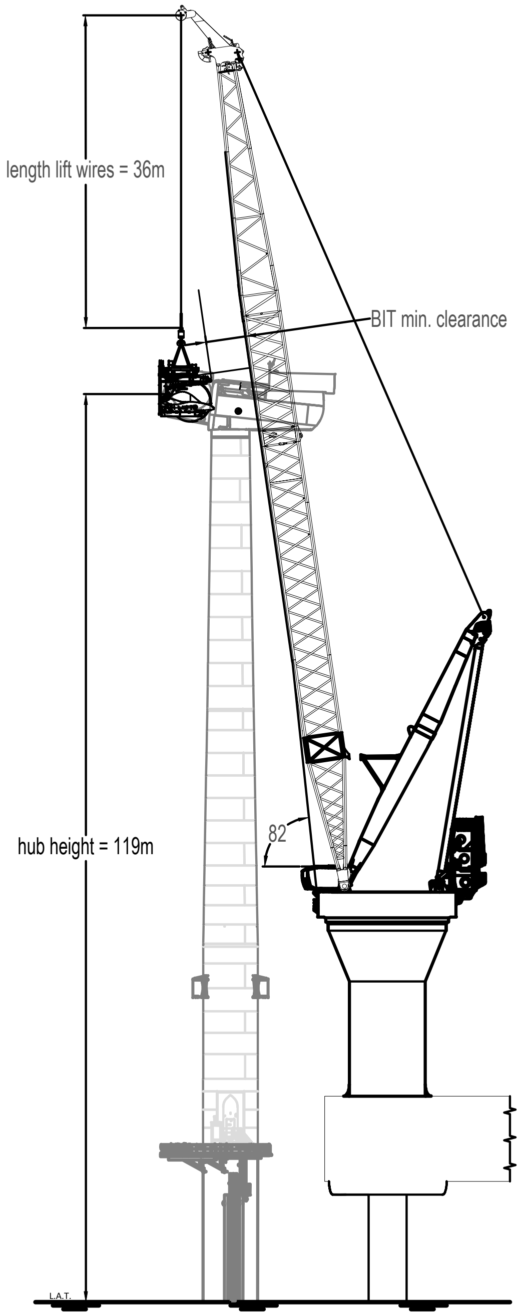

Figure 3.18: Overview lift installation plan

4

Model Results

This chapter presents the results and discussion of the results. The load cases are described in the first section. In section 4.2 the results for the installation of a 8.4MW turbine blade is given, which serves as a reference case. In the next section the results of a 12MW turbine blade are given and discussed. An eigenvalue analysis is performed for the 12MW turbine blade to obtain useful information about the dynamic behaviour of the lift setup.

4.1. Load Cases And Environmental Conditions

In this section the load cases are described which are used as input for the numerical simulations. For an overview of the load cases see table 4.1. Wind parameters are average wind speed and the wind direction relative to the blade orientation. Turbulence intensity, damping in system and the rotation of the blade in the BIT are treated in the sensitivity analysis.
In the reference load case RLC1 the wind direction varies. A wind direction perpendicular to the blade (0°) is expected to be worst case for installation. Because of the non-symmetric aerodynamic properties of the blade different results are expected for 45°,-45°and 135°. Blade installations only take place if the wind speed stays below the operational limited wind speed. For 8.4 MW blade this wind speed is around 12 m/s at a installation height of 105m. This operational limited wind speed is often imposed by the equipment used. Lower wind speeds, of 6 m/s and 9 m/s, and a higher wind speed of 15 m/s are also simulated in the reference load case RLC1. In load case LC1 for the 12MW turbine blade the same wind field characteristics and direction are selected just as for the reference load case RLC1. In this way the results can be compared to each other without changing the input of the system.

	Turbine size	$U_w[m/s]$	$\theta_{wind}[^{\circ}]$
RLC1	8.4	[6 9 12 15]	[-45 0 45 135]
LC1	12	[6 9]	[-45 0 45 135]

Table 4.1: Definition of load cases

A sensitivity analysis is performed to see how the results change when input parameters, such as damping, change related to their values used in the performed simulations. For an overview of the sensitivity cases see table 4.2. The results of the motion of the blade is expected to be sensitive to different pitch angles of the of the blade in the blade installation tool (SC1). Tower displacement motion is defined based on a period and certain amplitude. The fore-aft motion of the tower is considered for two different cases. For tower input 1 the frequency is 0.25Hz and amplitude 0.02m. The frequency is 0.25Hz and amplitude 0.06m for tower input 2 (SC2). These values are based on the results of a finite difference model and take into account the 1p and 3p frequencies of the tower. Damping sensitivity is analysed for 5 different damping percentages (SC3). In sensitivity case SC4 the influence of turbulence intensity of wind is investigated. A sudden change in wind speed increases the induced wind loads on the blade. In case of a low TI these changes are smaller compared to a high TI and different results

are expected.
For each sensitivity case only one input parameter changes. Values used in other analysis are 7°for the angle of the blade in the blade installation tool, tower input 1 for the tower displacement, 100% damping and a turbulence intensity of 0.12.

	Turbine size	$U_w[m/s]$	$\theta_{wind}[°]$	Sensitivity	Sensitivity values
SC1	12	9	45	Angle blade in BIT	76, -16, 0, 7, 17, 47, 52, 68, 85
SC2	12	9	45	Tower displacement	Tower input 1, Tower input 2
SC3	12	9	45	Damping	$50\%,80\%,\$100\%,120\%,150\%$
SC4	12	[6 9]	45	TI	0.06, 0.12, 0.14, 0.16

Table 4.2: Definition of sensitivity cases

4.2. Results Reference Case

In this section the results of the simulations for the reference case are given. First the blade root motion is analysed separately. In the second part the tower fore-aft motion is added to the blade root motion.

Blade Root Centre Motion

The motion of the blade root centre is considered first. As expected, higher wind speeds increases the maximum displacements of the blade root centre. Figure 4.2 shows the 30 minutes simulations results of the positions of the blade root centre in the xz plane.

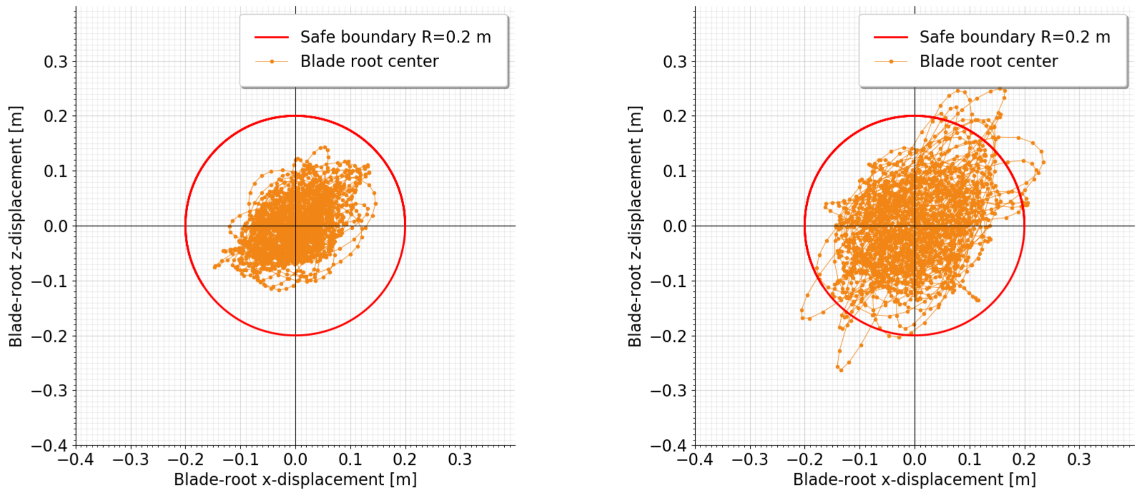

(a) $TI = 0.12 \quad V = 6m/s$ (b) $TI = 0.12 \quad V = 9m/s$

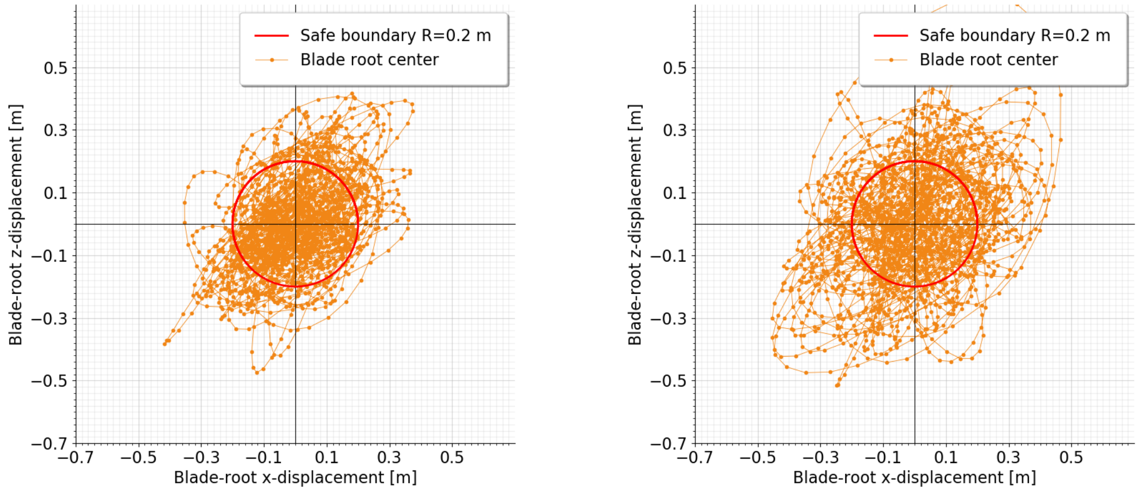

(c) $TI = 0.12 \quad V = 12m/s$ (d) $TI = 0.12 \quad V = 15m/s$

Figure 4.1: Track of the blade root center for 30-min simulations

The largest displacement seems to occur when the blade moves in both x- and z-direction and not along one particular axis. For wind speeds up to 9m/s single blade installation seems possible for an incoming wind direction of 45°. At a wind speed of 12m/s possible problems will occur during installation. For wind speeds higher and equal to 15 m/s blade installation is not possible and therefore

not analysed any further in the following sections. Blade aerodynamic forces and moments increase quadratically with higher wind speeds. This results in increase in blade root motions.
In figure 4.1 the results are shown for an incoming wind angle of 45°. Three other incoming wind angles used in simulations are -45°, 0°and 135°. For a different incoming wind angle the responses are expected to be different. In figure 4.2 the mean and standard deviation of the displacements are shown.

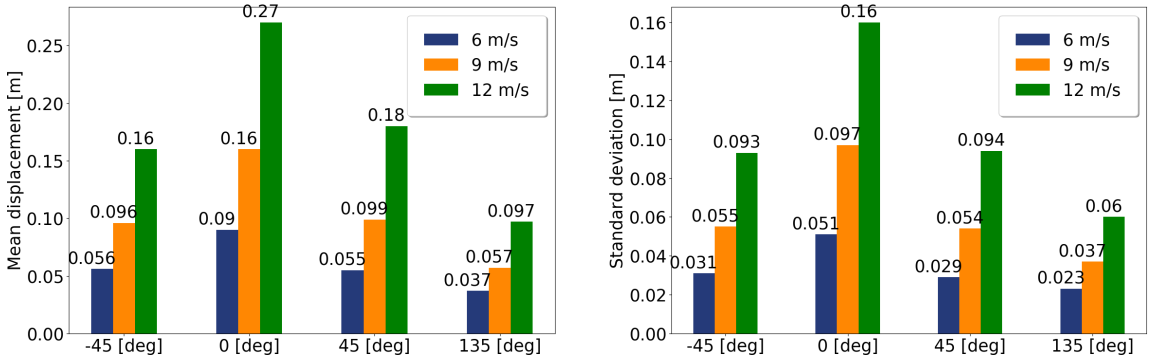

(a) Mean displacement

(b) Standard deviation displacement

Figure 4.2: Mean and standard deviation for 3 different wind speeds and 4 different angles

The responses for an incoming wind angle of -45°and 45° are smaller compared to a perpendicular wind field (incoming wind angle of 0°). For a incoming wind angle of 135° the wind comes from the other side of the blade, which is the trailing edge side of the blade instead of the leading edge side. The responses are smaller than the results for -45°and 45°angles. Beside the wind direction, the mean wind speed also influences the responses. If the wind speed is increased from $6m/s$ to $9m/s$ and from $9m/s$ to $12m/s$ the mean and standard deviation almost doubles. This is possible due to the fact that the aerodynamic forces are quadratic related to the wind speed.
In figure 4.4 the number of outcrossings is given for different incoming wind angles and three mean wind speeds. For the alignment phase the allowable outcrossing rate for a successful mating is $1.67 \cdot 10^{-2}$ Hz, which equals to one outcrossing of the safe boundary (0.2 m) per minute. The maximum outcrossing for a 30 minute simulation is therefore 30. The red line in figure 4.4 represents the limit of 30 outcrossings.

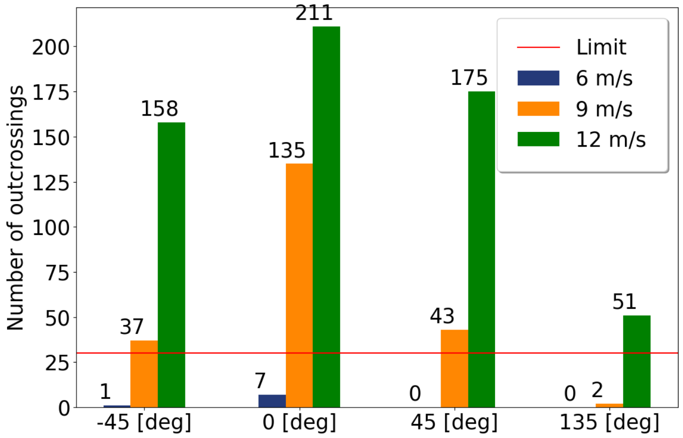

Figure 4.3: Mean displacement

Figure 4.4: Number of outcrossing of the safe boundary

For wind speeds lower or equal than 6 m/s the criterion is met. For wind speeds of 12 m/s and higher the criterion is exceeded and for 9 m/s the criterion is met for a small range of incoming wind angles.

4.2.1. Relative Motion Blade And Hub

In contrast to the responses of the blade, which depends on the wind field, the hub motion responses are governed by wave loads. Figure 4.5 shows the time series of the imposed hub centre movement. The hub motion does not outcrosses the safe boundary of 0.2 m, but has an effect on the number of outcrossings of the safe boundary when blade root motions are taken into account.

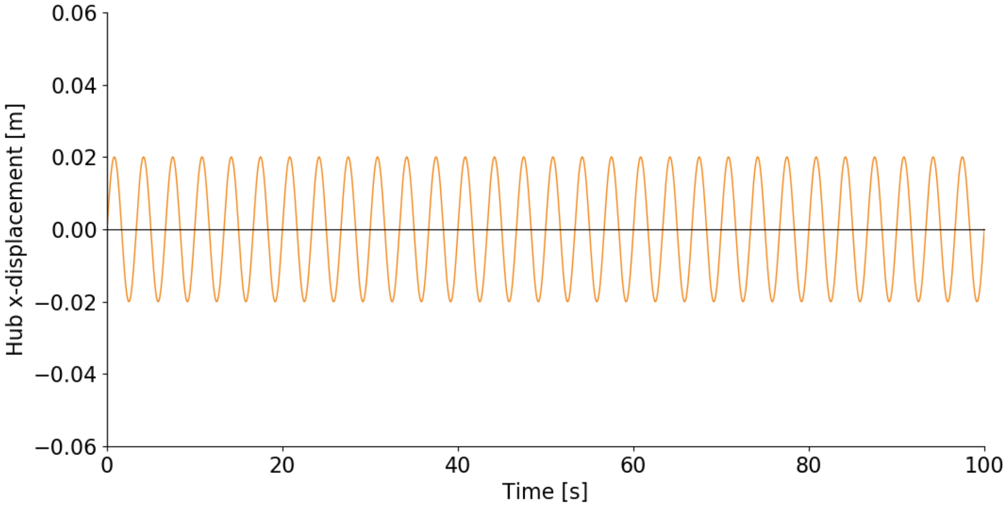

(a) $amplitude = 0.02m \quad f = 0.25Hz$

Figure 4.5: Track of the hub displacement in x-direction

Figure 4.6 displays the main effect of adding the relative motion of the blade to the hub for the number of outcrossings of the safe boundary.

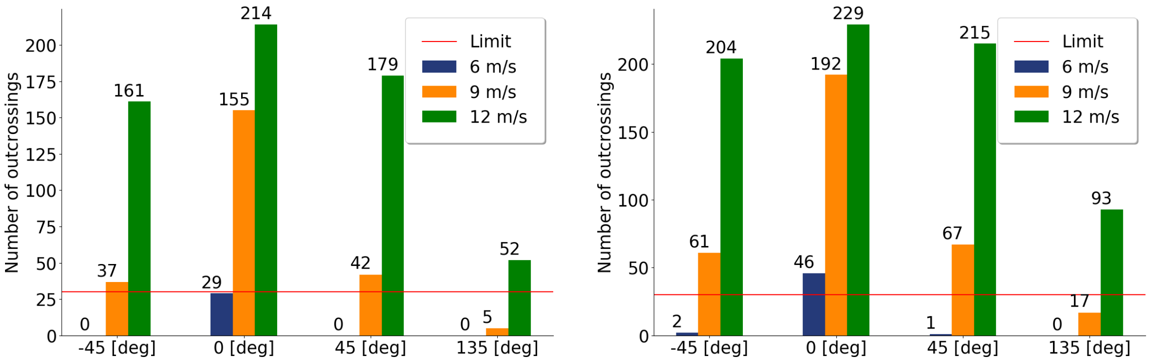

(a) Results for an imposed tower displacement with amplitude 0.02m

(b) Results for an imposed tower displacement with amplitude 0.06m

Figure 4.6: Number of outcrossing considering the relative motion between the blade root and hub

Using the tower displacement, as explained in section 3.7, the number of outcrossings increases compared to the number of outcrossings where the hub motions are neglected (see figure 4.3). It can be concluded that the relative motion of the blade root centre and hub can not be neglected. Relative motion between the two bodies is relevant in realistic offshore condition.

4.3. Results 12MW Turbine Blade

This section starts with the results of the eigenvalue analysis. In the second section the results of the simulations for the 12MW turbine blade are given. The results of the sensitivity analysis are described in the third section. Based on the results of these sections improvements are suggested in the fourth section. One particular solution, using an extra tagline, is elaborated in more detail.

4.3.1. Eigenvalue Analysis

The results of an eigenvalue analysis characterise the basic dynamic behaviour of the blade and how the blade will respond to external forces. Normal modes of vibration are associated with a specific natural frequency. The solution of the EOM for natural frequencies and their corresponding modes requires a reduced form of the EOM. Damping and external loading are set to zero. The EOM in matrix form reduces to

$$\mathbf{M\ddot{u}} + \mathbf{Ku} = 0 \tag{4.1}$$

where $\mathbf{M}$ is the mass matrix and $\mathbf{K}$ the stiffness matrix. Equation 4.1 is the equation of motion for undamped free vibration. To solve equation 4.1 the harmonic solution $\mathbf{u} = \boldsymbol{\phi} sin(\omega t)$ is substituted into the equation of motion

$$-\omega^2 \boldsymbol{\phi}\mathbf{M}\sin\omega t + \boldsymbol{\phi}\mathbf{K}\sin\omega t = 0 \tag{4.2}$$

with

$\boldsymbol{\phi}$ = Amplitude
ω = Angular undamped natural frequency
$\mathbf{u}$ = Displacement vector
$\mathbf{\ddot{u}}$ = Acceleration vector
t = Time

which after simplifying becomes

$$\left(\mathbf{K} - \omega^2\mathbf{M}\right)\boldsymbol{\phi} = 0 \tag{4.3}$$

By solving equation 4.3 the eigen periods and modes are obtained. As shown in table 4.3 the BIT with blade and hook coupled motions have 11 eigenmodes. In each eigenmode one or more motions dominate. For each eigenmode the natural period T_n is given in the last row of table 4.3.

Mode	1	2	3	4	5	6	7	8	9	10	11
α	-0.21	0	0.51	0	0	-0.05	0	0	0	0	0
β	0	0	0	0.01	-0.2	0	0	-0.1	0	-0.01	0
γ	0	0	0	0.01	0.04	0	0	0.99	0.21	0.29	0
δ	-0.17	0.23	0.21	0	0	0.97	-0.01	0	0	0	-0.48
ϵ	-0.68	-0.18	-0.52	0	0	0.01	-1	0	0	0	0.03
x	0	0	0	-0.1	-0.09	0	0	0.09	-0.75	-0.96	0
y	-0.04	-0.16	0.14	0	0	0.22	0	0	0	0	-0.88
z	0	0	0	0	0	0	0	0	-0.62	0.02	0
ζ	0	0.92	-0.38	0	0	0	0	0	0	0	0
η	0	0	0	0.99	0.97	0	0	-0.07	0.01	0.01	0
θ	-0.68	-0.19	-0.51	0	0	0	0	0	0	0	0
T_n	*18.6*	*15.7*	*5.18*	*4.55*	*2.4*	*0.693*	*0.415*	*0.111*	*0.088*	*0.069*	*0.029*

Table 4.3: Eigen modes and natural periods for BIT,blade and hook rigid body motions

The first 2 modes have relative long natural periods compared to the other modes. The first mode has a natural period of 18.6 seconds and corresponds to the rotation of the blade in the xy-plane. The dominant motion of second mode corresponds to the rotation of the blade around the x-axis, in the yz-plane. The natural periods of these modes are close to each other. Which can cause large blade root motions if the wind contains a lot of energy close to these frequencies. In figure 4.7 the dominant motion of the first and second mode are shown. The top picture shows a rotation of blade around the blade x-axis which corresponds to the second mode. The bottom picture shows the dominant motion of the first mode which corresponds to a rotation around the z-axis. A small rotation of the blade around the CoG, causes big displacements of the blade root centre. For the 12MW turbine blade the distance of the CoG to the blade root is larger. Therefore a rotation around the CoG causes even larger displacements compared to the 8.4MW turbine blade.

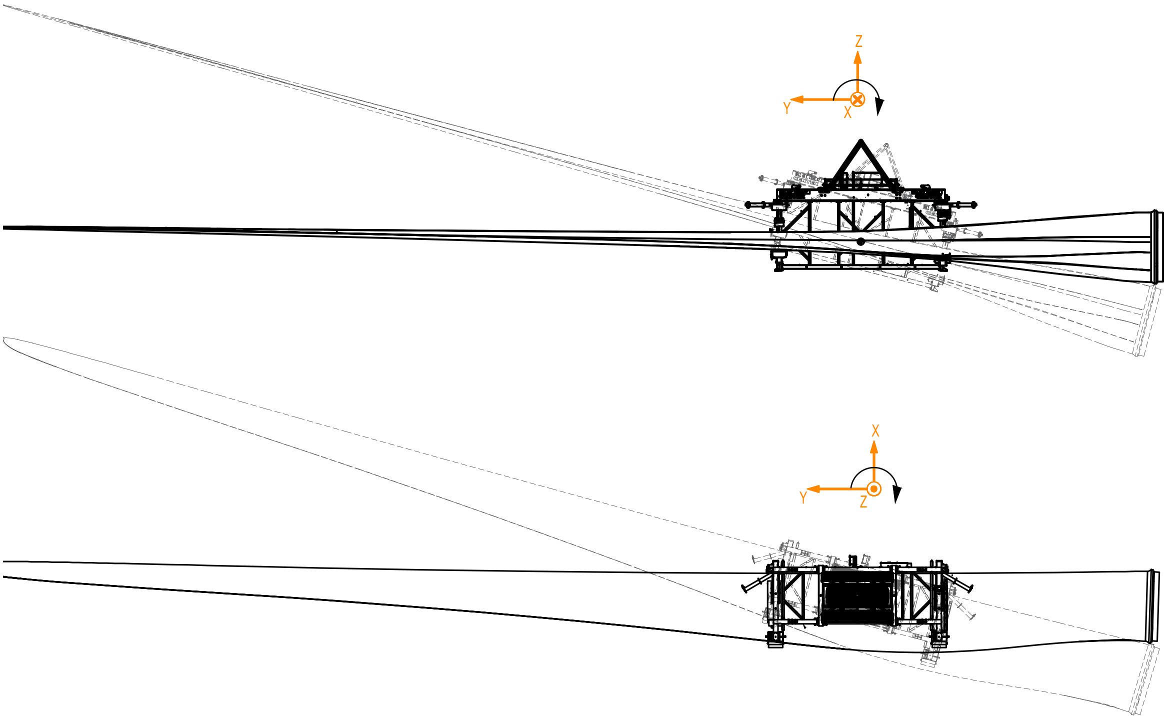

Figure 4.7: The dominant motion of the blade and BIT visualised: eigenmode 1 (bottom) and eigen mode 2 (top)

In figure 4.8 the wind spectrum is shown for a wind field with an average wind speed of 9m/s and turbulence intensity 0.12, created from a time series produced by the turbulence simulation tool (PyTurbSim). The top figure shows the wind speed for 500 seconds and the fluctuations due to turbulence. A fast fourier transform algorithm converts the wind speed signal in the time domain to a representation in the frequency domain. The wind field is created based on the Kaimal spectrum. Therefore the spectrum converted from the wind time series shows a similar graph compared to the Kaimal wind spectrum. In contrast to a wave spectrum, where the energy is centred around a certain frequency, the energy in the Kaimal wind spectrum is higher the lower the frequency (see figure 4.9). The lower the natural frequencies of the system the more they are excited. Figure 4.8 also shows the blade root displacement spectrum. In this spectrum the first and second mode of the system are plotted. The first two natural frequencies of the system are in the lower frequency part where the energy of wind spectrum is the largest. The first and second mode, corresponding to the rotation of the blade around the x-axis and z-axis, are excited the most. The excitations of the other 9 modes are negligible. Their natural frequencies are too high to get excited by the wind.

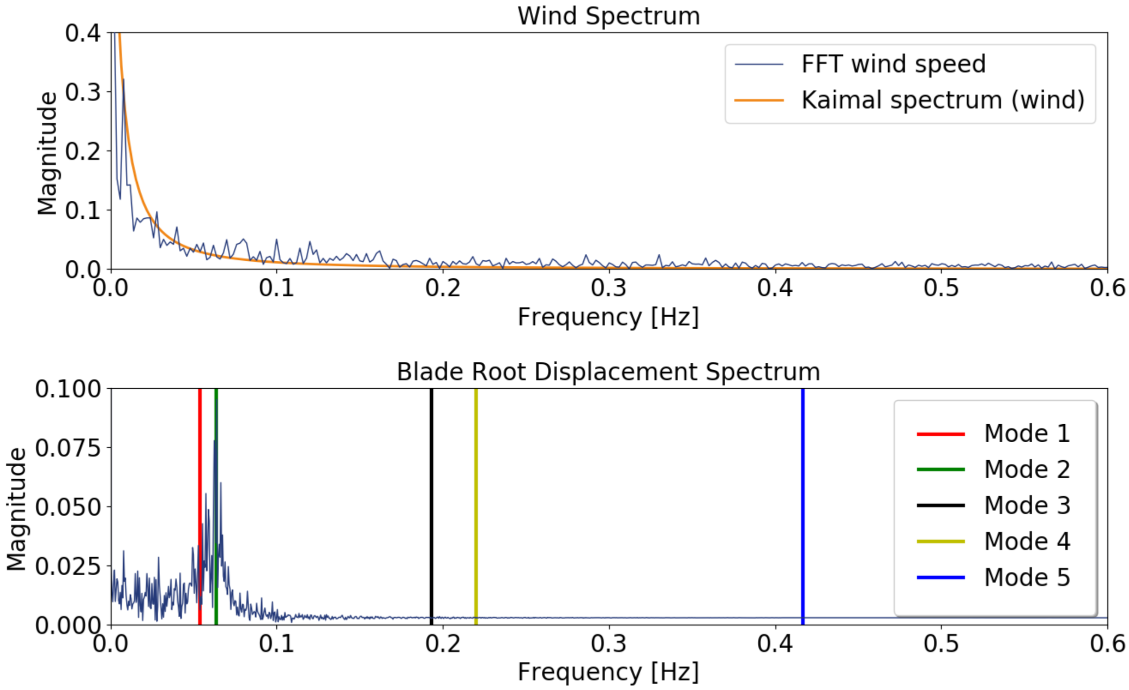

Figure 4.8: Wind speed spectrum (top) and blade root displacement frequency spectrum (bottom)

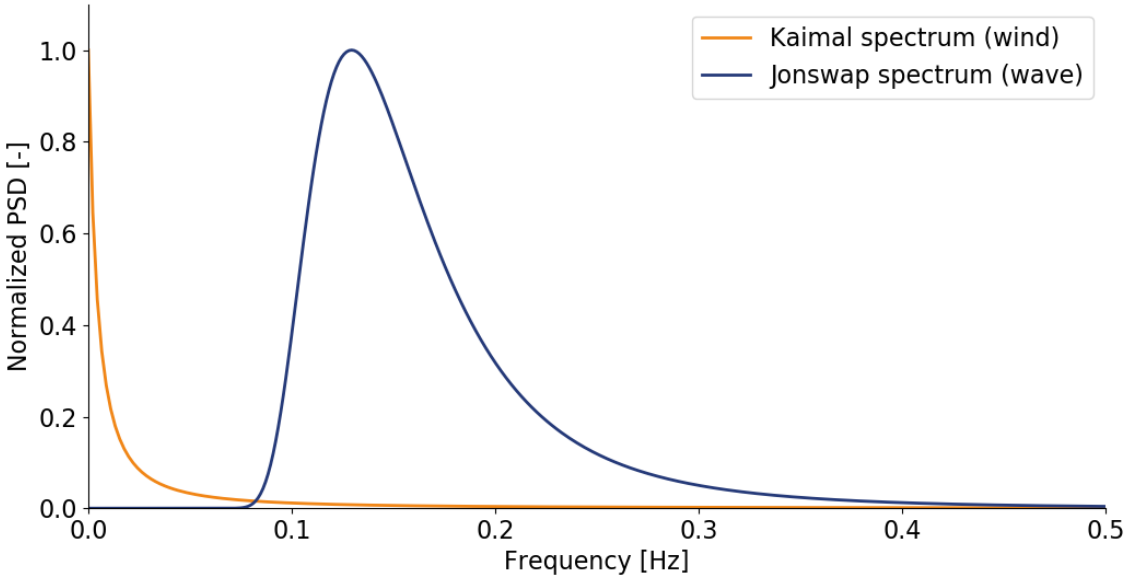

Figure 4.9: Kaimal and Jonswap spectrum

4.3.2. Simulation Results

Blade-Root Centre Motion

In this section, the simulation results for the 12MW blade are given. In comparison with the reference 8.4 MW blade the blade properties are changed. Mass, moment of inertia, and blade section properties are different. Changing these properties resulted in increasing blade root motions (see figure 4.10).

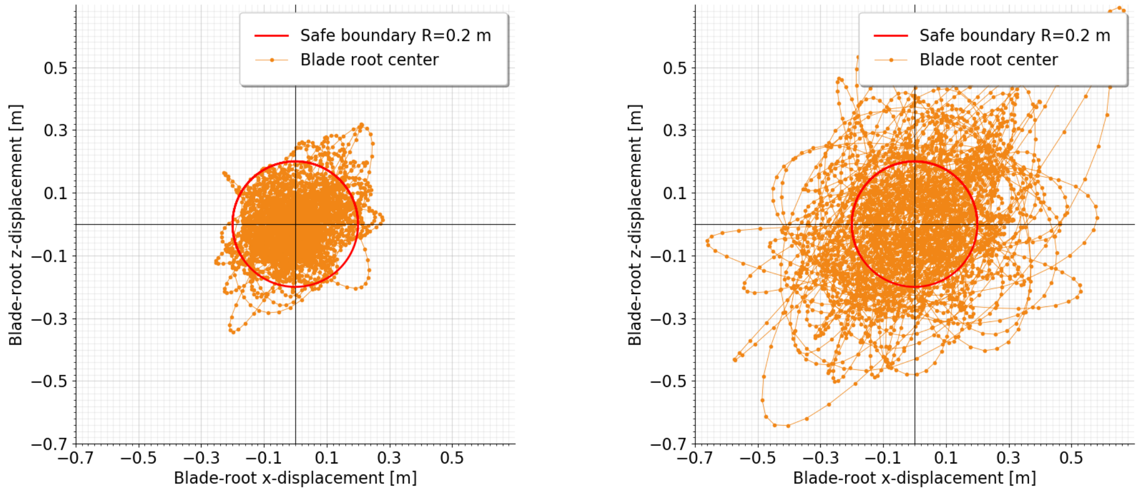

(a) $TI = 0.12 \quad V = 6m/s$

(b) $TI = 0.12 \quad V = 9m/s$

Figure 4.10: Track of the blade root center for 30-min simulations (12MW)

The operational wind speed limit decreased from around 10m/s for a 8.4MW blade to around 5m/s for a 12MW turbine blade for an incoming wind angle of 45 degrees. Figure 4.11 shows the decrease in workability when the wind speed limit decreases to 5m/s for the location at the Dogger Bank in the month August. The green part indicates the workable wind speeds.

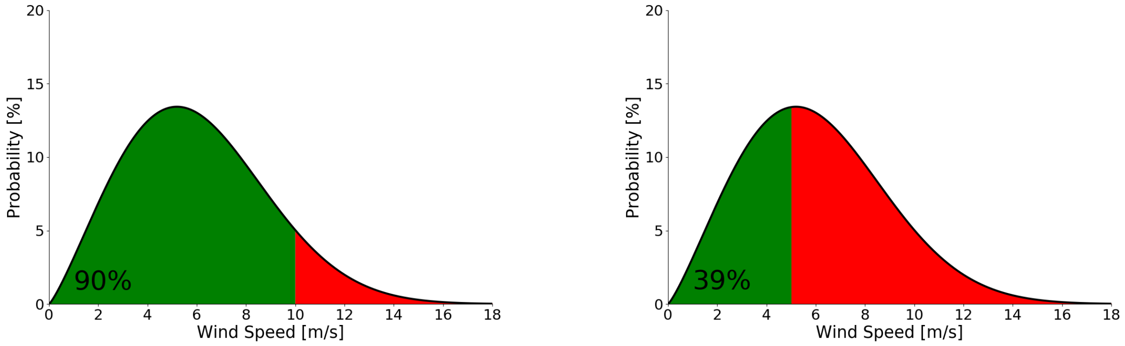

(a) Installation 8.4MW turbine blade

(b) Installation 12MW turbine blade

Figure 4.11: Workability for a 8.4MW (a) and 12MW (b) turbine blade installatin at the Dogger Bank in August

The decrease in the wind speed limit due to the fact that for the 12MW turbine blade the aerodynamic forces on the blade are bigger and therefore the aerodynamic moments increase as well. The second reason is the increase in distance of the CoG of the blade to the blade root centre. For a 8.4MW turbine blade this distance is 27m and for a 12MW turbine blade this distance increases to 34m. For an rotation of 1 degree around the CoG of the blade this correspond to an increase in displacement of $(34m - 27m) \cdot 1^{\circ} \cdot \frac{pi}{180} = 0.12m$. The increase in blade and BIT mass is the third reason for increasing blade root motions. The increase in mass decreases the natural frequencies of the system, which has

a negative impact on the motions of the blade root. Lower natural frequencies are excited more as explained in the previous section.
In figure 4.12 the results for vertical and horizontal displacement of the blade root centre and the moments are shown. The vertical and horizontal displacement of the root centre show similar behaviour. For most of the time a peak displacement in the horizontal plane is coupled with a peak displacement in the vertical plane. This reaction could be explained by taking a closer look at the modes of the system. The natural frequency of the first two modes are close to each other and their dominant motion is the rotation around the z-axis and x-axis respectively. If the wind speed frequency is close to these natural frequencies both mode 1 and 2 are triggered.
The bottom figure 4.12 shows the moment of the blade around the x- and z-axis over time. Fluctuations for the moment around the x-axis are larger compared to the moments around the z-axis. The bigger these fluctuations the larger the displacement in the blade root centre. This is why high turbulent wind could decrease workability.

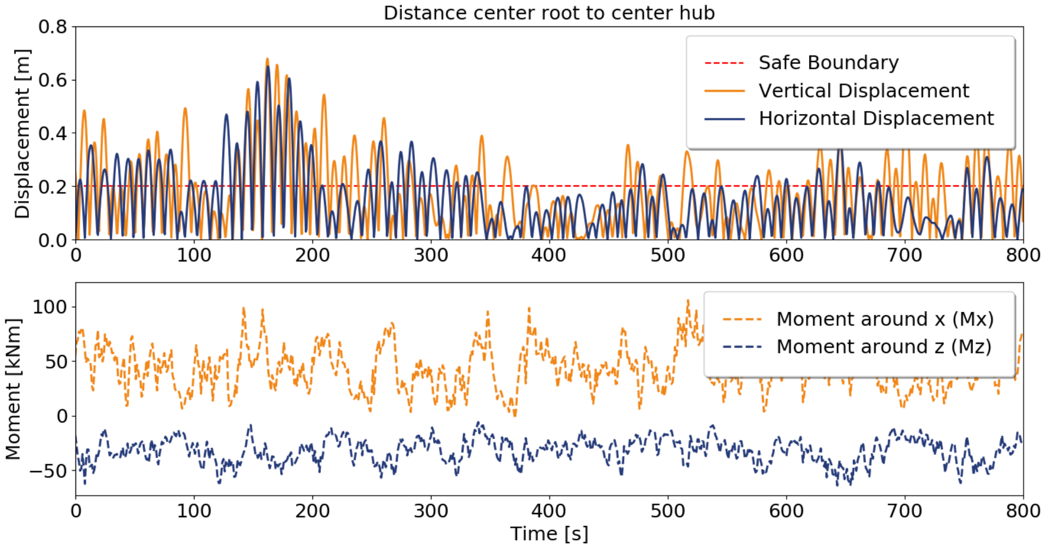

Figure 4.12: Track of the blade root (top figure) and moment (bottom figure)

Relative Motion Blade And Hub

Looking at figure 4.11a and 4.11b, it already appears to be difficult to install 12MW turbine blades and stay within the operational limits. Simulation results for a wind speed of 6 m/s and incoming wind direction angles of -45°,0°, 45° and 135° show that the maximum outcrossing number of 30 is exceeded. In figure 4.13a and figure 4.13b the mean and standard deviation are given respectively for the relative motion of the blade root and hub (for tower input 1).

Tagline Tension

The tagline master has a PFL of 30kN. If a wind peak suddenly affects the blade and the pull in the tagline exceeds 30kN, the TGM slides. This could lead to the dangerous situation where the blade is not in control anymore. Therefore the tagline tension is monitored during the simulations. The maximum tagline tension is around 32kN for wind speed around 9m/s and incoming wind direction 0°, which is above the PFL of the TGM. For the other simulations the limit wasn't exceeded.

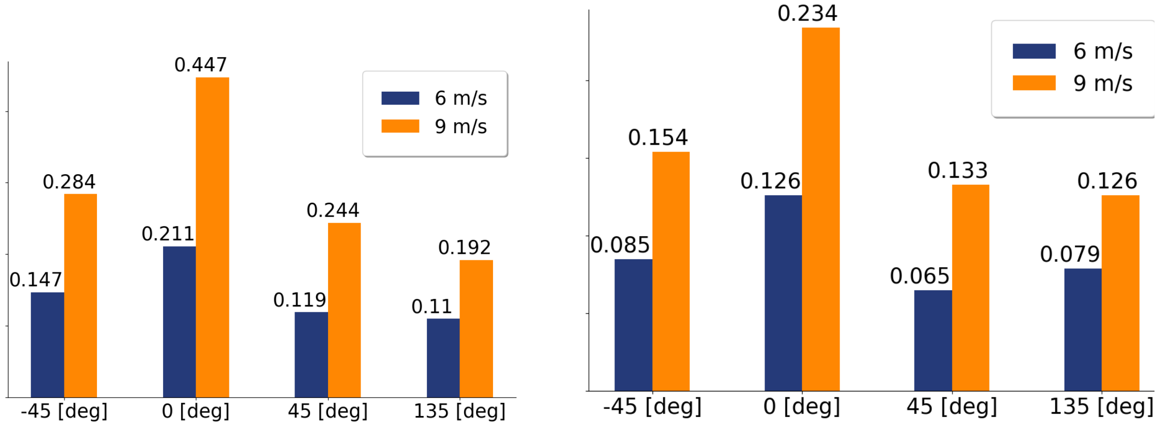

(a) Mean relative displacement (b) Standard deviation relative displacement

Figure 4.13: Mean and standard deviation of the relative motion between the blade root and hub

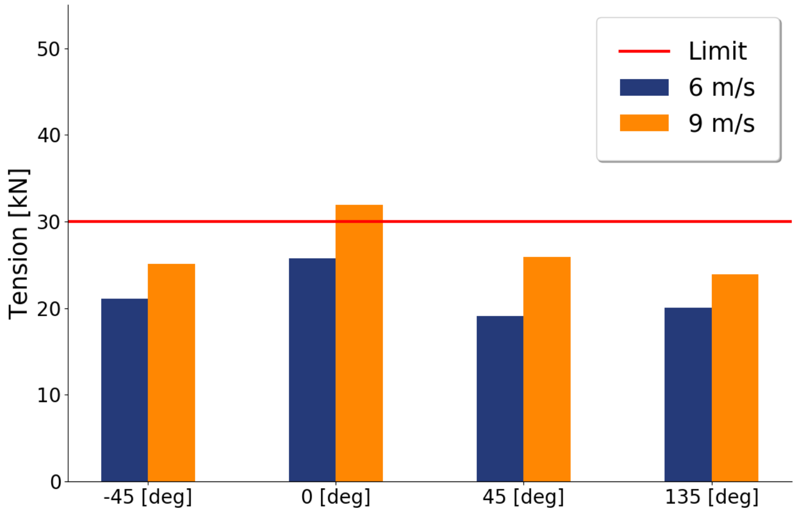

Figure 4.14: Maximum tagline tension for V = 6 m/s and V = 9 m/s

Root Y Displacement

Until this section, only the displacement of the blade root in the xz-plane is discussed. The displacement of the blade root towards the hub could also complicate the alignment process. Although this research focuses on the motion of the blade in the xz-plane, the motion of the blade root towards the hub should not be underestimated (see figure 4.15). At a wind speed of 6m/s the blade could move around 0.3m towards the hub in 5 seconds and for wind speeds around 9m/s the displacement could increase to 0.5m in 5 seconds. Which could lead to unsafe situations for workers.

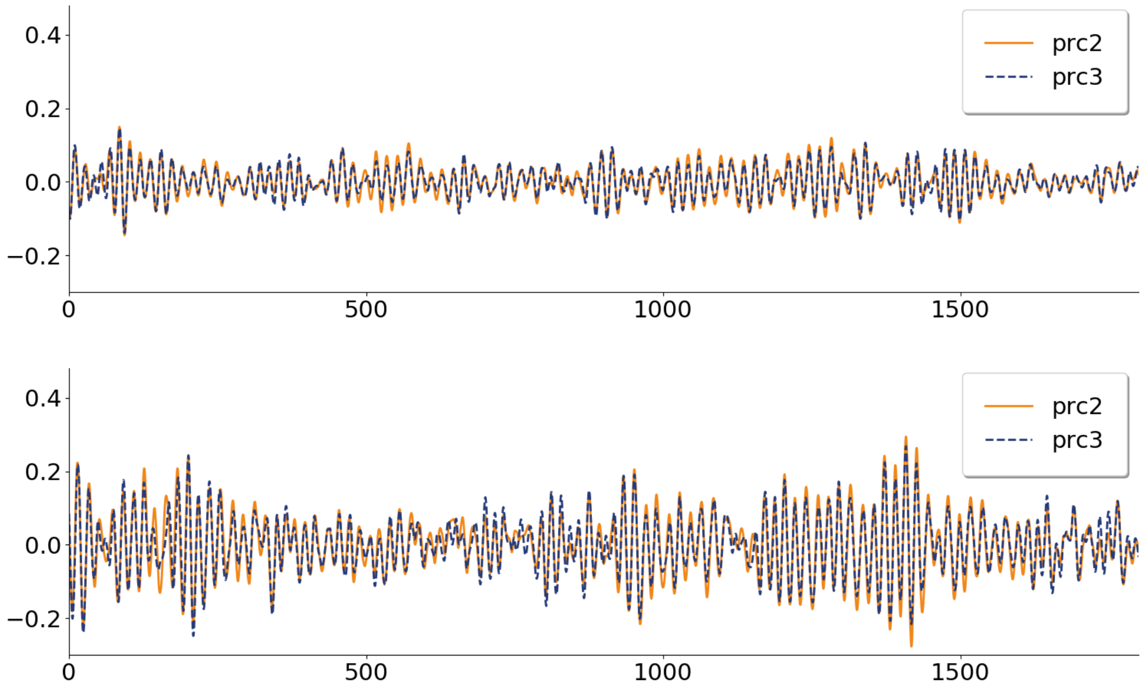

Figure 4.15: Motions of the blade root towards the hub for V = 6m/s (top) and V=9m/s (bottom)

4.3.3. Sensitivity Analysis

Blade Rotation in BIT

The distribution of aerodynamic forces and moments on the blade depends on the orientation of the blade in the BIT. A small rotation of the blade around the y_b axis changes the aerodynamic forces on the blade significant. Figure 4.16 compares the moment of the blade around the x-axis M_x and z-axis M_z for different angles of the blade ranging from -90° to 90°. The red line in 4.16 represents the angle of the blade used in the reference case and 12MW load cases (7°).

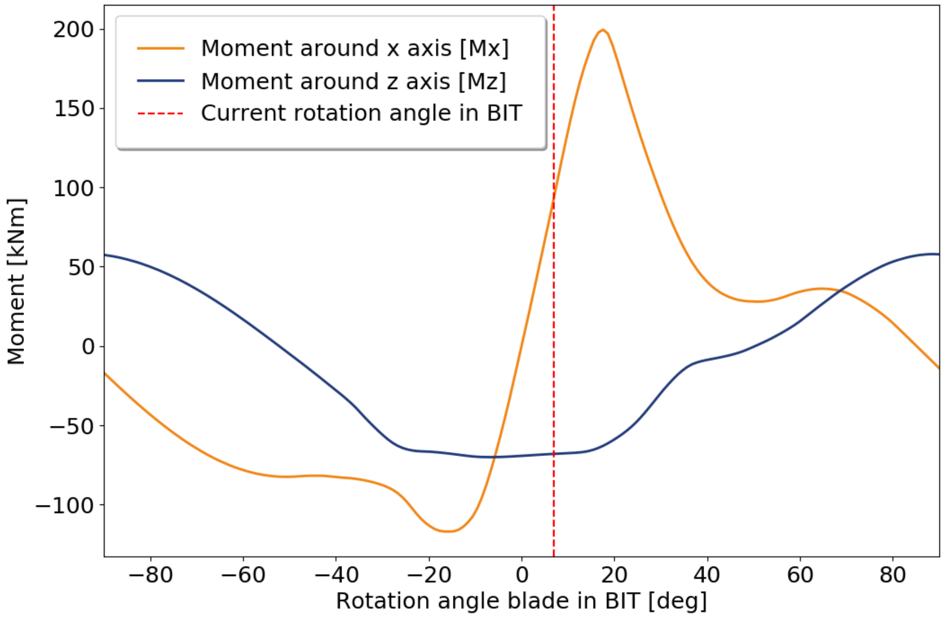

Figure 4.16: Blade aerodynamic moments around x and z axis for different blade angles in the BIT for a wind speed V = 10 m/s

The effect of the rotation angle of the blade in the BIT is studied. Figure 4.16 shows some interesting angles to investigate. For example the angles where one of the moments is zero: 0° for M_z and 52° for M_x. Other potential interesting angles are simulated and the results are shown in table 4.4. In this table the most favourable values are indicated in green cells and the most unfavourable in red.

Rotation blade in BIT [°]		-76	-16	0	7	17	47	52	68	85
Root center	$\mu_x[m]$	0.23	0.14	0.15	0.18	0.15	0.16	0.19	0.21	0.23
	$\mu_z[m]$	0.08	0.10	0.13	0.11	0.18	0.16	0.10	0.07	0.06
	$\sigma_x[m]$	0.17	0.10	0.11	0.13	0.11	0.12	0.14	0.16	0.17
	$\sigma_z[m]$	0.06	0.07	0.09	0.08	0.13	0.12	0.08	0.05	0.04
	Outcrossings	150	136	159	154	142	148	157	149	147
Blade motion	Roll [°]	0.15	0.18	0.22	0.20	0.32	0.27	0.18	0.12	0.10
	Yaw [°]	0.41	0.25	0.26	0.32	0.27	0.28	0.34	0.37	0.40
Forces	μ_{M_x} [kNm]	-21.9	-46.9	3.4	12.7	74.1	41.6	12.4	13.7	-1.0
	μ_{M_z} [kNm]	19.3	-28.2	-30.0	-0.8	-24.9	-29.5	1.7	15.5	24.4
	$\mu_{tagline[1]}$ [kN]	-16.8	-13.2	-13.0	-15.2	-13.6	-13.1	-15.4	-16.5	-17.2
	$\mu_{tagline[2]}$ [kN]	-13.9	-17.4	-17.4	-15.3	-17.1	-17.4	-15.1	-14.2	-13.6

Table 4.4: Simulation results for different angles of the blade in the BIT

A rotation of -16° of the blade reduces the number of outcrossing of the safe boundary and the mean displacement in x-direction (horizontal displacement) decreases with 22%. A reduction in vertical displacement of the blade root center can be accomplished by rotating the blade to 85°. In comparison with the 7° case the mean displacement of the root center in z-direction (vertical displacement) reduces with 46 %. The difference in the mean moment around the x-axis ranges from 74 kNm (17° case) to -1 kNm (85° case). For the moment around the z-axis the mean ranges from -30 kNm (0° case) to -0.8 kNm (7° case).

Effects Of Hub Motion

Figure 4.17 displays the main effect of adding the relative motion of the blade to the hub for the number of outcrossings of the safe boundary. The number of outcrossings increases if hub motion are taken into account. For larger hub motions the number of outcrossings increases further.

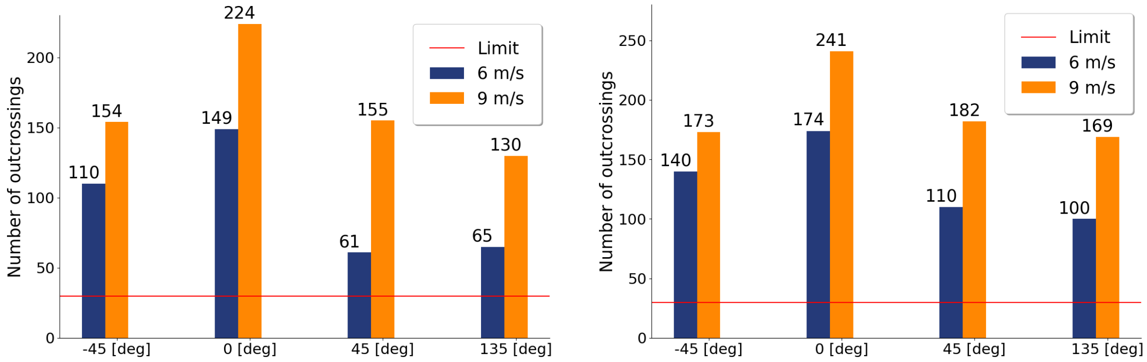

(a) Results for an imposed tower displacement with amplitude 0.02m

(b) Results for an imposed tower displacement with amplitude 0.06m

Figure 4.17: Number of outcrossing considering the relative motion between the blade root and hub

Damping

For different damping values simulations are performed to see how the model output changes. For five different damping cases the output results are shown in 4.5. For every damping case the result, in absolute values and relative values to the base case, are given. In the base case the damping values are equal to the ones used in the simulations. For the 50% and 80% case the damping values are decreased with 50% and 20% respectively. For the 120% and 150% case the damping values are increased with 20% and 50% respectively. Increasing the damping values leads to a decrease in the mean displacement, standard deviation and maximum displacement of the blade root. A decrease in damping values results in opposite results for the 50% case.

	50%		80%		Base case		120%		150%	
Output	Value	%	Value	%	Value	%	Value	%	Value	%
$\mu_{Blade-root}[m]$	0.36	26	0.26	-7.2	0.28	0	0.26	-7.4	0.24	-16
$\sigma_{Blade-root}[m]$	0.14	24	0.11	-1.2	0.11	0	0.11	-4.8	0.10	-10
$max_{Blade-root}[m]$	0.71	25	0.56	-1.2	0.57	0	0.55	-3.1	0.53	-6.7
$max_{Tagline}[kN]$	25	3.7	24	-0.82	24	0	24	-0.71	23	-1.2

Table 4.5: Simulation results for different damping values

Effects Of Turbulence Intensity

For four different turbulence intensity values simulations are performed at an average wind speed of 6 m/s and 9 m/s. The highest three TI values are according the normal offshore turbulence model (0.12,0.14 and 0.16). Simulations at TI 0.06 are performed to analyse the behaviour of the blade at a low TI value. The results show that the behaviour of the blade is sensitive to different turbulence intensities (see figure 4.18). Take the maximum blade root displacement for a wind speed of 9 m/s, the value at TI 0.16, which is around 1m, is over three times larger than the corresponding maximum blade root displacement at TI 0.06. The mean moment around the x- and z-axis of the blade experience a linear increasing trend with the increase of TI (see figure 4.18c). The maximum tension in the taglines also increase linear with the turbulence intensity (see figure 4.18d).

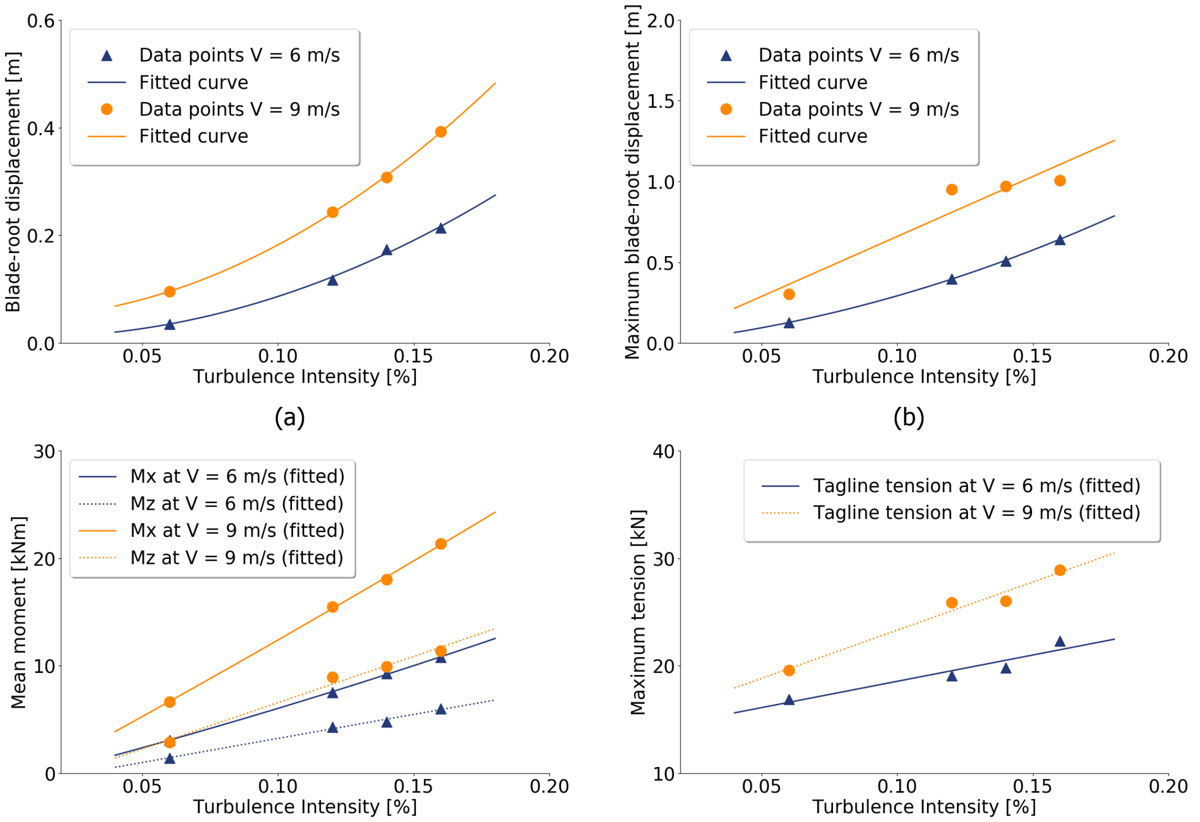

(a) (b)

(c) (d)

Figure 4.18: Results turbulence intensity sensitivity values

4.4. Improvements

The presented results in the previous sections can be used as input for the development of a new installation method or adjustment of the current lift setup to install blades. Based on the results and setup of the current tagline system it can be concluded that the current setup is not optimised for:

- Rotation around x-axis of the blade centre of gravity (indicated with 1 in figure 4.19)
- Rotation around z-axis of the blade centre of gravity (indicated with 2 in figure 4.19)
- Axial motion y-axis of the blade centre of gravity (indicated with 3 in figure 4.19)

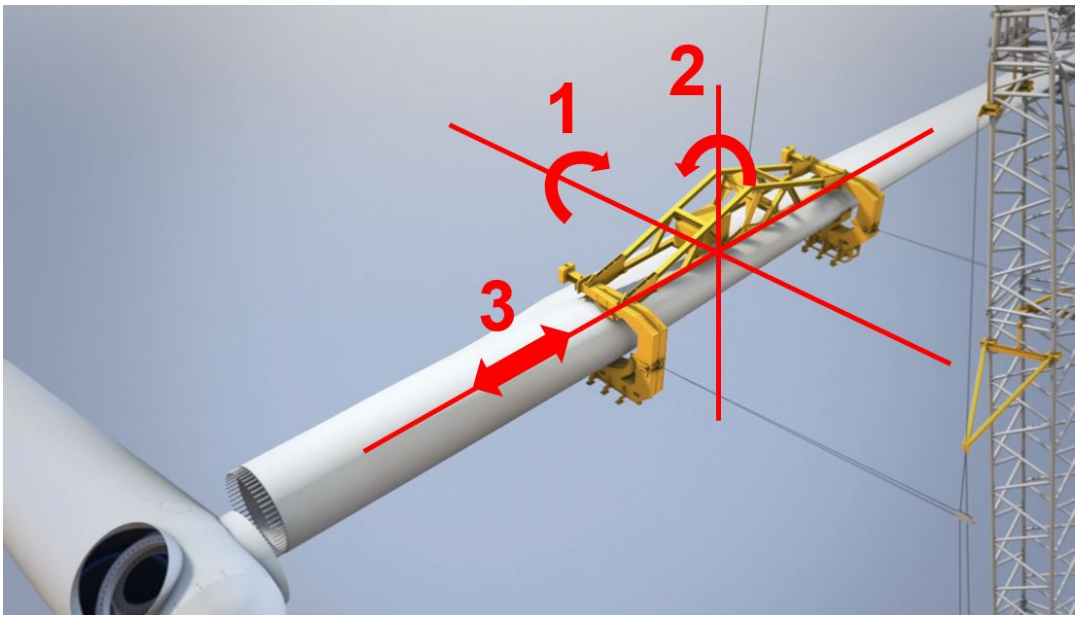

Figure 4.19: Tagline setup

To reduce the motions of the blade root, the motions of the blade centre of gravity should be reduced. To achieve this reduction multiple improvements could be made. These improvements should aim to increase the stiffness of the setup to increase the natural frequency of the first and second mode. The first improvement can be made by increasing the tagline tension. This will increase the lowest two natural frequencies and reduce the motions of the blade root. Figure 4.20 shows the difference in blade root motion for different tagline tensions at a wind speed of 9m/s. Although in the new situation the limit criteria are exceeded, the motions are decreased significant in the new situation.

The second improvement could be to attach the taglines more to the tip end and blade root end of the blade under a angle in the horizontal plane. The rotations in the blade, due to the wind induced moments, are easier to control if the distance between the attachment places of the taglines to the BIT are increased. The restoring moments are bigger for a wider setup. The attachment places depend on the blade installation tool that is provided by the turbine supplier. Therefore Van Oord is not in the position to make changes to this tool, although it is expected that increasing the width of the tagline attachment points could have a big effect on the dynamics of the blade.

The third improvement addresses the main three causes for the blade root motions displayed in figure 4.19. By adding an additional tagline (tagline 2) to the lift setup the motions of the blade root are reduced significant. This tagline setup is different from the tagline that is already in use in a number of ways. First of all, the pulley of the second tagline system doesn't slide over the guide wire but is attached to the crane at a predefined certain crane height. This increases the stiffness compared to the other tagline system. Furthermore, tagline 2 is installed under an angle in the vertical and horizontal plane (see 4.21). Tagline 2 is more effective in controlling the rotation of the blade around the x-axis (see figure 4.19) and therefore blade root motions in the vertical plane are reduced. The horizontal

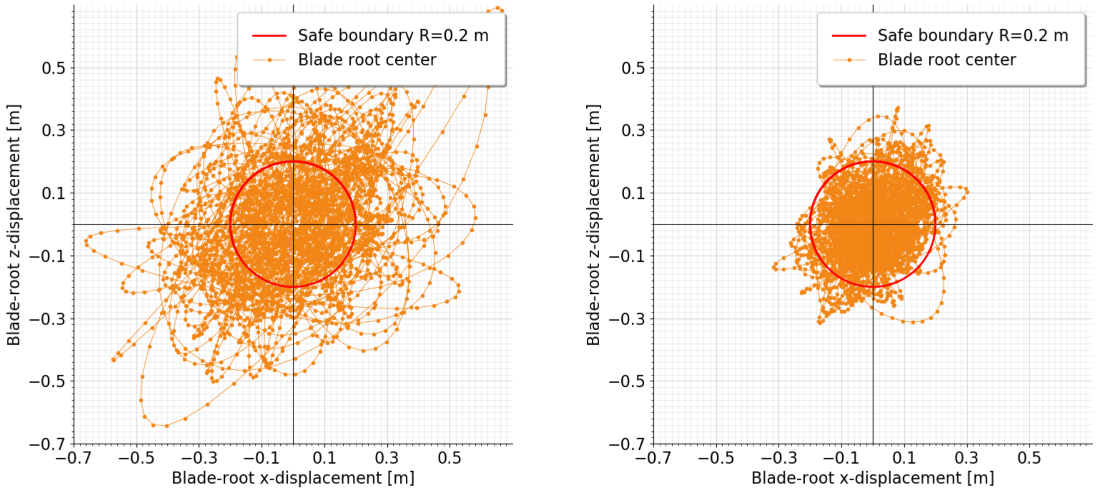

(a) Pretension tagline 15kN

(b) Pretension tagline 20kn

Figure 4.20: Track of the blade root center for 30-min simulations using a different tagline tension

angle in the second tagline system contributes to the reduction of the axial motion in y-direction of the blade.

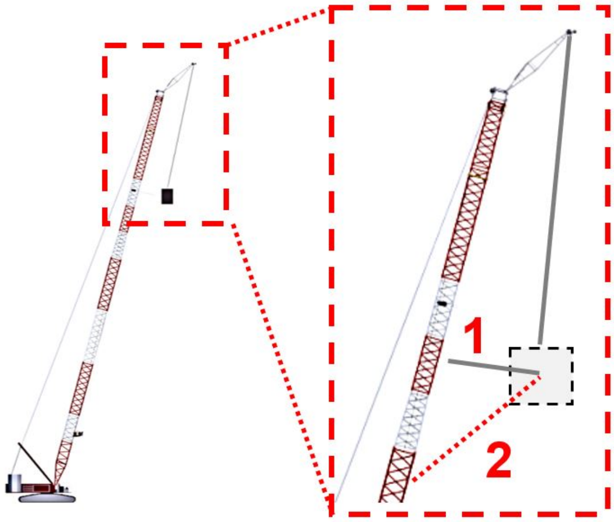

Figure 4.21: Additional tagline 2

The single lift blade installation procedure changes to the following:

1. The blade is lifted to hub height using tagline 1 and normal lifting procedures. The tension in the tagline 2 is zero and doesn't affect the installation.
2. At hub height, just before the alignment process initiates, the tension in tagline 2 increases to an optimum value for the lift setup. The tension in tagline 1 also changes to the preferred tagline tension.
3. The alignment of the blade root with the hub initiate following the normal lifting procedures.

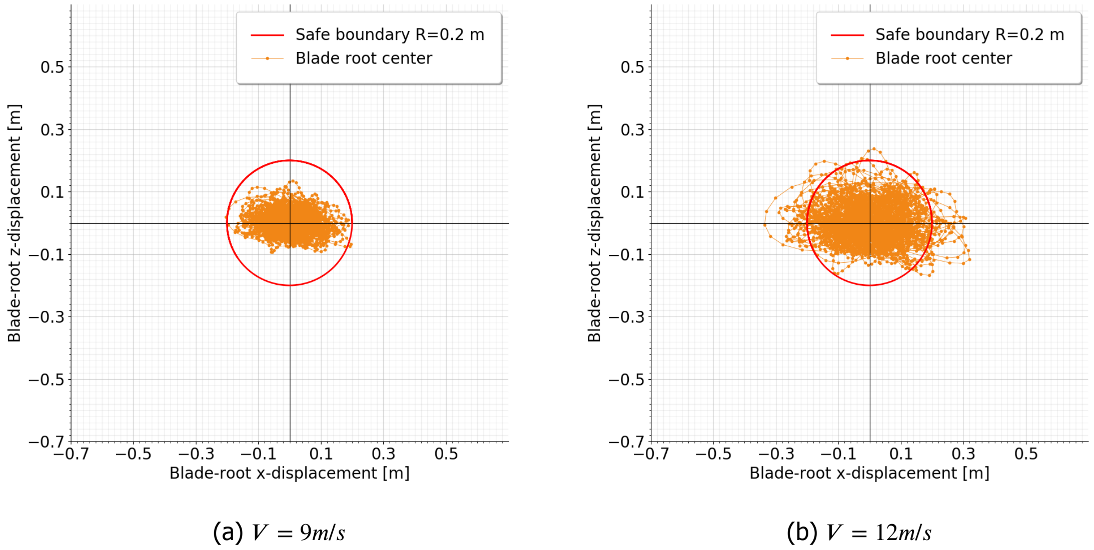

(a) $V = 9m/s$ (b) $V = 12m/s$

Figure 4.22: Track of the blade root centre with an additional tagline

Figure 4.22 shows the results for the new arrangement with an additional tagline. The blade root motions for a mean wind speed of $9m/s$ and $12m/s$ are reduced significantly. The reduction in blade root motions can be explained by taking a closer at the shift of the natural frequencies of the system. For the new lift setup the natural frequencies of the first and second mode are increased. Modes with higher natural frequencies are excited less due to the characteristics of the Kaimal wind spectrum, where the energy decreases non-linear for increasing frequencies. Furthermore the difference between the first and second natural frequency increased. As a results the blade root motion reduce. In figure 4.23 the natural frequencies and the corresponding blade root displacement spectrum are given for the old and new lift setup. In figure 4.24 the relative mean displacement in x,y and z direction are given for the different improvements. The distance R $(=\sqrt{x^2+y^2+z^2})$ gives the 3-D distance from the hub centre to the blade root centre. Increasing the tension or using an additional tagline both decreases the motion of the blade root.

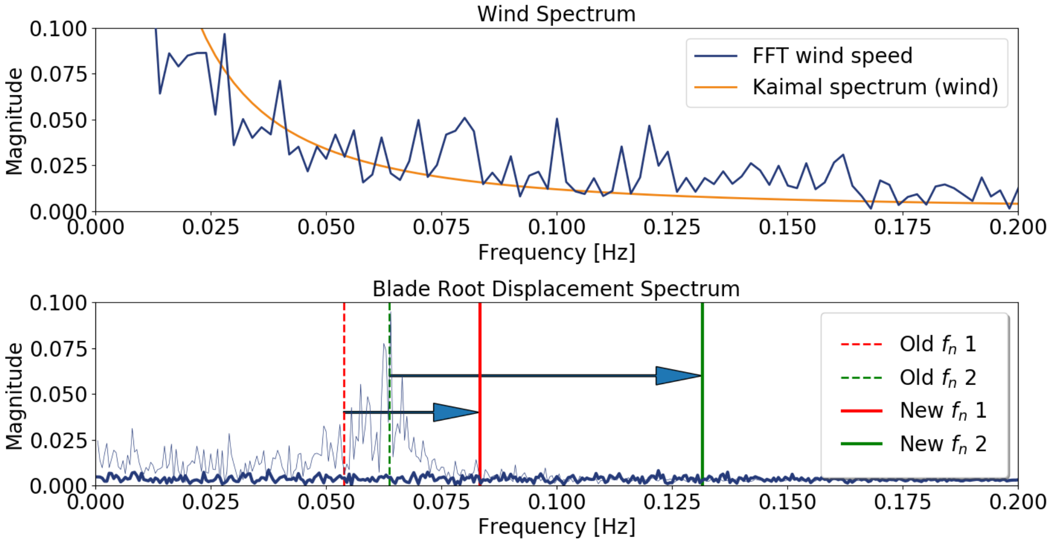

Figure 4.23: Wind spectrum (top) and blade root displacement spectrum for the old and new lift setup

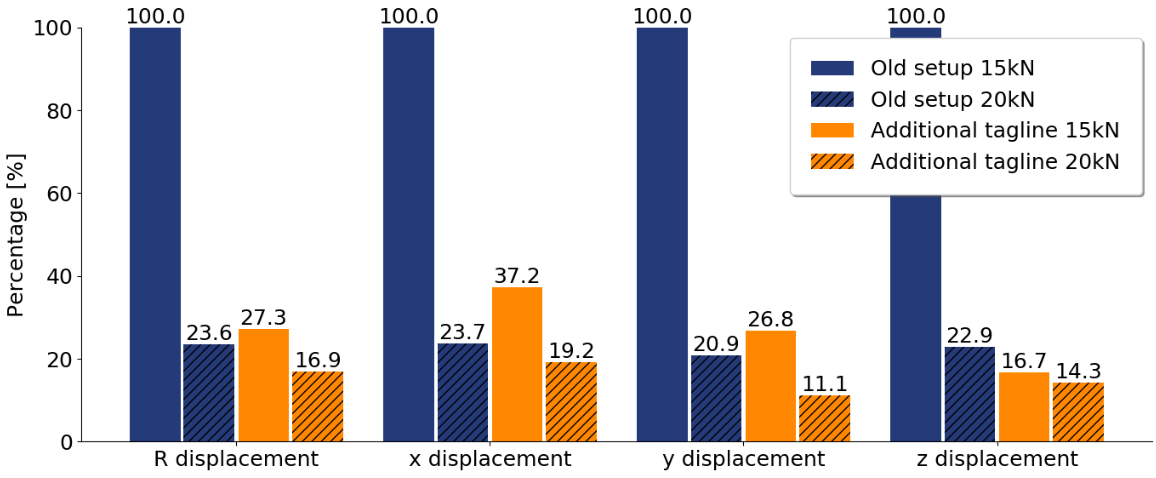

Figure 4.24: Results of the old setup compared to the results of the proposed improvements

5

Conclusion and Recommendations

5.1. Conclusions

This research addresses the feasibility of installing 12MW turbine blades. The research deals with the final installation phase: the alignment phase. The alignment phase is the most critical phase in the installation process of a turbine blade. A blade installation model for the alignment phase has been developed. For the motion of the hub an imposed displacement is considered. Time-domain simulations were conducted for the single blade installation alignment process for various wind conditions. An eigenvalue analysis is performed to determine the basic dynamic behaviour of the blade and how the blade will respond to external forces. In a sensitivity analysis the input variables (blade rotation, TI and damping) are changed to see how these changes affect the results. The most important conclusions are:

- The mean root displacement of a 107m blade (12MW) doubles compared to a 80 metre blade (8.4MW). The increase in blade mass decreases the natural frequencies of the system. Natural frequencies in the lower frequency range are excited by wind loading. The increase in blade length causes bigger displacement of the root for a rotation at the CoG of the blade. An increase in aerodynamic loads is the third cause for the increase in blade motion. Moments cause the blade to rotate and this rotation causes the blade root motions.
- A different rotation of the blade in the blade installation tool affects the root motions significant. A 69% reduction in mean displacement of vertical displacement could be achieved by rotating the blade 85°.
- Reduction in workability for 12MW turbine blade is expected to be around 60% considering wind conditions at the Dogger Bank.
- The current tagline setup is not optimal for installing 12MW turbine blades. Adding an extra tagline or increasing the tension reduces the motions by more than 80%.

The answers to the research questions can be found in F.

5.2. Recommendations

In this research the numerical model, used to study the alignment process of the blade, is simplified. For further research or application the following recommendations are given to improve the model:

- A limited number of environmental load cases are simulated. Performing simulations for a wider range of wind directions and wind velocities will give more information about the behaviour of the blade in different environmental conditions.
- An imposed displacement is used for the tower motions. This is a simplification, because tower motions are induced by wave and wind loads. Furthermore the motions of the tower hub can be in x and y direction (z direction is often negligible), but only the fore-aft motion of the tower is taken into account for this research. The number of blades installed in the hub also affects the hub motions and should be considered.

- The lift wires are assumed to be rigid and no elasticity in the lift wires is assumed. In reality the lift wires behave more like a spring. The taglines are modelled as a massless linear spring-damper system, which is a simplification of the real behaviour of taglines. In reality the taglines and guide wire system respond different. These assumptions were made to reduce the complexity of the model in order to decrease computational time.
- Crane and vessel dynamics are not accounted for in the model. The motions of the crane and vessel are assumed to be negligible relative to the blade motions in the alignment phase. For heavier blades this assumption could be incorrect and crane or vessel stiffness should be incorporated.
- The safe boundary is determined based on visual observations. It is recommended to determine the safe boundary based on the relating underlying aspects that cause problems if the motions become to big, such as a collision with the hub.

For future single lift blade installations a number recommendations are given:

- The focus of the installation method should be on the stabilisation of the blade root. The current tagline system stabilise the centre of the blade, but the blade root motions should be stabilised instead. These are caused by rotations and these rotations should be addressed.
- The angle of the blade in the blade installation tool should be considered. Aerodynamic forces vary for different blade angles and affect the dynamic behaviour of the blade.
- The current tagline setup is not optimal for the alignment phase of the blade and hub. Instead of looking for new (more expensive) solutions, the tagline system can be improved significant. For example by using an extra tagline under a different angle or using a different set up of the tagline system, which both requires more investigation.
- The installation procedures and lifting gear are often specified by turbine suppliers. Van Oord should aim to get involved in this process of determining installation procedures and lifting gear. For example, information about the aerodynamic properties of the blade could give a lot of valuable input for further research. Furthermore, design suggestions for the lift gear could be proposed to improve the alignment process.

A

Case Description

A.1. Restricted or Unrestricted operation

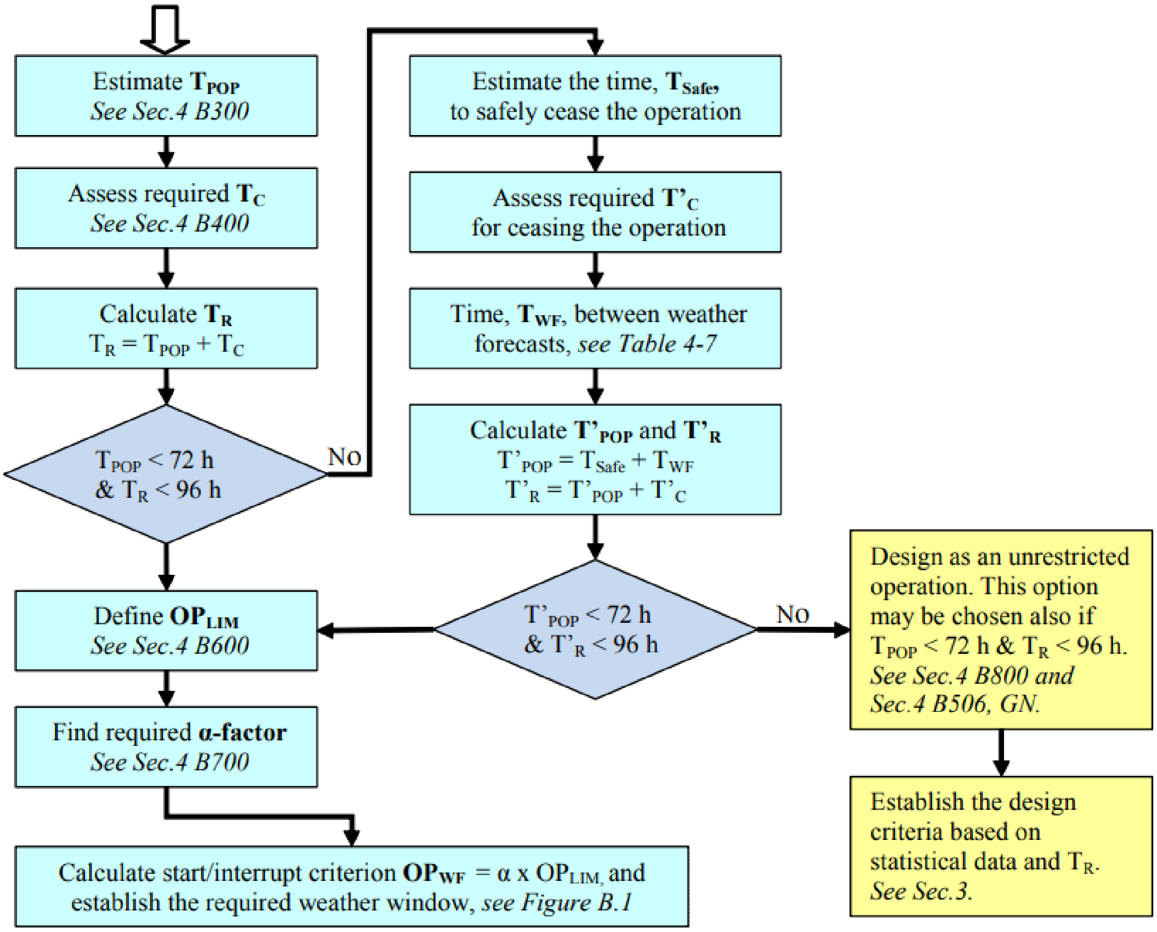

Figure A.1: Flow chart

A.2. Traverse system

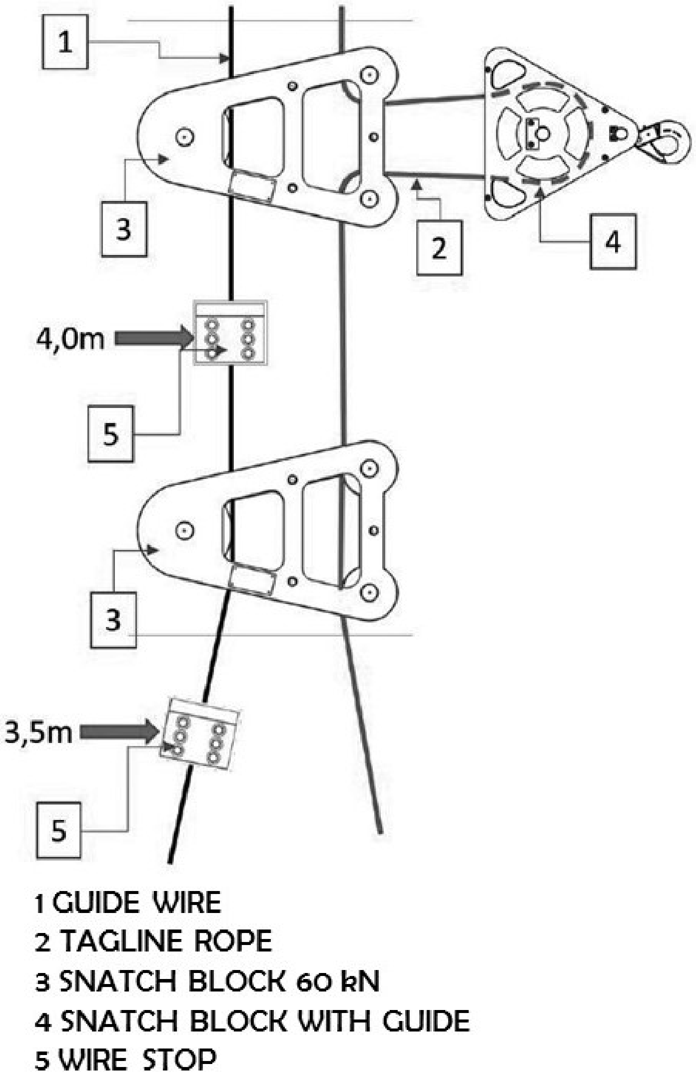

Figure A.2: Snatch Blocks

B

Model Verification

B.1. Simple Pendulum Motion Lift Wires

Newton's second law is applied to derive the analytical harmonic solution of the pendulum motion around the y-axis:

$$\tau = I\alpha \tag{B.1}$$

$$m_P g sin(\theta) L = m_P L^2 \frac{d^2\theta}{dt^2}. \tag{B.2}$$

Rearranging this equation and applying small angle approximation ($sin(\theta) = \theta$) gives

$$\frac{d^2\theta}{dt^2} - \frac{g}{L}\theta = 0 \tag{B.3}$$

Using the initial conditions, $\theta(0) = \theta_0$ and $\dot{\theta}_0 = 0$, the analytical solution becomes

$$\theta(t) = \theta_0 cos(\sqrt{\frac{g}{L}}t) \qquad \theta_0 << 1 \tag{B.4}$$

The solution of the pendulum motion around the x-axis is done using the same derivation:

$$\Theta(t) = \Theta_0 cos(\sqrt{\frac{g}{L}}t) \qquad \Theta_0 << 1 \tag{B.5}$$

B.2. Double Pendulum Motion Lift Wires

The position of m_1 and m_2 are

$$\mathbf{r_1} = -\frac{1}{2} l_1 \begin{bmatrix} sin(\theta_1) \\ cos(\theta_1) \end{bmatrix} \tag{B.6}$$

$$\mathbf{r_2} = 2\mathbf{r_1} - l_2 \begin{bmatrix} sin(\theta_2) \\ cos(\theta_2) \end{bmatrix} \tag{B.7}$$

the derivative of the position vector gives the velocity vectors

$$\dot{\mathbf{r}}_1 = -\frac{1}{2} l_1 \dot{\theta}_1 \begin{bmatrix} cos(\theta_1) \\ -sin(\theta_1) \end{bmatrix} \tag{B.8}$$

$$\dot{\mathbf{r}}_2 = 2\dot{\mathbf{r}}_1 - l_2 \begin{bmatrix} cos(\theta_2) \\ -sin(\theta_2) \end{bmatrix} \tag{B.9}$$

the derivative of the velocity vectors gives the acceleration vectors

$$\ddot{\mathbf{r}}_{\mathbf{1}} = -\frac{1}{2}l_1 \begin{bmatrix} \ddot{\theta}_1 cos(\theta_1) - \dot{\theta}_1^2 sin(\theta_1) \\ -\ddot{\theta}_1 sin(\theta_1) - \dot{\theta}_1^2 cos(\theta_1) \end{bmatrix} \quad \text{(B.10)} \qquad \ddot{\mathbf{r}}_{\mathbf{2}} = 2\ddot{\mathbf{r}}_{\mathbf{1}} - l_2 \begin{bmatrix} \ddot{\theta}_2 cos(\theta_2) - \dot{\theta}_2^2 sin(\theta_2) \\ -\ddot{\theta}_2 sin(\theta_2) - \dot{\theta}_2^2 cos(\theta_2) \end{bmatrix} \quad \text{(B.11)}$$

Forces

To solve Newton's second law $\mathbf{F} = m\ddot{\mathbf{r}}_{\mathbf{1/2}}$ the gravity and tension forces should be included in the equation. The derivation of constraint forces, such as tension, is not necessary if Langrangian mechanics are used. The tension (T) for m_1 and m_2 is in $-\mathbf{r_1}$ and $-\mathbf{r_2}$ direction, respectively. Tension T_2 Including gravitational forces gives

$$F_{x1} = T_1 sin(\theta_1) - T_2 cos(\theta_2 - \theta_1) sin(\theta_2) \quad \text{(B.12)} \qquad F_{z1} = T_1 cos(\theta_1) - T_2 cos(\theta_2 - \theta_1) - m_1 g sin(\theta_2) \quad \text{(B.13)}$$

$$F_{x2} = T_2 sin(\theta_2) \quad \text{(B.14)} \qquad F_{z2} = T_2 cos(\theta_2) - m_2 g \quad \text{(B.15)}$$

Equation of motions

The expression for the forces and accelerations of the particles are used to find the equation of motions

$$m_1\ddot{\mathbf{r}}_{\mathbf{1}} = \mathbf{F_1} \quad \text{(B.16)} \qquad m_2\ddot{\mathbf{r}}_{\mathbf{2}} = \mathbf{F_2} \quad \text{(B.17)}$$

The four EOMs become

$$\begin{aligned} m_1\ddot{r}_{x1} &= T_1 sin(\theta_1) - T_2 cos(\theta_2 - \theta_1) sin(\theta_2) && \text{(B.18)} \\ m_1\ddot{r}_{z1} &= T_1 cos(\theta_1) - T_2 cos(\theta_2 - \theta_1) - m_1 g sin(\theta_2) g && \text{(B.19)} \\ m_2\ddot{r}_{x1} &= T_2 sin(\theta_2) && \text{(B.20)} \\ m_2\ddot{r}_{z2} &= T_2 cos(\theta_2) - m_2 g. && \text{(B.21)} \end{aligned}$$

The number of equations is equal to the number of unknowns $(T_1, T_2, \theta_1, \theta_2)$. Maple is used to find expressions for $\ddot{\theta}_1$ and $\ddot{\theta}_2$. These are the equation to plug in any numerical method to analyse the system.

B.3. Symmetry M-Matrix

The kinetic energy term is defined as

$$E_{kin} = \frac{1}{2}\dot{\mathbf{q}}^{\mathbf{T}}\mathbf{M}\dot{\mathbf{q}} \quad \text{(B.22)}$$

Where $\dot{\mathbf{q}}$ represent the derivatives of the generalized coordinates. Define the symmetric part of matrix M as M_s and the asymmetric part of matrix M as M_a

$$\mathbf{M_s} = \frac{1}{2}(\mathbf{M} + \mathbf{M^T}) \quad \text{(B.23)} \qquad \mathbf{M_a} = \frac{1}{2}(\mathbf{M} - \mathbf{M^T}) \quad \text{(B.24)}$$

From equation B.23 and B.24 the following properties can be verified

$$\mathbf{M} = \mathbf{M_s} + \mathbf{M_a} \quad \text{(B.25)} \qquad \mathbf{M_s} = \mathbf{M_s^T} \quad \text{(B.26)} \qquad \mathbf{M_a^T} = -\mathbf{M_a} \quad \text{(B.27)}$$

The symmetric part of M is given in equation B.23 and the antisymmetric part in B.24. Using the formula for kinetic energy and substitution of equation B.25 gives

$$E_{kin} = \frac{1}{2}\dot{\mathbf{q}}^{\mathbf{T}}\mathbf{M}\dot{\mathbf{q}} = \frac{1}{2}\dot{\mathbf{q}}^{\mathbf{T}}(\mathbf{M_s} + \mathbf{M_a})\dot{\mathbf{q}} = \frac{1}{2}\dot{\mathbf{q}}^{\mathbf{T}}\mathbf{M_s}\dot{\mathbf{q}} + \frac{1}{2}\dot{\mathbf{q}}^{\mathbf{T}}\mathbf{M_a}\dot{\mathbf{q}} \quad \text{(B.28)}$$

Given that for any vector $\dot{\mathbf{q}}$ the equation $\dot{\mathbf{q}}^{\mathbf{T}}\mathbf{M_a}\dot{\mathbf{q}} = 0$ holds, the antisymmetric part of the mass matrix does not contribute to the kinetic energy in the system.

q1	*q2*	*q3*	*q4*	*q5*	*q6*	*q7*	*q8*	*q9*	*q10*	*q11*
0.61	0.57	0.52	0.25	0.46	0.49	0.48	0.95	0.97	0.72	0.57

Table B.1: Random verification input

q1	*q2*	*q3*	*q4*	*q5*	*q6*	*q7*	*q8*	*q9*	*q10*	*q11*
0.023	0.008	0.024	0.031	0.006	0.026	0.015	-5.4	0.009	0.006	0.028

Table B.2: Realistic verification input

17008000	0	1349260	1616070	260828	0	-798567	552944	0	0	0
0	23924200	4456170	-912184	-541155	971317	3526604	509233	0	0	0
1349260	4456170	253988	-17989	-44509	107612	-8068	62348	0	0	0
1616070	-912184	-17989	52640	24759	-17213	-53069	13614	0	0	0
260828	-541155	-44509	24759	4675	-13818	-10291	0	0	0	0
0	971317	107612	-17213	-13818	16000	0	0	0	0	0
-798567	3526604	-8068	-53069	-10291	0	16000	0	0	0	0
552944	509233	62348	13614	0	0	0	16000	0	0	0
0	0	0	0	0	0	0	0	19000000	0	0
0	0	0	0	0	0	0	0	0	500	0
0	0	0	0	0	0	0	0	0	0	19000000

Table B.3: Verification: M-matrix symmetry for random input values

23922500	0	9258	2386250	28130	0	-1151650	26777	0	0	0
0	23924200	4909890	-8150	-36895	1151960	221	9520	0	0	0
9258	4909890	267443	-361	-4085	127946	-179	3105	0	0	0
2386250	-8150	-361	65395	1563	-227	-63958	2008	0	0	0
28130	-36895	-4085	1563	25	-1009	-770	0	0	0	0
0	1151960	127946	-227	-1009	16000	0	0	0	0	0
-1151650	221	-179	-63958	-770	0	16000	0	0	0	0
26777	9520	3105	2008	0	0	0	16000	0	0	0
0	0	0	0	0	0	0	0	19000000	0	0
0	0	0	0	0	0	0	0	0	500	0
0	0	0	0	0	0	0	0	0	0	19000000

Table B.4: Verification: M-matrix symmetry for realistic input values

C

Tower Fore-Aft Motion

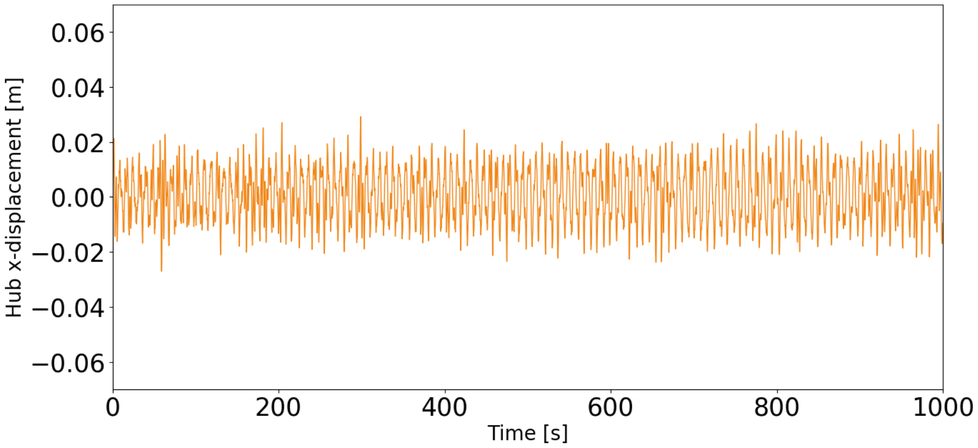

Figure C.1: Results fore-aft displacement hub for $h_s = 0.5m$

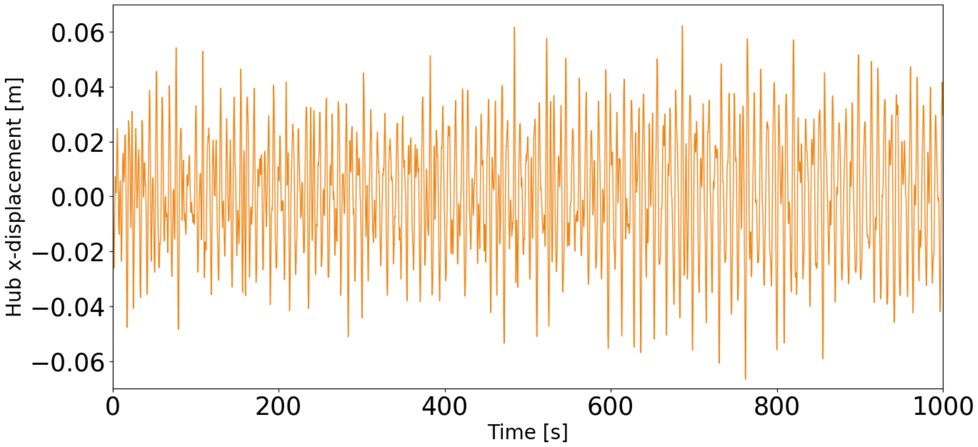

Figure C.2: Results fore-aft displacement hub for $h_s = 1m$

D

Blade

D.1. Blade Notes

Node	x_b	y_b	z_b	d_{cog}	θ_{twist}	l_{chord}	t_{rel}
1	0	-26.2	0	26.2	-14.5	5.4	100.0
2	0	-23.6	0	23.6	-14.5	5.4	99.7
3	0	-20.8	0	20.8	-14.5	5.4	95.3
4	0	-18.0	0	18.0	-14.4	5.5	86.0
5	0	-15.1	0	15.1	-13.9	5.6	73.9
6	0	-12.1	0	12.1	-12.5	5.9	61.1
7	0	-9.1	0	9.1	-10.6	6.1	50.4
8	0	-6.0	0	6.0	-8.9	6.2	43.0
9	0	-2.9	0	2.9	-7.8	6.2	38.3
10	0	0.2	0	0.2	-7.0	6.1	34.9
11	0	3.3	0	3.3	-6.4	6.0	32.4
12	0	6.4	0	6.4	-5.8	5.8	30.5
13	0	9.5	0	9.5	-5.2	5.6	29.1
14	0	12.6	0	12.6	-4.7	5.4	27.8
15	0	15.6	0	15.6	-4.1	5.2	26.8
16	0	18.5	0	18.5	-3.5	4.9	26.0
17	0	21.4	0	21.4	-2.9	4.7	25.3
18	0	24.2	0	24.2	-2.3	4.5	24.8
19	0	26.9	0	26.9	-1.7	4.2	24.5
20	0	29.5	0	29.5	-1.2	4.0	24.3
21	0	32.0	0	32.0	-0.7	3.8	24.1
22	0	34.5	0	34.5	-0.3	3.6	24.1
23	0	36.8	0	36.8	0.1	3.4	24.1
24	0	38.9	0	38.9	0.5	3.2	24.1
25	0	41.0	0	41.0	0.8	3.1	24.1
26	0	43.0	0	43.0	1.1	2.9	24.1
27	0	44.8	0	44.8	1.4	2.8	24.1
28	0	46.6	0	46.6	1.6	2.7	24.1
29	0	48.2	0	48.2	1.9	2.5	24.1
30	0	49.7	0	49.7	2.1	2.4	24.1
31	0	51.1	0	51.1	2.3	2.3	24.1
32	0	52.5	0	52.5	2.5	2.2	24.1
33	0	53.7	0	53.7	2.6	2.1	24.1
34	0	54.9	0	54.9	2.8	2.0	24.1
35	0	55.9	0	55.9	2.9	1.9	24.1
36	0	56.9	0	56.9	3.1	1.8	24.1
37	0	57.8	0	57.8	3.2	1.6	24.1
38	0	58.7	0	58.7	3.3	1.4	24.1
39	0	59.4	0	59.4	3.4	1.2	24.1
40	0	60.2	0	60.2	3.4	0.6	24.1

D.2. Segments

$Segment$	y_{begin}	y_{end}	x_{center}	y_{center}	z_{center}	$l_{segment}$	$A_{segment}$
1	-26.2	-23.6	0	-24.9	0	2.6	14.2
2	-23.6	-20.8	0	-22.2	0	2.7	14.4
3	-20.8	-18.0	0	-19.4	0	2.8	13.8
4	-18.0	-15.1	0	-16.5	0	2.9	12.8
5	-15.1	-12.1	0	-13.6	0	3.0	11.5
6	-12.1	-9.1	0	-10.6	0	3.0	10.1
7	-9.1	-6.0	0	-7.6	0	3.1	8.7
8	-6.0	-2.9	0	-4.5	0	3.1	7.8
9	-2.9	0.2	0	-1.4	0	3.1	7.0
10	0.2	3.3	0	1.7	0	3.1	6.4
11	3.3	6.4	0	4.9	0	3.1	5.8
12	6.4	9.5	0	8.0	0	3.1	5.3
13	9.5	12.6	0	11.0	0	3.1	4.8
14	12.6	15.6	0	14.1	0	3.0	4.4
15	15.6	18.5	0	17.1	0	2.9	3.9
16	18.5	21.4	0	20.0	0	2.9	3.6
17	21.4	24.2	0	22.8	0	2.8	3.2
18	24.2	26.9	0	25.6	0	2.7	2.9
19	26.9	29.5	0	28.2	0	2.6	2.6
20	29.5	32.0	0	30.8	0	2.5	2.4
21	32.0	34.5	0	33.3	0	2.4	2.1
22	34.5	36.8	0	35.6	0	2.3	1.9
23	36.8	38.9	0	37.8	0	2.2	1.7
24	38.9	41.0	0	40.0	0	2.1	1.6
25	41.0	43.0	0	42.0	0	2.0	1.4
26	43.0	44.8	0	43.9	0	1.8	1.3
27	44.8	46.6	0	45.7	0	1.7	1.1
28	46.6	48.2	0	47.4	0	1.6	1.0
29	48.2	49.7	0	48.9	0	1.5	0.9
30	49.7	51.1	0	50.4	0	1.4	0.8
31	51.1	52.5	0	51.8	0	1.3	0.7
32	52.5	53.7	0	53.1	0	1.2	0.7
33	53.7	54.9	0	54.3	0	1.2	0.6
34	54.9	55.9	0	55.4	0	1.1	0.5
35	55.9	56.9	0	56.4	0	1.0	0.4
36	56.9	57.8	0	57.4	0	0.9	0.4
37	57.8	58.7	0	58.2	0	0.8	0.3
38	58.7	59.4	0	59.1	0	0.8	0.2
39	59.4	60.2	0	59.8	0	0.7	0.2

E

Input Lift Plan

E.1. Lift wires

Parameter	Symbol	Unit	Value
	Lift Wires		
Mass	m_{AW} , m_{W}	kg	500
Mass moment of inertia	$\mathbf{I_{AW}}, \mathbf{I_{W}}$	$kg \cdot m^2$	$\begin{bmatrix}\mathbf{0}\end{bmatrix}$
Connection hoist jib ($\mathbf{p_1}$)	$\mathbf{p_1}$	m	$\begin{bmatrix}0 & -0.85 & 0\end{bmatrix}^T$
Connection hoist jib ($\mathbf{p_2}$)	$\mathbf{p_2}$	m	$\begin{bmatrix}0 & 0.85 & 0\end{bmatrix}^T$
CoGWW	$\mathbf{p_{CoGWW_{t=0}}}$	m	$\begin{bmatrix}0 & -0.85 & -18\end{bmatrix}^T$
CoGAW	$\mathbf{p_{CoGAW_{t=0}}}$	m	$\begin{bmatrix}0 & 0.85 & -18\end{bmatrix}^T$
Connection block catcher $\mathbf{p_3}$	$\mathbf{p_{3_{t=0}}}$	m	$\begin{bmatrix}0 & -0.85 & -36\end{bmatrix}^T$
Connection block catcher $\mathbf{p_4}$	$\mathbf{p_{4_{t=0}}}$	m	$\begin{bmatrix}0 & 0.85 & -36\end{bmatrix}^T$

Table E.1: Lift wires properties

E.2. Whip Hoist

Parameter	Symbol	Unit	Value
Whip Hoist Sheave			
Mass	m_{HS}	kg	$2.3 \cdot 10^3$
Mass moment of inertia	$\mathbf{I_{HS}}$	$kg \cdot m^2$	$\begin{bmatrix} 1.6 \cdot 10^3 & 0 & 0 \\ 0 & 0.40 \cdot 10^3 & 0 \\ 0 & 0 & 2.0 \cdot 10^3 \end{bmatrix}$
CoGHS	$\mathbf{p_{CoGHSt=0}}$	m	$\begin{bmatrix} 0 & 0 & -0.4 \end{bmatrix}^T$
Connection hook bearing $\mathbf{p_5}$	$\mathbf{p_{5t=0}}$	m	$\begin{bmatrix} 0 & 0 & -2 \end{bmatrix}^T$
Whip Hoist Hook Bearing			
Mass	m_{HB}	kg	$1.6 \cdot 10^3$
Mass moment of inertia	I_{HB}	$kg \cdot m^2$	$\begin{bmatrix} 1.2 \cdot 10^2 & 0 & 0 \\ 0 & 0.84 \cdot 10^2 & 0 \\ 0 & 0 & 1.2 \cdot 10^2 \end{bmatrix}$
CoGHB	$\mathbf{p_{CoGHBt=0}}$	m	$\begin{bmatrix} 0 & 0 & -0.5 \end{bmatrix}^T$
Connection hook $\mathbf{p_6}$	$\mathbf{p_{6t=0}}$	m	$\begin{bmatrix} 0 & 0 & -1 \end{bmatrix}^T$
Whip Hoist Hook			
Mass	m_H	kg	$1.0 \cdot 10^3$
Mass moment of inertia	I_H	$kg \cdot m^2$	$\begin{bmatrix} 1.7 \cdot 10^2 & 0 & 0 \\ 0 & 0.53 \cdot 10^2 & 0 \\ 0 & 0 & 2.0 \cdot 10^2 \end{bmatrix}$
CoGH	$\mathbf{p_{CoGH_{t=0}}}$	m	$\begin{bmatrix} 0 & 0 & -0.5 \end{bmatrix}^T$
Connection hook sling $\mathbf{p_{SH1}}$	$\mathbf{p_{SH1t=0}}$	m	$\begin{bmatrix} 0 & 0.2 & -0.5 \end{bmatrix}^T$
Connection hook sling $\mathbf{p_{SH2}}$	$\mathbf{p_{SH2t=0}}$	m	$\begin{bmatrix} 0 & -0.2 & -0.5 \end{bmatrix}^T$

Table E.2: Whip hoist properties

E.3. BIT and blade

Parameter	Symbol	Unit	Value
	BIT		
Mass	m_{BIT}	kg	$3.2 \cdot 10^4$
Mass moment of inertia	$\mathbf{I}_{\mathbf{BIT}}$	$kg \cdot m^2$	$\begin{bmatrix} 5.0 \cdot 10^5 & 0 & 0 \\ 0 & 4.0 \cdot 10^5 & 0 \\ 0 & 0 & 6.7 \cdot 10^5 \end{bmatrix}$
CoGBIT	$\mathbf{p}_{\mathbf{CoGBITt=0}}$	m	$\begin{bmatrix} 0 & 0 & -5.5 \end{bmatrix}^T$
Connection sling-BIT $\mathbf{p}_{\mathbf{SB1}}$	$\mathbf{p}_{\mathbf{SB1t=0}}$	m	$\begin{bmatrix} -1.1 & 2.5 & 3.0 \end{bmatrix}^T$
Connection sling-BIT $\mathbf{p}_{\mathbf{SB2}}$	$\mathbf{p}_{\mathbf{SB2t=0}}$	m	$\begin{bmatrix} -1.1 & -2.5 & 3.0 \end{bmatrix}^T$
Connection sling-BIT $\mathbf{p}_{\mathbf{SB3}}$	$\mathbf{p}_{\mathbf{SB3t=0}}$	m	$\begin{bmatrix} 1.1 & -2.5 & 3.0 \end{bmatrix}^T$
Connection sling-BIT $\mathbf{p}_{\mathbf{SB4}}$	$\mathbf{p}_{\mathbf{SB4t=0}}$	m	$\begin{bmatrix} 1.1 & 2.5 & 3.0 \end{bmatrix}^T$
Connection tagline-BIT $\mathbf{p}_{\mathbf{TB1}}$	$\mathbf{p}_{\mathbf{TB1t=0}}$	m	$\begin{bmatrix} 0 & 7.7 & 2.2 \end{bmatrix}^T$
Connection tagline-BIT $\mathbf{p}_{\mathbf{TB2}}$	$\mathbf{p}_{\mathbf{TB2t=0}}$	m	$\begin{bmatrix} 0 & -7.7 & 2.2 \end{bmatrix}^T$
Connection tagline-crane $\mathbf{p}_{\mathbf{TC1}}$	$\mathbf{p}_{\mathbf{TC1t=0}}$	m	$\begin{bmatrix} -6.4 & -6.0 & -45 \end{bmatrix}^T$
Connection tagline-crane $\mathbf{p}_{\mathbf{TC2}}$	$\mathbf{p}_{\mathbf{TC2t=0}}$	m	$\begin{bmatrix} -6.4 & 6.0 & -45 \end{bmatrix}^T$
	Blade (8.4 MW)		
Mass	m_{Blade}	kg	$3.5 \cdot 10^4$
Mass moment of inertia	I_{HB}	$kg \cdot m^2$	$\begin{bmatrix} 12.5 \cdot 10^6 & 0 & 0 \\ 0 & 0.24 \cdot 10^6 & 0 \\ 0 & 0 & 12.5 \cdot 10^6 \end{bmatrix}$
CoGBLADE	$\mathbf{p}_{\mathbf{CoGBLADEt=0}}$	m	$\begin{bmatrix} 0 & 0 & -5.5 \end{bmatrix}^T$
Blade root centre position $\mathbf{p}_{\mathbf{RC}_{\mathbf{t=0}}}$	$\mathbf{p}_{\mathbf{RC}_{\mathbf{t=0}}}$	m	$\begin{bmatrix} 0 & -24.4 & 0 \end{bmatrix}^T$
Blade root position $\mathbf{p}_{\mathbf{RC1}_{\mathbf{t=0}}}$	$\mathbf{p}_{\mathbf{RC1}_{\mathbf{t=0}}}$	m	$\begin{bmatrix} 0 & -24.4 & 2.6 \end{bmatrix}^T$
Blade root position $\mathbf{p}_{\mathbf{RC2}_{\mathbf{t=0}}}$	$\mathbf{p}_{\mathbf{RC2}_{\mathbf{t=0}}}$	m	$\begin{bmatrix} 2.6 & -24.4 & 0 \end{bmatrix}^T$
Blade root position $\mathbf{p}_{\mathbf{RC3}_{\mathbf{t=0}}}$	$\mathbf{p}_{\mathbf{RC3}_{\mathbf{t=0}}}$	m	$\begin{bmatrix} 0 & -24.4 & -2.6 \end{bmatrix}^T$
Blade root position $\mathbf{p}_{\mathbf{RC4}_{\mathbf{t=0}}}$	$\mathbf{p}_{\mathbf{RC4}_{\mathbf{t=0}}}$	m	$\begin{bmatrix} -2.6 & -24.4 & 0 \end{bmatrix}^T$

Table E.3: BIT and blade properties

F

Research questions

Sub-questions

What effect does wind have on the dynamics of a wind turbine blade in the mating phase?
Wind is the main cause for blade root motion. The mean displacement and standard deviation of the blade root increases rapidly when the wind speed increases. The results also depend on the incoming wind direction. A perpendicular wind direction is found to be the worst condition for installing blade. The workability improves at a wind direction of -45° and 45°. Improved workability is also expected for incoming wind directions between -45° and -90° and between 45° and 90°, because the wind velocity seen by the blade decreases further. An incoming wind direction of 135° results in smaller blade root motions than the -45° and 45° case. This decrease in blade root motion is due to different aerodynamic characteristics at the leading edge and at the trailing edge of the blade.

Under which environmental conditions will the movement of the blade relative to the hub stay within workable limits?
The mating process of the blade into the hub requires high precision. Compared to the installation of 8.4MW turbine blades the workability for the same environmental conditions will decrease. For wind speeds higher than 6m/s and a turbulence intensity of 0.12 the number of outcrossing per 30 minutes exceeds the limit of 30 for the wind direction angles between -45° and 45°. In the case the turbulence intensity drops to 0.06 (or lower) installation is feasible up to wind speeds of 9m/s.

What are the main causes for excessive blade root displacement?
The main causes for excessive blade root displacement are wind speed turbulence and the asymmetric lift setup. A sudden change in wind speed causes changes in drag and lift forces on the blade. Depending on the rotation of the blade in the blade installation tool, a change in the moment around the x-,y- and z-axis of the blade is induced. These changes in moment cause rotational accelerations of the blade and BIT. The rotational accelerations around the x- and z-axis results blade root displacement in the xz-plane. Forces in x-,y- and z-direction cause only small displacements, smaller than 0.01m, of the blade root motion. Also the moment around the y-axis of the blade (longitudinal axis) causes no significant motion of the blade root centre.

Are future blade installations expected to create an unsafe operation environment for employees?
The majority of serious injuries or fatalities from crane operations are sustained by workers who are close to the blade. In case workers are still close to the blade at the moment of mating the blade into the hub, possible dangerous situation could arise. The motion of the blade towards the hub could be close to 0.5 m in only a few seconds for 12MW turbine blades. Workers could get struck between the blade root flange and the hub flange. Therefore safety of the workers can't be guaranteed and a different lifting method should be considered.

Research-question

What effect on workability does the upscaling to future 12MW wind turbines have on the alignment process of single blade installation of turbine blades using a jack-up vessel?
Turbine blade root motions are caused by the aerodynamic moments of the blade around the x- and z-axis of the blade. Installing larger turbine blades will result in higher motions of the blade root and a decrease in workability. For the same wind speed, simulation results show that the mean and maximum displacement of the blade root doubles for a 12MW turbine blade compared to a 8.4MW turbine blade. This complicates the blade alignment process and the limit wind speed for which the blade can be alignment with the hub decreases from 10 m/s to around 5 m/s. Causing the workability to drop with 60%, compared to the 8.4MW turbine blade, and causes delays in the duration of a project at the Dogger Bank.

Bibliography

[1] Z. Ren, Z. Jiang, R. Skjetne, and Z. Gao, *Development and application of a simulator for offshore wind turbine blades installation,* Ocean Engineering 166, 380 (2018).

[2] Z. Ren, Z. Jiang, Z. Gao, and R. Skjetne, *Active tugger line force control for single blade installation,* Wind Energy, (2018).

[3] IRENA, *The power to change: Solar and wind cost reduction potential to 2025,* (2016).

[4] Det Norske Veritas, *DNV-OS-H101 Marine Operations, General,* (2011).

[5] Power Technology, *Dogger bank: profiling a true titan of wind power,* Retrieved from `https://www.power-technology.com/features/dogger-bank-profiling-true-titan-wind-power` (2017).

[6] H. J. Veenstra, *Geology of the dogger bank area, north sea,* Marine Geology 3, 245 (1965).

[7] Z. Jiang, *The impact of a passive tuned mass damper on offshore single-blade installation,* Journal of Wind Engineering and Industrial Aerodynamics 176, 65 (2018).

[8] Y. Zhao, Z. Cheng, P. Christian Sandvik, Z. Gao, and T. Moan, *An integrated dynamic analysis method for simulating installation of single blades for wind turbines*, Vol. 152 (2018) pp. 72–88.

[9] Orcina, *Rope/wire: Axial and bending stiffness,* Retrieved from `https://www.orcina.com/webhelp/OrcaFlex/Content/html/Ropewire,Axialandbendingstiffness.htm)` .

[10] Evolution, *Damping in a rolling bearing arrangement,* Retrieved from `http://evolution.skf.com/damping-in-a-rolling-bearing-arrangement` .

[11] M. Gaunaa, L. Bergami, S. Guntur, and F. Zahle, *First-order aerodynamic and aeroelastic behavior of a single-blade installation setup,* Journal of Physics: Conference Series 524, 012073 (2014).

[12] G. Chr, K. Ronold, and H. Jørgensen, *Ultimate loading of wind turbines,* (2019).

[13] NEN, *IEC 61400-3-1: Offshore wind turbine installations,* (2019).

[14] National Renewable Energy Lab, *Pyturbsim,* Retrieved from `http://lkilcher.github.io/pyTurbSim/` .

[15] L. Shampine and M. Reichelt, *The MATLAB ODE Suite,* SIAM Journal on Scientific Computing 18, 1 (1997).